



# HHS Public Access

Author manuscript

*J Med Chem.* Author manuscript; available in PMC 2022 June 26.

Published in final edited form as:

*J Med Chem.* 2022 May 12; 65(9): 6903–6925. doi:10.1021/acs.jmedchem.2c00266.

## Spiropyrimidinetrione DNA gyrase inhibitors with potent and selective antituberculosis activity

Preshendren Govender<sup>a</sup>,

Rudolf Müller<sup>a</sup>,

Kawaljit Singh<sup>a</sup>,

Virsinha Reddy<sup>a</sup>,

Charles J. Eyermann<sup>a</sup>,

Stephen Fienberg<sup>a</sup>,

Sandeep R. Ghorpade<sup>a</sup>,

Lizbé Koekemoer<sup>b</sup>,

Alissa Myrick<sup>b,#</sup>,

Dirk Schnappinger<sup>c</sup>,

Curtis Engelhart<sup>c</sup>,

Jaclynn Meshanni<sup>c,d</sup>,

Jo Ann W. Byl<sup>e</sup>,

Neil Osheroff<sup>e,f,g</sup>,

Vinayak Singh<sup>a,b</sup>,

Kelly Chibale<sup>a,b,\*</sup>,

Gregory S. Basarab<sup>a,h,\*</sup>

\*Corresponding Authors: Phone: +1-814-826-5988. greg.basarab@uct.ac.za, Phone: +27 21 650 2553. kelly.chibale@uct.ac.za.

<sup>†</sup>Current Address: Center for Global Infectious Disease Research, Seattle Children's Research Institute, Seattle, WA 98101, United States

<sup>#</sup>AM deceased in November 2019.

**Author Contributions.** Chemical synthesis, compound design and SAR expansion were performed by P.G., R.M., K.S., V.R. Computational and compound design support was provided by C.J.E. and S.F. Gyrase enzyme assay was performed by L.K. and Inspiralis Limited, UK. Biology data analyses was performed by A.M. and V.S. Screening against gyrase mutant strain was carried out by J.J. with data analysis by J.J. and T.P. Screening against gyrase hypomorph was conducted by C.A.E. and J.A.M. and the data was analyzed by C.A.E. and D.S. DNA cleavage reactions were carried out by J.A.W.B under the supervision of N.O. G.S.B. provided scientific and strategic guidance for the work and contributed the writing of the manuscript. S.R.G. provided scientific and strategic guidance for the work and wrote SAR, biology, DMPK, and conclusion sections of the manuscript. P.G. wrote synthesis and related experimental section. S.F. wrote computational section. Funding acquisition by K.C. along with scientific and strategic support and editing of the manuscript. All authors have given approval to the final version of the manuscript.

The authors declare no competing financial interest.

Supporting information includes Figure S1 (illustrations of moxifloxacin and QPT-1 crystal structures), Figure S2 (illustration of QPT-1 docking validation in Mtb DNA gyrase), the synthesis and characterization of inter- mediates, characteriazation of inactive isomers, the experimental method for the DNA gyrase supercoiling assay, the experimental methods for in vitro ADMET assays, sequence alignments of GyrA and GyrB (*M. tuberculosis*, *S. aureus* and *E. coli*), and QC data (NMR and UPLC-MS) for selected compounds (PDF)Coordinate files for *Mtb* gyrase binding models of compounds **5**, **6**, **10** and **42** (PDB).

Coordinate files for Mtb gyrase binding models of compound 5 (PDB)

Coordinate files for Mtb gyrase binding models of compound 6 (PDB)

Coordinate files for Mtb gyrase binding models of compound 10 (PDB)

Coordinate files for Mtb gyrase binding models of compound 42 (PDB)

Molecular formula strings and some data (CSV).

<sup>a</sup>Drug Discovery and Development Centre (H3D), Department of Chemistry, University of Cape Town, Rondebosch 7701, South Africa;

<sup>b</sup>Drug Discovery and Development Centre (H3D) South African Medical Research Council Drug Discovery and Development Research Unit, Department of Chemistry and Institute of Infectious Disease and Molecular Medicine, University of Cape Town, Rondebosch 7701, South Africa;

<sup>c</sup>Department of Microbiology and Immunology, Weill Cornell Medical College, New York, NY 10065 United States;

<sup>d</sup>Current affiliation: Department of Pharmacology and Toxicology, Rutgers University Ernest Mario School of Pharmacy, Piscataway, NJ 08854 United States;

<sup>e</sup>Department of Biochemistry, Vanderbilt University School of Medicine, Nashville, TN 37232 United States;

<sup>f</sup>Department of Medicine (Hematology/Oncology), Vanderbilt University School of Medicine, Nashville, TN 37232 United States;

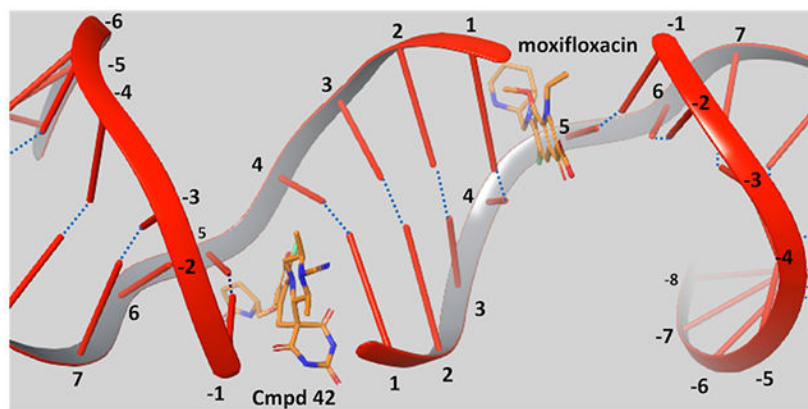
<sup>g</sup>VA Tennessee Valley Healthcare System, Nashville, Tennessee 37212, United States;

<sup>h</sup>Drug Discovery and Development Centre (H3D), Division of Clinical Pharmacology, Department of Medicine, University of Cape Town, Observatory, 7935, South Africa;

## Abstract

New antibiotics with either a novel mode-of-action (MoA) or novel mode-of-inhibition (MoI) are urgently needed to overcome the threat of drug-resistant tuberculosis (TB). The present study profiles new spiroimidinetriones (SPTs), DNA gyrase inhibitors having activity against drug resistant *Mycobacterium tuberculosis* (*Mtb*), the causative agent of TB. While the clinical candidate zoliflodacin has progressed to Phase 3 trials for the treatment of gonorrhoea, compounds herein demonstrated higher inhibitory potency against *Mtb* DNA gyrase (e.g., Compound **42** with an  $IC_{50} = 2.0$ ) and lower *Mtb* MICs (0.49  $\mu$ M for **42**). Notably, **42** and analogues showed selective *Mtb* activity relative to representative Gram-positive and Gram-negative bacteria. DNA gyrase inhibition was shown to involve stabilization of double-cleaved DNA while on-target activity was supported by hypersensitivity against a *gyrA* hypomorph. Finally, a docking model for SPTs with *Mtb* DNA gyrase was developed and a structural hypothesis was built for SAR expansion.

## Graphical Abstract



## Keywords

Tuberculosis; *Mycobacterium tuberculosis*; DNA gyrase; drug discovery; spiropyrimidinetriones

## INTRODUCTION

The increasing prevalence of *Mycobacterium tuberculosis* (*Mtb*), the causative agent of tuberculosis (TB), has been largely due to resistance to first- and second-line TB antibiotics and is exacerbating the global TB epidemic.<sup>1</sup> Multidrug resistant (MDR) *Mtb* strains resistant to both rifampicin (RIF) and isoniazid (INH), the most effective first-line drugs. Extensively drug resistant (XDR) *Mtb* strains are defined as those with MDR plus resistance to any fluoroquinolone (FQ) and one of the second line injectable drugs. As per the most recent World Health Organization report, in 2020 a global total of about 3 million people were diagnosed with pulmonary TB, of which 2.1 million showed rifampicin resistance and 202 000 showed MDR- or rifampicin-resistant TB (RR-TB).<sup>1</sup> Hence, there is an urgent need to replenish the TB drug discovery and development pipeline with new drug candidates having a novel mode-of-action (MoA) or novel mode-of-inhibition (MoI) of a known clinically validated target to combat resistance and to add to the arsenal of existing TB drugs.<sup>2</sup> Among the various approaches to overcome TB drug resistance, revisiting clinically validated targets by designing next generation compounds that overcome resistance or by identifying novel scaffolds that inhibit the validated targets differently remain worthwhile approaches to explore.<sup>3-4</sup> Herein, we present work around the spiropyrimidinetrione (SPT) class of compounds acting through the inhibition of DNA gyrase (hereafter referred to as gyrase), a clinically validated target for the treatment of TB.

DNA type II topoisomerases, comprised of the homologous enzyme gyrases and Topoisomerase IV, have drugs in the clinic representing four different classes of antibacterial agents.<sup>5-7</sup> Notably, these four classes that have all shown efficacy in humans avoid cross-resistance with one another. Gyrase is formed by two subunits each designated GyrA and GyrB operating as an A<sub>2</sub>B<sub>2</sub> complex, while Topoisomerase IV similarly is formed by two subunits each designated ParC and ParE in Gram-negative bacteria and GrlA and GrlB in Gram-positive bacteria. The primary role of gyrase is to adjust DNA topology by introducing negative supercoils necessary for DNA replication. Topoisomerase IV functions

primarily to decatenate replicating DNA, also necessary for replication. Notably, *Mtb* differs from most other human bacterial pathogens, including both Gram-negative and Gram-positive bacteria, in that it contains only one type II topoisomerase, namely gyrase, that carries out both supercoiling and decatenation.<sup>8-9</sup>

FQs comprise the most widely prescribed class of topoisomerase inhibitor (Figure 1) and are used for the treatment of a variety of bacterial infections.<sup>5, 7, 10</sup> Three FQs – moxifloxacin, levofloxacin and gatifloxacin – are currently used as second-line TB treatments. These compounds bind to a complex wherein both strands of the DNA are cleaved, covalently bonded to the topoisomerases.<sup>11-12</sup> As a second class of type II topoisomerase inhibitors, aminocoumarins are notable as competitive binders to the ATP-binding site situated well away from the topoisomerase DNA binding domain, a site that has received extensive investigation for inhibitor and drug design. Novobiocin, the leading example of an aminocoumarin, was on the market for Gram-positive infections associated with skin and respiratory tract infections for over 40 years, but its use was limited due to there being more potent drugs with better safety profiles and it was withdrawn in 2007.<sup>13</sup> Several other ATPase inhibitors have demonstrated potent *Mtb* activity,<sup>14-16</sup> though no clinical candidate has been revealed. Gepotidacin, representing a third class and having a novel triazaacenaphthylene moiety, inhibits type II topoisomerases at a distinct site from both FQs and aminocoumarins interacting with both DNA and the enzyme.<sup>17</sup> The compound shows broad spectrum activity against a variety of Gram-positive and Gram-negative pathogens and has progressed to Phase III clinical trials for treatment of uncomplicated urinary tract infection and urogenital gonorrhoea.<sup>18</sup> The quite diverse class of compounds represented by gepotidacin has been referred to as “novel bacterial topoisomerase inhibitors” (NBTIs) with several members having been identified with *Mtb* activity.<sup>19-22</sup> The SPT zoliflodacin, the leading compound of a fourth class of type II topoisomerase inhibitor, is currently in Phase 3 clinical trials as a single dose cure for uncomplicated gonorrhoea.<sup>23</sup> We have recently published an exploration of SPTs for the treatment of TB wherein activity was seen for a variety of analogues including zoliflodacin and the methyloxadiazole analogue **5** of Figure 1. Compound **5**, which showed higher *Mtb* activity than zoliflodacin, demonstrated cidal activity against the pathogen, activity against FQ-resistant *Mtb* strains and activity in a mouse infection model of TB.<sup>24</sup>

Here, we present the synthesis, structure-activity relationships (SAR) and biological assessments of an expanded series of SPTs with the goal of identifying a novel treatment for TB. One issue that is seen with FQs, ATPase inhibitors, quinolones and SPTs is that they have significant activity beyond *Mtb* against a broader spectrum of bacterial pathogens. It would be preferable to have a *Mtb*-selective agent to minimize the hardships stemming from the killing of commensal bacteria.<sup>25</sup> Furthermore, optimized dosing for treating TB may promote resistance in co-infections if such dosing were suboptimal against other pathogens. Therefore, activity of the new SPTs was determined against a Gram-positive and Gram-negative pathogen alongside *Mtb* towards understanding trends that would foster selectivity.

## Results and Discussions

### Model for SPTs within the *Mtb* gyrase binding site.

Despite the lack of cross resistance between FQs and SPTs across a variety of pathogens, moxifloxacin and a SPT analogue, QPT-1 (Figure 1), have been shown to share binding sites as determined via X-ray crystallography with the *Staphylococcus aureus* gyrase.<sup>26–27</sup> Gyrase creates a double stranded break with covalent phosphate bonds to Y123 (Y129 in *Mtb*) of GyrA, four bases apart on complementary DNA strands. Subsequently, a transported (T-segment) of duplex DNA is passed through, and the break is re-ligated. Moxifloxacin and other FQs bind at both the points of the double-stranded DNA breaks in both *S. aureus* and *Mtb* gyrase, inserting themselves between the base involved in a scissile bond and the –1 base and intercalating DNA bases (Figure 2A). Several GyrA residues lying beyond the  $\pi$ -stacking bases that sandwich the scaffold are associated with the moxifloxacin carboxylate and a  $Mg^{2+}$  and form part of the quinolone resistance-determining region (QRDR) including G88, A90, S91 and D94 (for *Mtb*, see Figure S1A and PDB 5BS8)<sup>28–29</sup> Like the FQs, QPT-1 forms  $\pi$ -stacking interactions with the complement of the –1 base as seen in its *S. aureus* co-crystal structure (Figure S1B). The pyrimidinetrione moiety extends into a region that is unoccupied by FQs and lies orthogonal to the scissile nucleotide and the Y123 phosphate acceptor. The two pyrimidinetrione NH groups each form a hydrogen bond with waters, one that bridges to the carboxylate of D437 and the other that bridges to the released ribose 3'-hydroxyl of the cleavage site DNA cytosine. The QPT-1 morpholino group is oriented towards the same solvated pocket as the chelated  $Mg^{2+}$  seen in the FQ binding mode. Residues abutting the morpholine ring include S84, S85, E88 and R92 of the GyrA QRDR (transformed to A90, S91, D94 and R98 in *Mtb* and to S89, A90, D93 and R97 in *E. coli*, see Supporting Information for GyrA and GyrB sequence alignments). The QPT-1 nitro group resides in a large open region lined by a tetrad of polar residues (R458, N475, N476 and E477). This region is occupied by the much larger tertiary amine of FQs at the protein interface with the –1 base complement. Sequence alignment showed that these residues are transformed to R482, N499, T500 and E501 in *Mtb* and K447, S464, Q465 and E466 in *E. coli*. Hence, the only difference between *Mtb* and *S. aureus* in the region is that of threonine to asparagine. Overall, functionality of similar polarity is retained across the three isozymes.

We generated a model for SPT binding to *Mtb* gyrase using the available *Mtb* gyrase structure with bound moxifloxacin (PDB 5BS8) and doubly cleaved DNA (Figure 2B). FQs and SPTs may stack with different bases at the site of DNA scission as suggested by optimal base sequences selected for co-crystallization work.<sup>30</sup> Several manipulations had to be made to the *Mtb* gyrase structure before SPT docking was possible. The *Mtb* structure was aligned with the QPT-1 *S. aureus* gyrase co-crystal structure (PDB 5CDM). Then the moxifloxacin ligand and its chelated  $Mg^{2+}$  ion were removed from one of the inhibitor binding sites, into which the QPT-1 ligand and the two bound waters associated with the pyrimidinetrione were transposed. An extended minimization of enzyme residues and DNA bases within a 7.5 Å radius of the transposed ligand in the *Mtb* structure was carried out. Following the minimization, QPT-1 was found to form a similar hydrogen bonding network around the pyrimidinetrione as was seen in its *S. aureus* co-crystal structure, that is with the D461 backbone NH H-bonding to the distal carbonyl and the two bound water molecules

H-bonding with each of the pyrimidinetrione NH groups. Additionally, as in the *S. aureus* co-crystal structure with QPT-1, one face of the SPT scaffold stacked on the adenosine-thymidine base pair (DNA -1 and DNA +5 relative to the scission sites) and the other face stacked on the guanosine DNA +1 base (relative to the scission site) while forming a tilted edge-to- $\pi$  interaction with a cytidine base in the +4 position of complementary DNA strand. A limitation of our model could be that nucleotide recognition for cleavage of DNA duplex may vary by inhibitor and gyrase isozyme,<sup>30</sup> as this transposition using a 24-mer DNA recognized by moxifloxacin may not be best recognized by QPT-1. Nonetheless, it is gratifying that the main contacts seen in this *Mtb* model mirror those seen in the *S. aureus* QPT-1 co-crystal structure offering a measure of validation. Notably, the pyrimidinetrione binding region might not have been predicted from the *Mtb* gyrase-moxifloxacin co-crystal structure alone.

After the SPT translocation and minimization, a Glide grid was generated from the ligand transposed structure<sup>31-32</sup> and validated by docking QPT-1 to afford a closely realigned pose. By extension, this pose aligned closely with that in the co-crystal of QPT-1 bound to the *S. aureus* gyrase with a negligible RMSD of 0.64 Å (Figure S2). Compound **5** was then docked into this validated grid (Figure 1) creating a pose in line with the QPT-1 binding mode wherein the pyrimidinetrione and morpholine moieties maintained their interactions at the binding site (Figure 3) and the fluorobenzisoxazole scaffold maintained the  $\pi$ -stacking interactions. The benzisoxazole oxygen atom abutted the tilted  $\pi$ -face of the cytosine. The methyloxadiazole extended well beyond the space surrounding the QPT-1 nitro group occupying a larger region bounded by the sidechains of the tetrad of GyrB polar residues (R482, N499, T500 and E501) as well as two consecutive DNA ribose rings and their phosphate bridge. The E501 carboxylate formed a salt bridge with the R482 guanidine and a H-bond with the T500 hydroxyl. The ring nitrogen atoms of the methyloxadiazole were positioned to accept a hydrogen bond from the guanidine of R482. Compound **5** also showed activity against *S. aureus* and *Escherichia coli* (Table 1) in line with similar binding interactions in the region surrounding the methyloxadiazole across species. As the region otherwise opens towards solvent along with apparent flexibility in the resident amino acid sidechains, there is considerable leeway in the diversity of substituents that can be tolerated on the benzisoxazole ring. At one level, the dockings of **5** and other compounds offer a measure of self-validation in that the benzisoxazole is tolerated for activity as is the variety of benzisoxazole substituents.

Overall, the modelling work pointed to two regions of the enzyme adjacent to the SPT molecule where it was deemed that further detailed SAR explorations would be fruitful as summarized in Figure 4. As already implied, the region surrounding the benzisoxazole R-substituent offers ample opportunity for variation, which aligns with extensive SAR work already published. Various compounds with *N*- or *O*-linked R-substituents having polar functionality (compounds **8-33**, Table 2 and 3) were designed to probe the tetrad of polar residues (R482, N499, T500 and E501) previously mentioned. The second binding region deemed exploitable surrounds the morpholine ring; this region is part of the QRDR and is considerably smaller and seemingly less amenable to incorporation of a broad array of substituents. By the model, the morpholine ring of SPTs adopted a chair conformation

placing the two methyl groups in equatorial orientations, while alternate conformations and orientations create a clash with stacking DNA bases. The surrounding region is where the FQ's chelate  $Mg^{2+}$  ion and is located between the scissile base, the -1 base and the enzyme. The immediate environment around the morpholine oxygen suggested a small accessible space for functionality in equatorial (or pseudo-equatorial) orientations. Hence compounds were made replacing the morpholine with substituted piperidines and piperazines (**34–45**, Table 4). The accessible space is bounded by the guanidine of the conserved R128 (R122 and R121 in *S. aureus* and *E. coli*, respectively) that displayed two occupancies for the sidechain guanidine in the moxifloxacin co-crystal structure with *Mtb* gyrase: one oriented towards a backbone DNA phosphate and the other to the carboxylate of the inhibitor, with the latter being chosen for the modelling. The pyrimidinetrione functionality was kept constant in the analogues herein, as it is perceived to be critical for potency based on the multiple hydrogen bond interactions and the snug fit in its binding pocket. To date, there are few published examples where the pyrimidinetrione was modified, and none where significant activity was observed.<sup>33</sup>

### Synthesis.

The literature synthesis of zoliflodacin **1** ends with the tertiary amino effect reaction (T-reaction) wherein chiral intermediate **46** and barbituric acid are heated at 110 °C to afford a thermodynamic 9:1 diastereomeric mixture; purification can be achieved by chromatography or crystallization (Scheme 1).<sup>34–36</sup> As the synthesis of **46** uses a rather expensive chiral (2*R*,6*R*)-2,6-dimethylmorpholine as a reactant,<sup>37–38</sup> we incorporated the inexpensive *meso*-2,6-dimethylmorpholine to set up the T-reaction in racemic form as depicted for the conversion of the transient intermediate aldehyde in Scheme 2. Hence, **47** with the *meso*-morpholine was prepared on a multi-gram scale as set out in the literature.<sup>37</sup> The chlorine atom of **47** was displaced with a variety of cyclic amines by refluxing in acetonitrile in the presence of DBU to give **48a-o** and with a variety of alcohols using NaH in DMF to give *O*-linked **48p-z**. Subsequent reaction of intermediates **48** with barbituric acid in ethanol containing HCl at 80 °C effected ketal hydrolysis to the transient aldehyde and *in situ* T-reaction to afford compounds **8–33** (Tables 2 and 3). As the T-reaction temperature was kept to the lower temperature of 80 °C, there was no formation of the other morpholine diastereomer as seen in Scheme 1.<sup>39–40</sup> The racemic mixtures (or diastereomeric mixtures when the R-substituent is chiral) were generally separated by chiral HPLC to give the enantiopure compounds. The stereochemistry of the isolated isomers could easily be assigned as the desired (2*R*,4*S*,4*a**S*) isomers invariably have a negative optical rotation and showed activity against *Mtb*. In the case of **20**, the corresponding ethyl ester (**S1**) was maintained through the T-reaction conditions and separated by chiral chromatography before being hydrolyzed with lithium hydroxide to the acid.

Scheme 3 exemplifies the sequence that was used to synthesize compounds whereby the dimethylmorpholine was changed to substituted piperazines. As mentioned, having an equatorially orientated substituent on the X-atom in Scheme 3 was predicted to interact with the conserved GyrA Arg128 of *Mtb*. Towards this, intermediate **49**<sup>37</sup> was assembled with the chiral oxazolidinone substituent on the benzisoxazole, set up for displacement of the fluorine atom *ortho* to the carboxaldehyde by various amines (syntheses of new amines

shown in Scheme S1–S2) to afford **50a-d**. Intermediates **50c** and **50d** were derived from **50a** by reacting with acetic anhydride and bromoacetonitrile, respectively. Compounds **34–37** were prepared from **50a-d** via the T-reaction with barbituric acid and were purified via chiral chromatography. The *N*-cyano analogue **38** was prepared by cyanation of racemic mixture of **34** with cyanogen bromide, followed by chromatographic separation on a chiral column.

Compounds **39–45** were made wherein the dimethylmorpholine ring was replaced with either a dimethylpiperidine or *N*-cyanodimethylpiperazine combining with more favorable benzisoxazole R-substituents (Scheme 4). For **39–43**, the syntheses involved the incorporation of amines (*meso*-1-cyano-2,6-dimethylpiperazine (**S5**) or *meso*-3,5-dimethylpiperidine) by S<sub>N</sub>Ar displacement of the fluorine *ortho* to the carboxaldehyde of **51**<sup>36</sup> to afford **52a-b**. Subsequently, the aldehydes were protected as the ethylene acetals affording **53a-b**. The R-substituents were then introduced by S<sub>N</sub>Ar displacement on the chlorobenzisoxazole using 1,2,4-triazol, (*S*)-3-hydroxypyrrolidine, (*R*)-3-hydroxypyrrolidine or (*S*)-5-(hydroxymethyl)pyrrolidin-2-one to afford **54a-e**. Finally, **54a-e** were transformed to **39–43** along with their diastereomeric or enantiomeric pairs by *in situ* acetal hydrolysis and T-reaction with barbituric acid. Compound **39** was only isolated as the racemic mixture as it did not succumb to separation of enantiomers, whereas **40–43** were separated from the corresponding isomers **40E–43E** via chiral chromatography. In Scheme 5, the known intermediate **55**<sup>41</sup> was treated with chiral (*R,R*)-2,6-dimethylpiperazine followed by cyanation with cyanogen bromide to afford **57** that is set up for the higher temperature T-reaction to afford **44**. For **45** (Scheme 5), **55** was treated with (*meso*-3*S*,4*r*,5*R*)-3,5-dimethylpiperidin-4-ol hydrochloride (supporting information intermediate **S11**, preparation outlined in Scheme S3) and reacted with barbituric acid in the T-reaction for subsequent purification by chiral chromatography. Importantly, the stereochemistry of **S11** was established to have the 4-hydroxyl *trans*-to the *cis*-dimethyl groups (see Figure S2). The stereochemistry was maintained on conversion to **45** as confirmed by <sup>1</sup>H-NMR spectroscopy, wherein the carbinol CH appears as a quartet with 9 Hz coupling consistent with a *trans*-diaxial orientation relative to the two hydrogens beneath each of the piperidine methyl groups. In the <sup>1</sup>H-NMR spectrum, there was a coincident 9 Hz coupling to the OH. Having the hydroxyl in the equatorial orientation was predicted to have a more favorable interaction in the enzyme binding site relative to the axial orientation wherein the OH would clash with the stacking guanosine base.

### Structure-activity relationships.

Analogues were profiled for the minimum inhibitor concentration (MIC) against *Mtb* as well as a Gram-positive (*S. aureus*) and Gram-negative (*E. coli*) pathogen, the latter two assays towards assessing selectivity for *Mtb* (Tables 1, 2, 3 and 4). Physical properties (solubility and logD) and cytotoxicity against HepG2 cells<sup>42ref</sup> were also determined; gratifyingly, solubilities for most of the compounds were high (>100 μM) and cytotoxicities (>50 μM) were low. Selected compounds were assessed for inhibition in gel based *Mtb* and *S. aureus* gyrase assays for correlation with whole cell activity. The SPTs of Table 1 showed considerably lower MIC values for *S. aureus* than those seen for *Mtb*, while the *E. coli* MICs were more variable. However, the SAR for *Mtb* activity diverges from that seen for *S. aureus* and *E. coli* as previously described.<sup>24</sup> The reasons for pathogen-to-pathogen divergence in



SAR could be differences in the inhibitor binding domain as the surrounding residues do vary despite being quite similar. Additionally, the optimal DNA cleavage sites and stacking bases that abut the inhibitors may differ depending on the pathogen. However, the data supports a larger influence of a second factor for the variable pathogen-to-pathogen SAR, namely the disparate nature of the outer cell envelope and efflux pumps among *Mtb*, Gram-positive and Gram-negative pathogens differentially affecting the compound permeability into the bacterial cytoplasm where gyrase is localized.<sup>43–44</sup> Indeed, the large influence of efflux was demonstrated for SPTs relative to *E. coli* activity, wherein considerably lower MICs (generally 200-fold or more) were seen for a *tolC*<sup>-</sup> efflux pump debilitated mutant relative to wild-type.<sup>36</sup> The key role of bacterial permeability is supported by comparing **5** with moxifloxacin (Table 1) wherein the former is 5-fold more potent as an inhibitor of *Mtb* gyrase inhibitor but 10-fold less active against the pathogen suggesting greatly enhanced permeability for the latter. It is worth noting that the gel-based DNA supercoiling assay requires a much higher amount of supercoiled DNA substrate to monitor conversion to relaxed DNA relative to concentrations encountered inside the cell. Hence, inhibitory potencies can often be considerably higher than MICs recorded in culture.

### SAR of benzisoxazole substituent.

The series of SPTs in Table 2 with pyrrolidine benzisoxazole substituents showed MICs as low as 4  $\mu\text{M}$  against *Mtb* and markedly higher MICs for both *S. aureus* and *E. coli*. For example, **8** with the *S*-hydroxypyrrolidine showed about equal activity relative to zoliflodacin against *Mtb* but was upwards of 200-fold less active against both *S. aureus* and *E. coli*. However, **8** ( $\log\text{D} = 1.4$ ) and zoliflodacin ( $\log\text{D} = 2.0$ ) showed comparable inhibitory potencies ( $\text{IC}_{50}\text{s} = 6.9$  and  $4.3$   $\mu\text{M}$ , respectively) against gyrase from *S. aureus*. Compound **7** ( $\log\text{D} = 1.6$ ) also showed a comparable *S. aureus* gyrase inhibitory potency ( $\text{IC}_{50} = 1.7$   $\mu\text{M}$ ) to zoliflodacin and was similarly active against the pathogen. The data are in line with correlations made previously for SPTs wherein higher lipophilicity was associated with higher bacterial cell permeability and lower MICs against *E. coli*.<sup>37</sup> Hence, it is apparent that permeability for *S. aureus* and *E. coli*, whether it is due to passive outer cell envelop diffusion or active efflux, is much more sensitive to compound polarity than is *Mtb*. Compound **9** with the (*R*)-hydroxypyrrolidine maintained the *Mtb* activity compared to **8**. A binding model supports that both the *R*- and *S*-hydroxypyrrolidine configurations can form a favorable H-bond with the sidechain hydroxyl of T500 or the guanidine of R482. Incorporation of a second hydroxyl onto the pyrrolidine forming the dihydroxypyrrolidine diastereomers **10**, **11** and **12** were well-tolerated. A binding model for **10** (Figure 5A), the most active of the three, suggests H-bond interactions with both T500 and R482. The  $\text{IC}_{50}\text{s}$  for gyrase from both *Mtb* and *S. aureus* (16 and 6.6  $\mu\text{M}$ , respectively) were similar to the values seen for **8**, as were the MICs against *Mtb*, *S. aureus* and *E. coli*, providing further confirmation that bacterial permeability is driving selectivity for *Mtb*. The methoxypyrrolidine **13** ( $\text{IC}_{50} = 77$   $\mu\text{M}$  against gyrase,  $\text{MIC} = 31$   $\mu\text{M}$ ) showed diminished *Mtb* activity relative to **8** suggesting that the hydroxyl group better donates a H-bond versus being on the receiving end of a H-bond and, indeed, the T500 hydroxyl looks to be tied up with a H-bond to E501. The *Mtb* gyrase  $\text{IC}_{50}$ 's for **8**, **10**, **14** and **19** were equal to or only around 2-fold higher than the value for moxifloxacin (10  $\mu\text{M}$ ), yet *Mtb* MICs were considerably worse, again attributable to inferior bacterial permeability for SPTs. Compound

**15** with 3-methyl-3-hydroxypyrrolidine (obtained as a mixture of inseparable diastereomers) showed a significant loss of *Mtb* activity (MIC >125  $\mu$ M); both configurations for the compound place the methyl substituent in a clash with T500 that is thought to receive a H-bond from the hydroxyl. Compounds **16** and **17** with the basic 3-aminopyrrolidine and 3-methylaminopyrrolidine showed 9 to 16-fold higher MICs compared to **8**. As **16** was only about 2-fold less potent against *Mtb* gyrase relative to moxifloxacin, it is likely that the positively charged basic amine diminishes bacterial permeability accounting for the lower antibacterial activity. Interestingly, **18** and **19** with 3-F and 3-CN-pyrrolidines, respectively, retained *Mtb* activities similar to **8**, suggesting that both functionalities can interact productively to the surrounding enzyme functionality. Notably, **18** being more lipophilic than **8**, showed improved activity against *S. aureus* and *E. coli*. Compound **20** with the 3-pyrrolidine carboxylate substituent showed significantly lower *Mtb* activity (MIC >125  $\mu$ M) indicating intolerance for the charged carboxylate group for binding affinity and/or diminished bacterial permeability. The two 3-hydroxypiperidine diastereomers **21** and **22** had moderate MICs indicating a slightly less favorable positioning of the hydroxyl group and a limitation of the 6-membered ring relative to the pyrrolidine.

Another series of *Mtb* active SPTs were identified having heterocycles in a two-atom bridge linked to the benzisoxazole through an ether oxygen (Table 3). Compound **23** with the pyrrolidinone heterocycle showed a high *Mtb* gyrase inhibitory potency (IC<sub>50</sub> = 2.6  $\mu$ M) and a low *Mtb* MIC (1.0  $\mu$ M). Compound **24** with the epimeric configuration at the lactam ring was found to be inactive (MIC >125  $\mu$ M); however, the compound was extremely insoluble in aqueous media, which might compromise the expression of activity. The reason for extremely low solubility for **24** is not understood and may involve extraordinary tight packing in a crystal lattice. Capping of the lactam NH of **23** with methyl affording **25** was detrimental to *Mtb* activity by 4-fold. Replacing the lactam with a lactone as in **26** and **27** reduced the activity 2- to 4-fold compared to **23**. Oxazolidinones **28** and **29** maintained *Mtb* MICs of 2  $\mu$ M. Changing the attachment of the 2-atom linker to the lactam ring from the 5- to 4-position (compounds **30** and **31**) was also well-tolerated for *Mtb* activity with MICs = 2  $\mu$ M. As well, **32** with 3-atom linker was ~4-fold less active than **23**. Finally in Table 3, **33** with a 2-atom linker to the methyloxadiazole was considerably less active than the compounds otherwise. Overall, these observations indicate considerable leeway in the region surrounding the benzisoxazole, though there is a measure of specific binding.

### SAR of morpholine modifications.

In general, modifications of the morpholine ring of SPTs showed little leeway for variation (Table 4), in line with the docking model. Compound **43** with dimethylpiperidine was 16-fold less active than the corresponding morpholine matched pair **23**. The binding model has the axial hydrogen for the CH<sub>2</sub> for O replacement approaching a stacking DNA base, which may contribute to the lower activity. However, relative to **8** and **23**, **43** was more active against *S. aureus* and *E. coli*, in line with improved permeability due to the piperidine increasing the logD about one unit over the morpholine. For *S. aureus*, it is hypothesized that the optimal DNA stacking for the inhibition complex is different such that binding with the piperidine would be favored, though structural work with a variety of DNA duplex motifs would need to be carried out for confirmation. Replacing the morpholine with a piperidine

substituted at the 4-position by an equatorial hydroxyl (compound **45**) led to a 10-fold reduction in *Mtb* activity relative to the matched pair **5** of Table 1.

Piperazine derivatives were made eliminating the potential negative impact of the axial hydrogen atom of the piperidine. Compound **34** with the weakly basic 2,6-dimethylpiperazine and various *N*-substituted analogues thereof such as *N*-hydroxy **35**, *N*-acetyl **36** and *N*-cyanomethyl **37** showed considerably lower *Mtb* activity (>125  $\mu\text{M}$ ). It is likely that *N*-acetyl derivative **36** alters the conformation of piperidine ring clashing with the adjacent methyl groups and is too large to fit into the adjacent space. The *N*-cyanomethyl group is also likely too large to fit into the space. The parent piperazine and *N*-hydroxypiperazine may not make favorable interactions especially for the former if it is likely protonated at physiological pH. However, the *N*-cyano analogue **38**, was nearly 2-fold more active against *Mtb* than its matched pair, zoliflodacin; the compound also showed significant activity (though lower than zoliflodacin) against *S. aureus* and *E. coli*. Hence, the series of compounds **39-42** maintaining the *N*-cyanopiperazine in place of the morpholine but varying the R-substituent were made, consistently showing about equal activity to the corresponding matched pair. Compound **39** (MIC = 0.9  $\mu\text{M}$ ) with the triazole benzisoxazole substituent was 2-fold more active relative to its matched pair **7** (MIC = 2.0  $\mu\text{M}$ ); since **39** could only be isolated as the racemate, the active enantiomer could have a 4-fold lower MIC. Notably, **39** showed lower HepG2 cytotoxicity (>300 versus 26  $\mu\text{M}$ ) compared to **7** of Table 1, which might be associated with incompatibility of the *N*-cyanopiperazine with the human orthologs, topoisomerase IIa and topoisomerase IIb.<sup>37</sup> Compound **42** showed the highest activity against *Mtb* (MIC = 0.49  $\mu\text{M}$ ) of the *N*-cyanopiperazines as well as potent inhibition (IC<sub>50</sub> = 2.6  $\mu\text{M}$ ) of *Mtb* gyrase while retaining many of the same attributes as its morpholine matched pair **23**, including selectivity relative to *S. aureus* and *E. coli* activity, high solubility and clean cytotoxicity at the highest concentration tested (300  $\mu\text{M}$ ). Figure 5B shows a proposed model of the *N*-cyano group within the surrounding region of the gyrase QRDR wherein the piperazine maintains a conformation to display the two methyl and cyano groups in pseudo-equatorial orientations. The cyano extends out towards the guanidine of the conserved GyrA R128, the residue assuming an orientation similar to that seen in the moxifloxacin co-crystal structure wherein it bridged to the inhibitor carboxylate. The pyrrolidinone tethered off the benzisoxazole reaches over to T500. Though the equivalent of T500 in *S. aureus* and *E. coli* are N476 and Q465, it is possible that these residues contribute to variations in pathogen MICs. However, there is a fair statistical correlation ( $R^2 = 0.8$ ) between *Mtb* inhibitory potency and MIC for the ten compounds where the first value was determined (Figure 6). The ten compounds displayed broad range of lipophilicity (logD's 0.16– 2.3); a poor correlation was seen for SPTs with a similar logD range against *E. coli*.<sup>30</sup> Again the data indicate that *E. coli* and *S. aureus* SPT permeability are more sensitive to compound lipophilicity than is *Mtb*, in line with what has already been noted for **10**. Explicitly, more polar compounds are apparently better able to transit into the *Mtb* cytoplasm relative to Gram-positive and Gram-negative bacteria.

### Mode-of-action characterization.

To validate that *Mtb* gyrase is the primary target of SPTs and to confirm the on-target activity, we evaluated whether conditional depletion of GyrA in *Mtb* would sensitize the

growth inhibitory effects of SPTs. Previously, **5** was shown to be devoid of cross-resistance to two strains of *Mtb* having point mutations (A90V and G88C) in GyrA that impart resistance to FQs.<sup>24</sup> Herein, an anhydrotetracycline (ATc)-regulated conditional knockdown mutant (hypomorph) in the Tet-ON configuration underexpressing *gyrA*<sup>46</sup> was assessed for inhibitory activity by SPTs. Due to the sensitivity of *gyrA* hypomorph to ATc and the nature of the assay, we compared both MIC<sub>50</sub> (for 50% growth inhibition) and MIC (for 99% growth inhibition) and calculated the fold-hypersensitivity in the form of the ratio (WT/hypomorph MICs, Table 5) thereby getting a reading of variations in the concentration response curves. The *gyrA* hypomorph consistently displayed hypersusceptibility to SPTs versus wildtype H37Rv control, similar to and/or greater than what is seen for moxifloxacin confirming that the SPTs inhibit *Mtb* growth via enzymatic inhibition of gyrase (Table 5). Rifampicin as a negative control validated that the MIC differences are not artefacts due to fitness of the hypomorph construct. These data support the conclusion that SPTs operate by inhibition of gyrase *Mtb* thereby thwarting DNA replication. However, it is well understood that varying enzyme levels could be complicated by the formation of DNA strand breaks, which also contributes to cell death via the SOS response (see below).<sup>24, 48</sup> A much more involved investigation would be needed to assess the influence of increasing and decreasing levels of either *gyrA* and *gyrB* (or both simultaneously) to understand the relative role to cell cidity around blocking DNA replication versus generating DNA strand breaks.

We also set out to determine whether the inhibitory mechanism of SPTs correlates with stabilization of the doubly cleaved complex of DNA with gyrase as had been demonstrated for other pathogens.<sup>5, 7, 10</sup> Assays were carried out via incubation of *Mtb* gyrase with negative supercoiled plasmid in the presence of drug, and, after denaturing, DNA was analyzed by gel electrophoresis (Figure 7).<sup>47</sup> Both moxifloxacin and **23** displayed similar accumulations of double-stranded cleaved DNA (linear DNA), supporting that they operate by binding to DNA doubly cleaved to *Mtb* gyrase and supporting the binding model that has been used herein. It is likely that there is a contribution to cidity associated with production of the cleaved DNA due to induction of the cellular hypersensitive SOS response.<sup>24, 48</sup> Taken together with the hypomorph data, the MoIs for SPTs and FQs are similar in that they show bactericidal activity by inhibition of gyrase. That SPTs are not cross-resistant to gyrase mutations that impart decreased FQ sensitivity likely invokes that SPTs are unaffected by the association of the QRDR with FQ-Mg<sup>2+</sup> complexes.<sup>49</sup>

## Conclusion

Compounds were identified with improved *Mtb* activity over the two previously characterized compounds, zoliflodacin and **5**. Importantly, a docking model for SPTs was developed using a *Mtb* gyrase crystal structure to build a structural hypothesis for the observed SAR. The selectivity seen for *Mtb* over other Gram-positive and Gram-negative bacteria (as exemplified by *S. aureus* and *E. coli*, respectively) was attributed to compound lipophilicity and differential bacterial permeability. Hence, SPTs are less sensitive to changes in lipophilicity relative to permeability in mycobacteria, and selectivity was not due to drastic differences in target inhibition. The benefit for such selectivity would be ease of dosing in the clinic by minimizing the upset due to disruption of beneficial gastrointestinal microbiota and by removing the pressure for resistance development to the class when

co-infection occurs. Previous publications around SPTs disclose compounds that displayed both *S. aureus* and *E. coli* activities. The compounds of Table 1, including moxifloxacin, show activity against *Mtb* and appreciable cross-over to the other pathogens. Two parts of the SPT molecule were identified for analogue optimization leading to expansion of SAR over what had previously been established. First, the scaffold benzisoxazole substituent was modified to afford novel substituents with *N*-linked hydroxypyrrolidines and with heterocycles linked via an *O*-linked two-atom bridge. Second, replacing the morpholine with an *N*-cyanopiperazine, hypothesized to interact with the conserved Arg128, was shown to be operable for inhibition of gyrase representing perhaps the only SPT morpholine modification disclosed to date that maintains target potency and antibacterial activity. Overall, **42** having the pyrrolidinone heterocycle linked to the benzisoxazole and the *N*-cyanopiperazine replacement for morpholine provided the highest *Mtb* activity herein, while maintaining favorable solubility and low cytotoxicity. Notably, the mode-of-inhibition for a representative SPT (compound **23**) correlated with binding to the DNA cleaved complex of *Mtb* gyrase in line with observations seen for other pathogens. The significance is that gyrase functions differently in *Mtb* due to its enhanced role for decatenation in addition to supercoiling, yet its interaction with the SPT is similar. Previously it was shown that SPTs are not cross-resistant with FQs despite the shared mode-of-action; herein we showed that the *Mtb* activity is due to gyrase inhibition as demonstrated by the upward shift in MICs against the down-regulated *gyrA* hypomorph. These studies thus lay the foundation for further compound optimization of activity towards achieving in vivo efficacy and identifying a valuable treatment for TB.

## Experimental section

### MIC assays.

The minimum inhibitory concentration (MIC) that inhibits 90% of growth of the bacterial population was determined using the broth micro-dilution method against the *M. tuberculosis* H37RvMa strain (ATCC 27294), as described earlier.<sup>50</sup> MIC values represent the average of at least two biological replicates. Briefly, a 10 mL culture of the *M. tuberculosis* H37RvMa strain was grown to an optical density (OD<sub>600</sub>) of 0.6 – 0.7. Duplicate two-fold serial dilutions of the test compounds were prepared across 10 wells in a 96-well microtiter plate, in a volume of 50 µL, after which, 50 µL of the diluted *M. tuberculosis* culture (1:500) was added to each well in the plate. The final volume per well was 100 µL. A positive growth (DMSO =< 2.5%), a negative growth (Rifampicin at 2xMIC), and a Rifampicin dose response (range 0.15 – 0.0002 µM) controls were used to measure the contamination and/or plate-to-plate variations. The microtiter plate was sealed in a secondary container and incubated at 37°C with humidification. The AlamarBlue (Bio-Rad) reagent was added to each well of the assay plate at day 7 and incubated for 24 h. The measurement of MIC values was done at day 8, either visually (the lowest concentration of compound displaying no visible growth was scored as the MIC, blue colour – no growth, pink/purple colour - growth) or by measuring relative fluorescence (excitation 540 nm; emission 590 nm) using a SpectraMax i3x Plate reader. The raw fluorescent data were used to calculate % inhibition using a 4-parameter curve fit protocol (Softmax® Pro 6 Version 6.5.1).

### MICs against *gyrA* hypomorph.

Wild-type H37Rv and *gyrA*-FDAS-TetON-1 were grown in 7H9 broth (supplemented with 5 g/L bovine serum albumin, 2 g/L dextrose, 0.85 g/L NaCl, 0.2% glycerol, and 0.05% Tyloxapol, and +50 µg/mL Hygromycin, +25 µg/mL Streptomycin, +500 ng/mL Anhydrotetracycline for the *gyrA* hypomorph) in a humidified incubator at 37 °C and 5% CO<sub>2</sub> until logarithmic growth was reached. The cultures were washed with fresh drug-free 7H9 and suspended to an OD<sub>580</sub> of 0.01. The diluted suspensions were added to 384-well black, clear-bottom plates at 50 µL/well, containing 16-point 2-fold drug dilutions in DMSO in triplicate, for a final DMSO concentration of 1%. Plates were wrapped with aluminum foil in stacks of no more than six and incubated at 37 °C and 5% CO<sub>2</sub> in a humidified incubator. The OD<sub>580</sub> of the plates was read after incubating 11 days. Growth data was normalized to inhibitor-free wells, and MIC values were determined by fitting the normalized data to a Gompertz model in GraphPad Prism. MIC values represent the average of two replicates.

### DNA cleavage.

DNA cleavage reactions were based on the procedure of Aldred *et al.*<sup>47</sup> Negatively supercoiled pBR322 plasmid DNA was prepared from *E. coli* using a Plasmid Mega Kit (Qiagen) as described by the manufacturer. Reactions were carried out in the presence or absence of **23** or moxifloxacin (LKT) and contained 100 nM wild-type (1.5:1 GyrA:GyrB ratio) and 10 nM negatively supercoiled pBR322 in a total volume of 20 µL of 10 mM Tris-HCl (pH 7.5), 40 mM KCl, 6 mM MgCl<sub>2</sub>, 0.1 mg/mL bovine serum albumin, and 10% glycerol. 20 mM stocks of **23** and moxifloxacin were made with 100% DMSO and stored at -20 °C. Dilutions (200 µM) of each compound was made in 40% DMSO. Reactions were incubated at 37 °C for 10 min. Covalent gyrase-cleaved DNA complexes were trapped by adding 2 µL of 4% sodium dodecyl sulfate followed by 1 µL of 375 mM Na<sub>2</sub>EDTA and 2 µL of 0.8 mg/mL Proteinase K (Affymetrix). Reaction mixtures were incubated at 45 °C for 30 min to digest the enzyme. Samples were mixed with 2 µL of 60% sucrose, 10 mM Tris-HCl (pH 7.9), 0.5% bromophenol blue; and 0.5% xylene cyanol FF and incubated at 45 °C for 2 min before loading onto 1% agarose gels. Reaction products were subjected to electrophoresis in 40 mM Tris-acetate (pH 8.3) and 2 mM EDTA containing 0.5 µg/mL ethidium bromide. DNA bands were visualized with medium-range ultraviolet light and quantified them using an Alpha Innotech digital imaging system. DNA single- or double-stranded cleavage was monitored by the conversion of supercoiled plasmid to nicked or linear molecules.

### Docking model generation.

The *Mtb* gyrase structure was prepared from the crystal structure (PDB ID: 5BS8)<sup>27</sup> co-crystallised in complex with moxifloxacin using the Maestro Protein Preparation wizard. The dsDNA portion of the structure was solved for two strands with alternate sequences on the same coordinates. With two DNA strands (chains D and E; F and G), the F and G chains were deleted while saving their two Mg<sup>2+</sup> ions to coordinate with the two moxifloxacin molecules from the D and E chains. With the overlapping DNA chains removed, the missing covalent bonds between the catalytic Y129 residues and the scissile bases were added.

The charges around the moxifloxacin binding site were then corrected to give zero order bonds between the ligand and its coordinating  $Mg^{2+}$  ions. The Maestro protein preparation wizard<sup>51</sup> preprocess was then run,<sup>52</sup> followed by the H-bond optimizer, water removal and restrained minimization. Once minimized, the *S. aureus* gyrase co-crystal structure with QPT-1 (PDB ID: 5CDM)<sup>26</sup> was aligned with the prepared *Mtb* gyrase structure and prepared using the Protein preparation wizard. Once minimized, the QPT-1 and the two water molecules mediating a hydrogen bond between the two pyrimidinetrione NH groups and the receptor were transposed into the *Mtb* gyrase structure followed by a 7.5 Å radius minimization around the transposed ligand using Prime.<sup>53</sup> The minimized structure was then inspected and the aromatic portion of the transposed QPT-1 ligand was found to stack with the adenine base of the -1 DNA cleavage site, forming a hydrogen bond between the distal pyrimidinetrione carbonyl and the backbone amide of D461 as seen analogously in the *S. aureus* crystal structure.

The minimized structure was then validated by creating a docking grid around the new ligand binding site using the Glide grid generation tool.<sup>31-32</sup> The grid was centered around the transposed ligand using a hydrogen bond constraint with the backbone amide of D461. Docking QPT-1 into this grid using Glide SP precision reproduced this pose exactly. Tests also suggested rotating the  $\alpha$ - $\beta$  torsion of T500 by 180° would help break the hydrogen bond with its neighboring E501 freeing up these residues for possible polar and H-bond interactions with various substituents on the benzisoxazole. Two docking grids were therefore created to sample both possible T500 orientations. All ligands were then docked into both grids using Glide SP docking enforcing the hydrogen bond constraint. Docked ligand poses were then visually inspected before Prime MM-GBSA calculations with 5 Å radius of minimization with the R482 residue fixed.

## Chemistry.

All reagents and solvents were obtained from commercial sources and used as received. Compound **1** (moxifloxacin) was purchased from Sigma-Aldrich. The following compounds<sup>37</sup> **4**,<sup>38</sup> **5**,<sup>34</sup> **7**,<sup>41</sup> **47**,<sup>37</sup> **49**,<sup>37</sup> **51**,<sup>36</sup> and **55**<sup>41</sup> were prepared according to literature procedures. Reactions were monitored by thin layer chromatography (TLC) using Merck TLC silica gel 60 F254 aluminium-backed precoated plates and were visualized by ultraviolet light at 254 nm. Purification of compounds was carried out by either column chromatography on silica gel 60 (Fluka), particle size 0.063–0.2 mm (70–230 mesh ASTM), as the stationary phase, or by preparative HPLC using a Waters' HPLC fitted with a X-bridge C18 5 $\mu$ m OBD column (4.6 × 150 mm); organic phase: 10 mM ammonium acetate (pH 3.7) in HPLC grade methanol, aqueous phase: 10 mM ammonium acetate (pH 3.7) in HPLC grade water; flow rate = 15.00 mL/min; detector: photodiode array (PDA). Isomers were separated by chiral HPLC using a Waters' HPLC fitted with a Chiralpak IA (5  $\mu$ m, 20mm diameter × 250mm) or Chiralpak IC (5  $\mu$ m, 20mm diameter × 250mm) column with HPLC grade solvents (see individual compounds for specific details); flow rate = 15.00 mL/min; detector: photodiode array (PDA). Optical rotations were measured with an Autopol I-S3 (single wavelength) using a 1.5 mL glass cell with a 10 cm path length. All target compounds and intermediates were characterized by <sup>1</sup>H NMR, <sup>13</sup>C NMR, <sup>19</sup>F NMR and/or MS. NMR spectra were recorded on either a Varian Mercury-300 (<sup>1</sup>H 300.1 MHz, <sup>13</sup>C 75.5

MHz) or Bruker-400 ( $^1\text{H}$  400.2 MHz,  $^{13}\text{C}$  100.6 MHz,  $^{19}\text{F}$  377 MHz) instrument using  $\text{CDCl}_3$ ,  $\text{MeOH}-d_4$  or  $\text{DMSO}-d_6$  as solvents. The  $^1\text{H}$  NMR data are reported as follows: chemical shift in parts per million ( $\delta$ ) downfield of tetramethylsilane (TMS), multiplicity (s = singlet, bs = broad singlet, d = doublet, t = triplet, q = quartet, dd = doublets of doublets, dt = triplets of doublets and m = multiplet), coupling constant (Hz), and integrated value. The  $^{13}\text{C}$  and  $^{19}\text{F}$  NMR spectra were measured with complete proton decoupling. LC-MS analysis was performed using an Agilent® 1260 Infinity Binary Pump, Agilent® 1260 Infinity Diode Array Detector (DAD), Agilent® 1290 Infinity Column Compartment, Agilent® 1260 Infinity Standard Autosampler, and a Agilent® 6120 Quadrupole (Single) MS, with APCI/ESI multimode ionisation source. The purities were determined by Agilent® LCMS/MS (*Method 1*) or Waters' HPLC (*Method 2*) using X-bridge C18  $5\mu\text{m}$  column ( $4.6 \times 150$  mm); organic phase: 10 mM Ammonium acetate (pH 3.7) in HPLC grade methanol, aqueous phase: 10 mM Ammonium acetate (pH 3.7) in HPLC grade water; flow rate = 1.20 mL/min; detector: photodiode array (PDA). The purities of all compounds were found to be >95% or otherwise stated.

**(2R,4S,4aS)-11-fluoro-8-((S)-3-hydroxypyrrolidin-1-yl)-2,4-dimethyl-1,2,4,4a-tetrahydro-2'H,6H-spiro[isoxazolo[4,5-g][1,4]oxazino[4,3-a]quinoline-5,5'-pyrimidine]-2',4',6'(1'H,3'H)-trione (8).**—A mixture of **48a** (293mg, 1.21 mmol) and pyrimidine-2,4,6(1*H*, 3*H*, 5*H*)-trione (170mg, 1.33mmol) in 10mL of EtOH and 1mL of 2M HCl was heated to 80°C for 16H. The solvents were removed, and the reaction mixture was precleaned by flash chromatography on silica gel, using a 4g column (over 16min) and a linear gradient 0–10% (DCM:0.05M  $\text{NH}_3$  in MeOH). The major band was isolated and contained a mixture of isomers. The mixture was separated using chiral chromatography (hexane:EtOH, 50:50, isocratic, 15mL/min, Daicel IA column). Compound **8** was isolated as a white solid (150 mg, 26%).  $^1\text{H}$  NMR (300 MHz, MeOD)  $\delta$  7.06 (s, 1H), 4.60 – 4.39 (m, 1H), 4.12 – 4.02 (m, 1H), 3.98 – 3.88 (m, 1H), 3.86 – 3.73 (m, 1H), 3.72 – 3.47 (m, 4H), 3.43 – 3.33 (m, 1H), 3.22 – 3.18 (m, 1H), 3.08 – 2.88 (m, 2H), 2.14 – 1.87 (m, 2H), 1.11 (d,  $J = 6.2$  Hz, 3H), 0.90 (d,  $J = 6.3$  Hz, 3H).  $^{13}\text{C}$  NMR (101 MHz, MeOD)  $\delta$  172.75, 169.43, 160.00, 154.73 (d,  $J = 12.8$  Hz), 151.13, 136.40 (d,  $J = 239.5$  Hz), 136.18, 122.21, 117.30, 110.15, 74.29, 73.87, 71.77, 66.50, 58.14 (d,  $J = 9.8$  Hz), 57.90, 55.48, 47.84, 41.22, 35.03, 18.97, 18.64. RP-HPLC  $t_{\text{R}} = 2.939$  min (method 1, purity 95%); LC-MS APCI,  $m/z$  472.1  $[\text{M}-\text{H}]^-$  (anal. calcd. for  $\text{C}_{22}\text{H}_{24}\text{FN}_5\text{O}_6$ ,  $m/z = 473.5$ ).  $[\alpha]_{\text{D}}^{20} = -128.2^\circ$  (c 0.26, MeOH).

**(2R,4S,4aS)-11-fluoro-8-((R)-3-hydroxypyrrolidin-1-yl)-2,4-dimethyl-1,2,4,4a-tetrahydro-2'H,6H-spiro[isoxazolo[4,5-g][1,4]oxazino[4,3-a]quinoline-5,5'-pyrimidine]-2',4',6'(1'H,3'H)-trione (9).**—Prepared following the preparation of **8** using **48b** (229 mg, 0.56 mmol) and pyrimidine-2,4,6(1*H*, 3*H*, 5*H*)-trione (79 mg, 0.62 mmol). Chiral column chromatography using hexane:EtOH (65:35, isocratic, 15mL/min, Daicel IA column). White solid (44 mg, 17%).  $^1\text{H}$  NMR (300 MHz, MeOD)  $\delta$  7.18 (s, 1H), 4.62 – 4.49 (m, 1H), 4.28 – 4.14 (m, 1H), 4.09 – 4.01 (m, 1H), 3.97 – 3.59 (m, 5H), 3.59 – 3.41 (m, 1H), 3.35 (d,  $J = 4.6$  Hz, 1H), 3.23 – 3.00 (m, 2H), 2.25 – 1.97 (m, 2H), 1.22 (d,  $J = 6.2$  Hz, 3H), 1.01 (d,  $J = 6.3$  Hz, 3H).  $^{13}\text{C}$  NMR (101 MHz, MeOD)  $\delta$  171.17, 167.85, 158.37, 153.13 (d,  $J = 12.8$  Hz), 149.57, 134.68 (d,  $J = 119.8$  Hz), 134.52, 120.68, 115.66, 108.49, 72.68, 72.24, 70.11, 64.91, 56.51 (d,  $J = 9.7$  Hz), 56.21, 53.89, 46.25, 39.60, 33.40,



17.37, 17.05. RP-HPLC  $t_R$  = 2.929 min (method 1, purity 99%); LC-MS APCI,  $m/z$  472.1 [M-H]<sup>-</sup> (anal. calcd. for C<sub>22</sub>H<sub>24</sub>FN<sub>5</sub>O<sub>6</sub>,  $m/z$  = 473.5).  $[\alpha]_D^{20}$  = -165.2° (c 0.27, MeOH).

**(2R,4S,4aS)-8-((3R,4R)-3,4-dihydroxypyrrolidin-1-yl)-11-fluoro-2,4-dimethyl-1,2,4,4a-tetrahydro-2'H,6H-spiro[isoxazolo[4,5-g][1,4]oxazino[4,3-a]quinoline-5,5'-pyrimidine]-2',4',6'(1'H,3'H)-trione (10).**—Prepared following the preparation of **8** using **48c** (481 mg, 1.14 mmol) and pyrimidine-2,4,6(1*H*, 3*H*, 5*H*)-trione (160 mg, 1.25 mmol). Chiral column chromatography using hexane:EtOH (70:30, isocratic, 15mL/min, Daicel IA column). White solid (119 mg, 21%). <sup>1</sup>H NMR (300 MHz, MeOD) δ 7.09 (d, *J* = 3.3 Hz, 1H), 4.17 – 4.01 (m, 3H), 4.00 – 3.89 (m, 1H), 3.86 – 3.63 (m, 4H), 3.58 – 3.45 (m, 1H), 3.31 – 3.15 (m, 2H), 3.10 – 2.92 (m, 2H), 1.09 (d, 3H), 0.90 (d, *J* = 6.4, 3.3 Hz, 3H). <sup>13</sup>C NMR (101 MHz, MeOD) δ 172.76, 169.44, 160.14, 154.74 (d, *J* = 12.9 Hz), 151.14, 136.41 (d, *J* = 240.0 Hz), 136.23, 122.25, 117.25, 110.09, 76.61 (2C), 74.32, 73.89, 66.47, 58.55, 58.15 (d, *J* = 9.5 Hz), 55.58 (2C), 41.22, 18.98, 18.65. RP-HPLC  $t_R$  = 2.831 min (method 1, purity 98%); LC-MS APCI,  $m/z$  488.1 [M-H]<sup>-</sup> (anal. calcd. for C<sub>22</sub>H<sub>24</sub>FN<sub>5</sub>O<sub>7</sub>,  $m/z$  = 489.5).  $[\alpha]_D^{20}$  = -133.2° (c 0.26, MeOH).

**(2R,4S,4aS)-8-((3S,4S)-3,4-dihydroxypyrrolidin-1-yl)-11-fluoro-2,4-dimethyl-1,2,4,4a-tetrahydro-2'H,6H-spiro[isoxazolo[4,5-g][1,4]oxazino[4,3-a]quinoline-5,5'-pyrimidine]-2',4',6'(1'H,3'H)-trione (11).**—Prepared following the preparation of **8** using **48d** (142 mg, 0.34 mmol) and pyrimidine-2,4,6(1*H*, 3*H*, 5*H*)-trione (47 mg, 0.37 mmol). Chiral column chromatography using hexane:EtOH (65:35, isocratic, 15mL/min, Daicel IA column). Off-white solid (10 mg, 6%). <sup>1</sup>H NMR (300 MHz, MeOD) δ 7.25 (s, 1H), 4.23 (d, *J* = 3.6 Hz, 3H), 4.17 (d, *J* = 2.2 Hz, 1H), 4.06 (d, *J* = 8.8 Hz, 1H), 3.98 – 3.79 (m, 4H), 3.55 (d, *J* = 10.8 Hz, 2H), 3.16 – 3.05 (m, 2H), 1.22 (d, *J* = 6.2 Hz, 3H), 1.01 (d, *J* = 6.3 Hz, 3H). <sup>13</sup>C NMR (151 MHz, MeOD) δ 171.14, 167.81, 158.52, 153.21, 149.54, 135.57, 134.60, 133.98, 120.82, 115.61, 108.44, 74.94, 72.66, 72.24, 64.91, 56.51, 54.47, 53.94, 42.40, 39.57, 17.36, 17.03. RP-HPLC  $t_R$  = 2.856 min (method 1, purity 99%); LC-MS APCI,  $m/z$  488.1 [M-H]<sup>-</sup> (anal. calcd. for C<sub>22</sub>H<sub>24</sub>FN<sub>5</sub>O<sub>7</sub>,  $m/z$  = 489.5).  $[\alpha]_D^{20}$  = -137.8° (c 0.26, MeOH).

**(2R,4S,4aS)-8-((3R,4S)-3,4-dihydroxypyrrolidin-1-yl)-11-fluoro-2,4-dimethyl-1,2,4,4a-tetrahydro-2'H,6H-spiro[isoxazolo[4,5-g][1,4]oxazino[4,3-a]quinoline-5,5'-pyrimidine]-2',4',6'(1'H,3'H)-trione (12).**—Prepared following the preparation of **8** using **48e** (589 mg, 1.39 mmol) and pyrimidine-2,4,6(1*H*, 3*H*, 5*H*)-trione (196 mg, 1.53 mmol). Chiral column chromatography using hexane:EtOH (70:30, isocratic, 15mL/min, Daicel IA column). White solid (42 mg, 6%). <sup>1</sup>H NMR (300 MHz, MeOD) δ 7.19 (s, 1H), 4.37 – 4.27 (m, 2H), 4.24 – 4.13 (m, 1H), 3.85 – 3.70 (m, 3H), 3.59 – 3.47 (m, 2H), 3.41 – 3.35 (m, 1H), 3.20 – 3.04 (m, 2H), 1.86 – 1.72 (m, 2H), 1.22 (d, *J* = 6.2 Hz, 3H), 1.01 (d, *J* = 6.4 Hz, 3H). <sup>13</sup>C NMR (151 MHz, MeOD) δ 171.14, 167.84, 158.33, 153.15 (d, *J* = 12.8 Hz), 149.54, 134.75 (d, *J* = 239.7 Hz), 134.61, 120.78, 115.57, 108.27, 72.67, 72.24, 70.83, 64.89, 56.51 (d, *J* = 9.7 Hz), 53.84, 52.76, 52.50, 39.54, 24.23, 17.36, 17.04. RP-HPLC  $t_R$  = 2.826 min (method 1, purity 99%); LC-MS APCI,  $m/z$  488.1 [M-H]<sup>-</sup> (anal. calcd. for C<sub>22</sub>H<sub>24</sub>FN<sub>5</sub>O<sub>7</sub>,  $m/z$  = 489.5).  $[\alpha]_D^{20}$  = -116.0° (c 0.25, MeOH).

**(2R,4S,4aS)-11-fluoro-8-((S)-3-methoxypyrrolidin-1-yl)-2,4-dimethyl-1,2,4,4a-tetrahydro-2'H,6H-spiro[isoxazolo[4,5-g][1,4]oxazino[4,3-a]quinoline-5,5'-pyrimidine]-2',4',6'(1'H,3'H)-trione (13).**—Prepared following the preparation of **8** using **48f** (255 mg, 0.61 mmol) and pyrimidine-2,4,6(1*H*, 3*H*, 5*H*)-trione (85 mg, 0.67 mmol). Chiral column chromatography using hexane:EtOH:DCM (70:20:10, isocratic, 15mL/min, Daicel IA column). Off-white solid (32 mg, 11%). <sup>1</sup>H NMR (300 MHz, MeOD) δ 7.16 (s, 1H), 4.23 – 4.11 (m, 2H), 4.09 – 3.99 (m, 1H), 3.97 – 3.73 (m, 2H), 3.73 – 3.44 (m, 5H), 3.38 (s, 3H), 3.15 – 3.05 (m, 2H), 2.27 – 2.02 (m, 2H), 1.22 (d, *J* = 6.2 Hz, 3H), 1.01 (d, *J* = 6.4 Hz, 3H). <sup>13</sup>C NMR (101 MHz, MeOD) δ 171.15, 167.79, 158.64, 153.30 (m), 149.46, 134.82 (d, *J* = 218.1 Hz), 134.60, 120.73, 115.57, 108.69, 79.82, 72.69, 72.22, 65.06, 56.58 (m), 55.39, 54.03, 53.38, 46.35, 39.74, 30.28, 17.33, 16.98. RP-HPLC *t*<sub>R</sub> = 3.046 min (method 1, purity 99%); LC-MS APCI, *m/z* 486.1 [M-H]<sup>-</sup> (anal. calcd. for C<sub>23</sub>H<sub>26</sub>FN<sub>5</sub>O<sub>6</sub>, *m/z* = 487.5). [α]<sub>D</sub><sup>20</sup> = -149.4° (c 0.24, MeOH).

**(2R,4S,4aS)-11-fluoro-8-((S)-3-(hydroxymethyl)pyrrolidin-1-yl)-2,4-dimethyl-1,2,4,4a-tetrahydro-2'H,6H-spiro[isoxazolo[4,5-g][1,4]oxazino[4,3-a]quinoline-5,5'-pyrimidine]-2',4',6'(1'H,3'H)-trione (14).**—Prepared following the preparation of **8** using **48g** (279 mg, 0.66 mmol) and pyrimidine-2,4,6(1*H*, 3*H*, 5*H*)-trione (93 mg, 0.73 mmol). Chiral column chromatography using hexane:EtOH:DCM (80:15:5, isocratic, 15mL/min, Daicel IA column). Off-white solid (73 mg, 23%). <sup>1</sup>H NMR (300 MHz, MeOD) δ 7.17 (s, 1H), 4.24 – 4.10 (m, 1H), 4.12 – 3.99 (m, 1H), 3.98 – 3.74 (m, 2H), 3.74 – 3.46 (m, 6H), 3.40 – 3.35 (m, 1H), 3.19 – 3.01 (m, 2H), 2.66 – 2.45 (m, 1H), 2.25 – 2.00 (m, 1H), 1.94 – 1.76 (m, 1H), 1.22 (d, *J* = 6.2 Hz, 3H), 1.01 (d, *J* = 6.3 Hz, 3H). <sup>13</sup>C NMR (151 MHz, MeOD) δ 171.12, 167.83, 158.29, 153.09 (d, *J* = 12.7 Hz), 149.53, 134.74 (d, *J* = 239.5 Hz), 134.51, 120.61, 115.76, 108.51, 72.66, 72.24, 64.87, 63.22, 56.49 (d, *J* = 9.8 Hz), 53.88, 50.90, 48.15, 41.04, 39.58, 27.44, 17.37, 17.05. RP-HPLC *t*<sub>R</sub> = 3.027 min (method 1, purity 99%); LC-MS APCI, *m/z* 486.1 [M-H]<sup>-</sup> (anal. calcd. for C<sub>23</sub>H<sub>26</sub>FN<sub>5</sub>O<sub>6</sub>, *m/z* = 487.5). [α]<sub>D</sub><sup>20</sup> = -137.3° (c 0.25, MeOH).

**11-fluoro-8-(3-hydroxy-3-methylpyrrolidin-1-yl)-2,4-dimethyl-1,2,4,4a-tetrahydro-2'H,6H-spiro[isoxazolo[4,5-g][1,4]oxazino[4,3-a]quinoline-5,5'-pyrimidine]-2',4',6'(1'H,3'H)-trione (15).**—Prepared following the preparation of **8** using **48h** (22 mg, 0.050 mmol) and pyrimidine-2,4,6(1*H*, 3*H*, 5*H*)-trione (7 mg, 0.060 mmol) (*Note: compound isolated as a mixture of isomers*). Pale yellow solid (9 mg, 36%). <sup>1</sup>H NMR (300 MHz, DMSO-*d*<sub>6</sub>) δ 11.46 (br s, 2H), 7.36 (s, 1H), 4.07 (d, *J* = 13.6 Hz, 1H), 3.93 (d, *J* = 8.7 Hz, 1H), 3.88 – 3.38 (m, 5H), 3.16 – 3.00 (m, 1H), 2.95 (d, *J* = 14.2 Hz, 1H), 2.47 – 2.19 (m, 4H), 1.14 (d, *J* = 6.1 Hz, 3H), 0.89 (d, *J* = 6.3 Hz, 3H). RP-LC *t*<sub>R</sub> = 1.060 min (method 2, purity 100%); LC-MS ESI, *m/z* 486.2 [M-H]<sup>-</sup> (anal. calcd. for C<sub>23</sub>H<sub>26</sub>FN<sub>5</sub>O<sub>6</sub>, *m/z* = 487.5).

**(2R,4S,4aS)-8-((S)-3-aminopyrrolidin-1-yl)-11-fluoro-2,4-dimethyl-1,2,4,4a-tetrahydro-2'H,6H-spiro[isoxazolo[4,5-g][1,4]oxazino[4,3-a]quinoline-5,5'-pyrimidine]-2',4',6'(1'H,3'H)-trione (16).**—Prepared following the preparation of **8** using **48i** (192 mg, 0.38 mmol) and pyrimidine-2,4,6(1*H*, 3*H*, 5*H*)-trione (53 mg, 0.42 mmol). Chiral column chromatography

using hexane:0.1% Et<sub>2</sub>NH in EtOH (65:35, isocratic, 15mL/min, Daicel IA column). Beige solid (10 mg, 6%). <sup>1</sup>H NMR (300 MHz, MeOD) δ 7.20 (s, 1H), 4.23 – 4.14 (m, 1H), 4.08 – 4.02 (m, 1H), 3.96 – 3.86 (m, 1H), 3.85 – 3.70 (m, 3H), 3.69 – 3.56 (m, 1H), 3.42 – 3.34 (m, 1H), 3.17 – 3.01 (m, 3H), 2.39 – 2.19 (m, 1H), 2.02 – 1.92 (m, 2H), 1.22 (d, *J* = 6.2 Hz, 3H), 1.01 (d, *J* = 6.3 Hz, 3H). <sup>13</sup>C NMR (101 MHz, MeOD) δ 171.65, 168.27, 158.34, 153.21 (d, *J* = 13.0 Hz), 150.17, 134.77 (d, *J* = 239.6 Hz), 134.64, 120.87, 115.61, 108.42, 72.72, 72.24, 64.95, 56.57, 55.12, 53.80, 50.66, 46.55, 42.14, 39.65, 17.35, 17.04. RP-UPLC *t*<sub>R</sub> = 0.677 min (method 2, purity 99%); LC-MS ESI, *m/z* 471.2 [M-H]<sup>-</sup> (anal. calcd. for C<sub>22</sub>H<sub>25</sub>FN<sub>6</sub>O<sub>5</sub>, *m/z* = 472.5). [α]<sub>D</sub><sup>20</sup> = -94.° (c 0.22, MeOH).

**(2R,4S,4aS)-11-fluoro-2,4-dimethyl-8-((S)-3-(methylamino)pyrrolidin-1-yl)-1,2,4,4a-tetrahydro-2'H-spiro[isoxazolo[5',4':4,5]benzo[1,2-b][1,4]oxazino[4,3-d][1,4]oxazine-5,5'-pyrimidine]-2',4',6'(1'H,3'H)-trione (17).**

—Prepared following the preparation of **8**

using **48j** (365 mg, 0.70 mmol) and pyrimidine-2,4,6(1H, 3H, 5H)-trione (99 mg, 0.77 mmol). Chiral column chromatography using hexane:0.1% Et<sub>2</sub>NH in EtOH (50:50, isocratic, 15mL/min, Daicel IA column). Off-white solid (41 mg, 11%). <sup>1</sup>H NMR (300 MHz, MeOD) δ 7.23 (s, 1H), 4.22 – 4.12 (m, 1H), 4.08 – 4.01 (m, 1H), 3.95 – 3.83 (m, 1H), 3.82 – 3.68 (m, 2H), 3.68 – 3.54 (m, 1H), 3.51 – 3.38 (m, 2H), 3.18 – 2.96 (m, 3H), 2.48 (s, 3H), 2.36 – 2.20 (m, 1H), 2.05 – 1.92 (m, 2H), 1.22 (d, *J* = 6.2 Hz, 3H), 1.01 (d, *J* = 6.3 Hz, 3H). <sup>13</sup>C NMR (151 MHz, MeOD) δ 171.43, 168.06, 158.33, 153.20 (d, *J* = 12.7 Hz), 149.91, 134.76 (d, *J* = 239.3 Hz), 134.63, 120.86, 115.63, 108.39, 72.69, 72.24, 64.91, 58.95, 56.49 (d, *J* = 9.5 Hz), 53.81, 52.82, 46.65, 39.59, 32.86, 30.11, 17.35, 17.03. RP-HPLC *t*<sub>R</sub> = 2.569 min (method 1, purity 95%); LC-MS APCI, *m/z* 485.1 [M-H]<sup>-</sup> (anal. calcd. for C<sub>23</sub>H<sub>27</sub>FN<sub>6</sub>O<sub>5</sub>, *m/z* = 486.5). [α]<sub>D</sub><sup>20</sup> = -88.6° (c 0.28, MeOH).

**(2R,4S,4aS)-11-fluoro-8-((S)-3-fluoropyrrolidin-1-yl)-2,4-dimethyl-1,2,4,4a-tetrahydro-2'H,6H-spiro[isoxazolo[4,5-g][1,4]oxazino[4,3-a]quinoline-5,5'-pyrimidine]-2',4',6'(1'H,3'H)-trione (18).**

—Prepared following the preparation of **8** using **49k** (247 mg, 0.60 mmol) and pyrimidine-2,4,6(1H, 3H, 5H)-trione (85 mg, 0.66 mmol). Chiral column chromatography using hexane:EtOH:EtOAc (70:5:25, isocratic, 15mL/min, Daicel IA column). Off-white solid (52 mg, 18%).

<sup>1</sup>H NMR (300 MHz, MeOD) δ 7.17 (s, 1H), 5.53 – 5.26 (m, 1H), 4.25 – 4.13 (m, 1H), 4.10 – 3.99 (m, 1H), 3.94 – 3.86 (m, 1H), 3.84 – 3.61 (m, 4H), 3.39 – 3.26 (m, 2H), 3.22 – 2.98 (m, 2H), 2.45 – 2.07 (m, 2H), 1.22 (d, *J* = 6.2 Hz, 3H), 1.01 (d, *J* = 6.3 Hz, 3H). <sup>13</sup>C NMR (151 MHz, MeOD) δ 171.10, 167.86, 158.17, 153.19 (d, *J* = 12.9 Hz), 149.52, 134.74 (d, *J* = 239.9 Hz), 134.65, 120.80, 115.49 (d, *J* = 3.4 Hz), 108.27, 93.27, 92.11, 72.67, 72.25, 64.85, 56.52 (d, *J* = 9.6 Hz), 54.77 (d, *J* = 23.0 Hz), 46.04, 39.61, 31.75 (d, *J* = 21.7 Hz), 17.37, 17.04. RP-UPLC *t*<sub>R</sub> = 0.959 min (method 2, purity 99%); LC-MS ESI, *m/z* 474.1 [M-H]<sup>-</sup> (anal. calcd. for C<sub>22</sub>H<sub>23</sub>F<sub>2</sub>N<sub>5</sub>O<sub>5</sub>, *m/z* = 475.5). [α]<sub>D</sub><sup>20</sup> = -144.6° (c 0.27, MeOH).

**(S)-1-((2R,4S,4aS)-11-fluoro-2,4-dimethyl-2',4',6'-trioxo-1,1',2,3',4,4a,4',6'-octahydro-2'H,6H-spiro[isoxazolo[4,5-g][1,4]oxazino[4,3-a]quinoline-5,5'-pyrimidin]-8-yl)pyrrolidine-3-carbonitrile (19).**

—Prepared following the preparation of **8** using **48l** (109 mg, 0.26 mmol) and

pyrimidine-2,4,6(1*H*, 3*H*, 5*H*)-trione (37 mg, 0.29 mmol). Chiral column chromatography using hexane:0.1% Et<sub>2</sub>NH in EtOH (55:45, isocratic, 15mL/min, Daicel IA column). Off-white solid (6 mg, 5%). <sup>1</sup>H NMR (300 MHz, MeOD) δ 7.23 (s, 1H), 4.23 – 4.15 (m, 1H), 4.08 – 4.03 (m, 1H), 3.97 – 3.84 (m, 2H), 3.84 – 3.75 (m, 2H), 3.75 – 3.63 (m, 1H), 3.56 – 3.44 (m, 1H), 3.17 – 3.06 (m, 2H), 3.04 – 2.93 (m, 2H), 2.53 – 2.29 (m, 2H), 1.22 (d, *J* = 6.2 Hz, 3H), 1.01 (d, *J* = 6.3 Hz, 3H). <sup>13</sup>C NMR (151 MHz, MeOD) δ 171.73, 168.35, 158.02, 153.34 (d, *J* = 12.5 Hz), 150.30, 134.78, 134.71 (d, *J* = 240.2 Hz), 121.28, 120.24, 115.32, 108.01, 72.71, 72.23, 64.96, 56.49 (d, *J* = 9.4 Hz), 51.23, 42.20, 39.58, 29.38, 27.87, 17.34, 17.03, 10.53. RP-HPLC *t*<sub>R</sub> = 2.764 min (method 1, purity 96%); LC-MS APCI, *m/z* 481.2 [M-H]<sup>-</sup> (anal. calcd. for C<sub>23</sub>H<sub>23</sub>FN<sub>6</sub>O<sub>5</sub>, *m/z* = 482.5). [α]<sub>D</sub><sup>20</sup> = -89.6° (c 0.12, MeOH).

**(S)-1-((2R,4S,4aS)-11-fluoro-2,4-dimethyl-2',4',6'-trioxo-1,1',2,3',4,4a,4',6'-octahydro-2'H,6H-spiro[isoxazolo[4,5-g][1,4]oxazino[4,3-a]quinoline-5,5'-pyrimidin]-8-yl)pyrrolidine-3-carboxylic acid (20).**—To a solution

of ethyl (*S*)-1-((2*R*,4*S*,4*aS*)-11-fluoro-2,4-dimethyl-2',4',6'-trioxo-1,1',2,3',4,4*a*,4',6'-octahydro-2'*H*,6*H*-spiro[isoxazolo[4,5-*g*][1,4]oxazino[4,3-*a*]quinoline-5,5'-pyrimidin]-8-yl)pyrrolidine-3-carboxylate (**S1**) (20 mg, 0.038mmol) in 1mL (1,4-dioxane:H<sub>2</sub>O, 3:1), lithium hydroxide monohydrate (4.8mg, 0.110mmol) was added. The reaction mixture was heated at 30°C for 1 h. The mixture was cooled and neutralized with 2M HCl to pH 6. Organic solvent was removed under reduced pressure and the remaining water removed on the freeze dryer overnight. To remove any salts present, the remaining residue was taken up in a minimum amount of MeOH and passed through a 2g Salicycle (SPE-R5123003–064) propylsulfonic acid cartridge. The cartridge was pre-washed with MeOH. Pressure was used to move the solvent through the cartridge. The solvent was removed, and material dried to afford **20** as a white solid (8 mg, 36%). <sup>1</sup>H NMR (300 MHz, MeOD) δ 7.19 (s, 1H), 4.19 (d, *J* = 12.6 Hz, 2H), 4.04 (d, *J* = 8.8 Hz, 1H), 3.97 – 3.85 (m, 1H), 3.83 – 3.65 (m, 6H), 3.19 – 3.03 (m, 2H), 2.40 – 2.23 (m, 2H), 1.21 (d, *J* = 6.1 Hz, 3H), 1.00 (d, *J* = 6.2 Hz, 3H). <sup>13</sup>C NMR (151 MHz, MeOD) δ 175.24, 171.11, 167.83, 158.15, 153.17 (d, *J* = 13.1 Hz), 149.51, 134.68 (d, *J* = 240.0 Hz), 134.60, 120.82, 115.62, 108.36, 72.66, 72.23, 64.88, 56.49 (d, *J* = 9.6 Hz), 53.86, 50.39, 50.28, 42.72, 39.53, 28.35, 17.35, 17.03. RP-UPLC *t*<sub>R</sub> = 0.896 min (method 2, purity 99%); LC-MS ESI, *m/z* 500.1 [M-H]<sup>-</sup> (anal. calcd. for C<sub>23</sub>H<sub>24</sub>FN<sub>5</sub>O<sub>7</sub>, *m/z* = 501.5). [α]<sub>D</sub><sup>20</sup> = -120.3° (c 0.08, MeOH).

**(2R,4S,4aS)-11-fluoro-8-((S)-3-hydroxypiperidin-1-yl)-2,4-dimethyl-1,2,4,4a-tetrahydro-2'H,6H-spiro[isoxazolo[4,5-g][1,4]oxazino[4,3-a]quinoline-5,5'-pyrimidine]-2',4',6'(1'H,3'H)-trione (21).**—Prepared following the preparation

of **8** using **48n** (109 mg, 0.26 mmol) and pyrimidine-2,4,6(1*H*, 3*H*, 5*H*)-trione (36 mg, 0.28 mmol). Chiral column chromatography using hexane:EtOH (65:35, isocratic, 15mL/min, Daicel IA column). Off-white solid (64 mg, 51%). <sup>1</sup>H NMR (300 MHz, MeOD) δ 7.16 (s, 1H), 4.24 – 4.12 (m, 1H), 4.09 – 4.00 (m, 1H), 3.98 – 3.74 (m, 4H), 3.70 – 3.57 (m, 2H), 3.18 – 3.05 (m, 3H), 3.06 – 2.94 (m, 1H), 2.07 – 1.97 (m, 1H), 1.97 – 1.85 (m, 1H), 1.75 – 1.47 (m, 2H), 1.22 (d, *J* = 6.2 Hz, 3H), 1.01 (d, *J* = 6.3 Hz, 3H). <sup>13</sup>C NMR (101 MHz, MeOD) δ 171.91, 168.62, 161.81, 154.41 (d, *J* = 13.3 Hz), 150.31, 135.09, 135.56 (d, *J* = 239.9 Hz), 121.80, 116.29, 116.26, 109.17, 73.46, 73.03, 66.17, 65.68, 57.30 (d, *J* = 9.8 Hz), 55.44, 54.68, 40.43, 32.96, 22.93,

18.17, 17.85. RP-HPLC  $t_R$  = 3.018 min (method 1, purity 99%); LC-MS APCI,  $m/z$  486.1 [M-H]<sup>-</sup> (anal. calcd. for C<sub>23</sub>H<sub>26</sub>FN<sub>5</sub>O<sub>6</sub>,  $m/z$  = 487.5).  $[\alpha]_D^{20}$  = -124.3° (c 0.27, MeOH).

**(2R,4S,4aS)-11-fluoro-8-((R)-3-hydroxypiperidin-1-yl)-2,4-dimethyl-1,2,4,4a-tetrahydro-2'H,6H-spiro[isoxazolo[4,5-g][1,4]oxazino[4,3-a]quinoline-5,5'-pyrimidine]-2',4',6'(1'H,3'H)-trione (22).**—Prepared following the preparation

of **8** using **48o** (251 mg, 0.60 mmol) and barbituric acid (84 mg, 0.66 mmol). Chiral column chromatography using hexane:EtOH (65:35, isocratic, 15mL/min, Daicel IA column). Off-white solid (86 mg, 30%). <sup>1</sup>H NMR (300 MHz, MeOD) δ 7.20 (s, 1H), 4.19 (dd,  $J$  = 14.2, 2.2 Hz, 1H), 4.05 (d,  $J$  = 8.8 Hz, 1H), 3.99 – 3.74 (m, 5H), 3.73 – 3.59 (m, 1H), 3.40 – 3.28 (m, 1H), 3.20 – 2.93 (m, 4H), 2.10 – 1.86 (m, 1H), 1.84 – 1.62 (m, 1H), 1.62 – 1.45 (m, 1H), 1.22 (d,  $J$  = 6.2 Hz, 3H), 1.01 (d,  $J$  = 6.4 Hz, 3H). <sup>13</sup>C NMR (101 MHz, MeOD) δ 171.91, 168.62, 161.88, 154.45 (d,  $J$  = 12.9 Hz), 150.31, 135.58 (d,  $J$  = 240.3 Hz), 135.14, 121.88, 116.28, 109.19, 73.46, 73.03, 66.22, 65.69, 57.29 (d,  $J$  = 9.5 Hz), 55.48, 54.72, 48.70, 40.45, 32.96, 22.96, 18.16, 17.83. RP-HPLC  $t_R$  = 3.002 min (method 1, purity 99%); LC-MS APCI,  $m/z$  486.1 [M-H]<sup>-</sup> (anal. calcd. for C<sub>23</sub>H<sub>26</sub>FN<sub>5</sub>O<sub>6</sub>,  $m/z$  = 487.5).  $[\alpha]_D^{20}$  = -163.2° (c 0.29, MeOH).

**(2R,4S,4aS)-11-fluoro-2,4-dimethyl-8-(((S)-5-oxopyrrolidin-2-yl)methoxy)-1,2,4,4a-tetrahydro-2'H,6H-spiro[isoxazolo[4,5-g][1,4]oxazino[4,3-a]quinoline-5,5'-pyrimidine]-2',4',6'(1'H,3'H)-trione (23).**—Prepared

following the preparation of **8** using **48p** (265 mg, 0.61 mmol) and pyrimidine-2,4,6(1*H*, 3*H*, 5*H*)-trione (86 mg, 0.67 mmol). Chiral column chromatography using hexane:EtOH (50:50, isocratic, 15mL/min, Daicel IA column). Off-white solid (42 mg, 14%). <sup>1</sup>H NMR (300 MHz, DMSO-*d*<sub>6</sub>) δ 7.87 (s, 1H), 7.09 (s, 1H), 4.35 – 4.19 (m, 2H), 4.11 – 4.02 (m, 1H), 4.02 – 3.91 (m, 2H), 3.84 – 3.63 (m, 2H), 3.57 – 3.46 (m, 1H), 3.15 – 3.03 (m, 1H), 2.94 – 2.83 (m, 1H), 2.82 – 2.68 (m, 1H), 2.25 – 2.13 (m, 2H), 1.95 – 1.88 (m, 1H), 1.14 (d,  $J$  = 6.2 Hz, 3H), 0.88 (d,  $J$  = 6.3 Hz, 3H). <sup>13</sup>C NMR (101 MHz, MeOD) δ 179.75, 172.65, 169.14, 166.07, 153.65 (d,  $J_{CF}$  = 31.2 Hz), 135.43 (d,  $J_{CF}$  = 25.1 Hz), 133.29, 122.81, 113.34, 105.81, 72.76, 72.48, 72.21, 65.18, 56.52 (d,  $J_{CF}$  = 9.7 Hz), 53.65, 53.43, 42.24, 39.53, 29.51, 22.58, 17.31, 17.04. RP-UPLC  $t_R$  = 0.901 min (method 2, purity 100%); LC-MS ESI,  $m/z$  500.1 [M-H]<sup>-</sup> (anal. calcd. for C<sub>23</sub>H<sub>24</sub>FN<sub>5</sub>O<sub>7</sub>,  $m/z$  = 501.5).  $[\alpha]_D^{20}$  = -135.8° (c 0.27, MeOH).

**(2R,4S,4aS)-11-fluoro-2,4-dimethyl-8-(((R)-5-oxopyrrolidin-2-yl)methoxy)-1,2,4,4a-tetrahydro-2'H,6H-spiro[isoxazolo[4,5-g][1,4]oxazino[4,3-a]quinoline-5,5'-pyrimidine]-2',4',6'(1'H,3'H)-trione (24).**—Prepared

following the preparation of **8** using **48q** (346 mg, 0.79 mmol) and pyrimidine-2,4,6(1*H*, 3*H*, 5*H*)-trione (112 mg, 0.87 mmol). Chiral column chromatography using hexane:EtOH:DCM (60:20:20, isocratic, 15mL/min, Daicel IA column). Beige solid (42 mg, 14%). <sup>1</sup>H NMR (300 MHz, DMSO-*d*<sub>6</sub>) δ 11.56 (s, 2H), 7.89 (s, 1H), 7.12 (s, 1H), 4.40 – 4.18 (m, 2H), 4.13 – 4.03 (m, 1H), 3.97 (dd,  $J$  = 13.1, 6.5 Hz, 2H), 3.85 – 3.74 (m, 1H), 3.74 – 3.62 (m, 1H), 3.62 – 3.50 (m, 1H), 3.18 – 3.03 (m, 1H), 2.97 – 2.86 (m, 1H), 2.35 – 2.06 (m, 3H), 1.99 – 1.82 (m, 1H), 1.14 (d,  $J$  = 6.2 Hz, 3H), 0.89 (d,  $J$  = 6.3 Hz, 3H). <sup>13</sup>C NMR (151 MHz, DMSO-*d*<sub>6</sub>) δ 177.35, 171.37, 168.10, 166.29, 153.17 (d,  $J$  = 12.4 Hz), 149.95, 135.69, 134.24 (d,  $J$  = 240.7 Hz), 123.16, 114.50,

105.76, 73.26, 72.52, 72.15, 64.88, 56.82 (d,  $J = 7.4$  Hz), 53.57, 52.55, 39.07, 30.05, 23.14, 18.67, 18.59. RP-UPLC  $t_R = 0.910$  min (method 2, purity 100%); LC-MS ESI,  $m/z$  500.1 [M-H]<sup>-</sup> (anal. calcd. for C<sub>23</sub>H<sub>24</sub>FN<sub>5</sub>O<sub>7</sub>,  $m/z = 501.5$ ).  $[\alpha]_D^{20} = -185.1^\circ$  (c 0.35, MeOH).

**(2R,4S,4aS)-11-fluoro-2,4-dimethyl-8-(((S)-1-methyl-5-oxopyrrolidin-2-yl)methoxy)-1,2,4,4a-tetrahydro-2'H,6H-spiro[isoxazolo[4,5-g][1,4]oxazino[4,3-a]quinoline-5,5'-pyrimidine]-2',4',6'(1'H,3'H)-trione (25).**—Prepared following the preparation of **8** using **48r** (208 mg, 0.46 mmol) and pyrimidine-2,4,6(1*H*, 3*H*, 5*H*)-trione (65 mg, 0.51 mmol).

Chiral column chromatography using hexane:EtOH:2-propanol (65:35:5, isocratic, 15mL/min, Daicel IA column). Beige solid (66 mg, 28%). <sup>1</sup>H NMR (300 MHz, DMSO-*d*<sub>6</sub>)  $\delta$  7.10 (s, 1H), 4.62 – 4.33 (m, 2H), 4.13 – 4.02 (m, 1H), 4.00 – 3.89 (m, 2H), 3.83 – 3.72 (m, 1H), 3.72 – 3.63 (m, 1H), 3.63 3.51 (m, 1H), 3.15 – 3.03 (m, 1H), 2.94 – 2.83 (m, 1H), 2.78 (s, 3H), 2.47 – 2.32 (m, 1H), 2.28 2.11 (m, 2H), 2.01 – 1.84 (m, 1H), 1.16 – 1.12 (m, 3H), 0.88 (d,  $J = 6.3$  Hz, 3H). <sup>13</sup>C NMR (151 MHz, DMSO)  $\delta$  175.24, 171.86, 168.49, 166.19, 153.13 (d,  $J_{CF} = 12.8$  Hz), 150.49, 135.76, 134.17 (d,  $J_{CF} = 240.1$  Hz), 123.44, 114.18, 105.51, 72.58, 72.23, 70.74, 64.89, 58.49, 56.73 (d,  $J_{CF} = 9.3$  Hz), 53.42, 38.95, 30.12, 28.13, 21.07, 18.53, 18.48. RP-UPLC  $t_R = 0.941$  min (method 2, purity 100%); LC-MS ESI,  $m/z$  514.2 [M-H]<sup>-</sup> (anal. calcd. for C<sub>24</sub>H<sub>26</sub>FN<sub>5</sub>O<sub>7</sub>,  $m/z = 515.5$ ).  $[\alpha]_D^{20} = -149.0^\circ$  (c 0.24, MeOH).

**(2R,4S,4aS)-11-fluoro-2,4-dimethyl-8-(((S)-5-oxotetrahydrofuran-2-yl)methoxy)-1,2,4,4a-tetrahydro-2'H,6H-spiro[isoxazolo[4,5-g][1,4]oxazino[4,3-a]quinoline-5,5'-pyrimidine]-2',4',6'(1'H,3'H)-trione (26).**—Prepared following the preparation of **8** using **48s** (247 mg,

0.57 mmol) and pyrimidine-2,4,6(1*H*, 3*H*, 5*H*)-trione (80 mg, 0.62 mmol). Chiral column chromatography using hexane:EtOH:MTBE:DCM (45:5:30:20, isocratic, 15mL/min, Daicel IC column). Off-white solid (28 mg, 10%). <sup>1</sup>H NMR (300 MHz, DMSO-*d*<sub>6</sub>)  $\delta$  11.82 (br s, 1H), 11.46 (br s, 1H), 7.15 (s, 1H), 4.99 – 4.93 (m, 1H), 4.61 – 4.52 (m, 1H), 4.53 – 4.44 (m, 1H), 4.12 – 4.03 (m, 1H), 3.98 – 3.91 (m, 1H), 3.83 – 3.74 (m, 1H), 3.72 – 3.64 (m, 1H), 3.62 – 3.56 (m, 1H), 3.17 – 3.03 (m, 1H), 2.97 – 2.86 (m, 1H), 2.62 – 2.54 (m, 2H), 2.42 – 2.26 (m, 1H), 2.16 – 2.05 (m, 1H), 1.14 (d,  $J = 6.1$  Hz, 3H), 0.89 (d,  $J = 6.3$  Hz, 3H). <sup>13</sup>C NMR (101 MHz, DMSO-*d*<sub>6</sub>)  $\delta$  177.38, 171.32, 168.09, 166.05, 153.28 (d,  $J = 12.9$  Hz), 149.89, 135.81, 131.58 (d,  $J = 303.7$  Hz), 123.41, 114.35, 105.57, 77.60, 72.51, 72.16, 72.01, 64.90, 56.82 (d,  $J = 9.0$  Hz), 53.67, 39.03, 28.32, 23.45, 18.67, 18.59. RP-UPLC  $t_R = 0.954$  min (method 2, purity 98%); LC-MS ESI,  $m/z$  501.1 [M-H]<sup>-</sup> (anal. calcd. for C<sub>23</sub>H<sub>23</sub>FN<sub>4</sub>O<sub>8</sub>,  $m/z = 502.5$ ).  $[\alpha]_D^{20} = -118.2^\circ$  (c 0.26, MeOH).

**(2R,4S,4aS)-11-fluoro-2,4-dimethyl-8-(((R)-5-oxotetrahydrofuran-2-yl)methoxy)-1,2,4,4a-tetrahydro-2'H,6H-spiro[isoxazolo[4,5-g][1,4]oxazino[4,3-a]quinoline-5,5'-pyrimidine]-2',4',6'(1'H,3'H)-trione (27).**—Prepared following the preparation of **8** using **48t** (191 mg, 0.44 mmol) and pyrimidine-2,4,6(1*H*, 3*H*, 5*H*)-trione (62 mg, 0.48 mmol). Chiral column chromatography using hexane:EtOH:MTBE:DCM (45:5:30:20, isocratic, 15mL/min, Daicel IC column). Off-white solid (24 mg, 10%). <sup>1</sup>H NMR (300 MHz, DMSO-*d*<sub>6</sub>)  $\delta$  7.15 (s, 1H), 5.01 – 4.89 (m, 1H), 4.60 – 4.51 (m, 1H), 4.51 – 4.41 (m, 1H), 4.13 – 4.02 (m, 1H), 3.98 – 3.90 (m, 1H), 3.85 – 3.73

(m, 1H), 3.71 – 3.63 (m, 1H), 3.61 – 3.53 (m, 1H), 3.16 – 3.04 (m, 1H), 2.92 (d,  $J = 14.3$  Hz, 1H), 2.62 – 2.53 (m, 2H), 2.42 – 2.25 (m, 1H), 2.17 – 2.04 (m, 1H), 1.14 (d,  $J = 6.1$  Hz, 3H), 0.89 (d,  $J = 6.4$  Hz, 3H).  $^{13}\text{C}$  NMR (101 MHz, DMSO- $d_6$ )  $\delta$  177.37, 171.32, 168.07, 166.07, 153.27 (d,  $J = 13.1$  Hz), 149.88, 135.79, 134.28 (d,  $J = 240.4$  Hz), 123.37, 114.35, 105.57, 77.64, 72.52, 72.16, 72.06, 64.88, 56.83 (d,  $J = 9.3$  Hz), 53.63, 39.05, 28.31, 23.44, 18.67, 18.59. RP-UPLC  $t_{\text{R}} = 0.954$  min (method 2, purity 95%); LC-MS ESI,  $m/z$  501.1  $[\text{M-H}]^-$  (anal. calcd. for  $\text{C}_{23}\text{H}_{23}\text{FN}_4\text{O}_8$ ,  $m/z = 502.5$ ).  $[\alpha]_{\text{D}}^{20} = -152.8^\circ$  (c 0.23, MeOH).

**(2R,4S,4aS)-11-fluoro-2,4-dimethyl-8-(((R)-2-oxooxazolidin-4-yl)methoxy)-1,2,4,4a-tetrahydro-2'H,6H-spiro[isoxazolo[4,5-g][1,4]oxazino[4,3-a]quinoline-5,5'-pyrimidine]-2',4',6'(1'H,3'H)-trione (28).**—Prepared

following the preparation of **8** using **48u** (276 mg, 0.63 mmol) and pyrimidine-2,4,6(1*H*, 3*H*, 5*H*)-trione (89 mg, 0.69 mmol). Chiral column chromatography using hexane:EtOAc (55:45, isocratic, 15mL/min, Daicel IA column). Off-white solid (34 mg, 11%).  $^1\text{H}$  NMR (300 MHz, DMSO- $d_6$ )  $\delta$  7.93 (s, 1H), 7.07 (s, 1H), 4.51 – 4.41 (m, 1H), 4.35 (dd,  $J = 6.2, 3.9$  Hz, 2H), 4.29 – 4.19 (m, 2H), 4.12 – 4.03 (m, 1H), 3.98 – 3.90 (m, 1H), 3.85 – 3.72 (m, 1H), 3.71 – 3.60 (m, 2H), 3.17 – 3.05 (m, 1H), 2.95 – 2.84 (m, 1H), 1.14 (d,  $J = 6.1$  Hz, 3H), 0.89 (d,  $J = 6.3$  Hz, 3H).  $^{19}\text{F}$  NMR (377 MHz, DMSO)  $\delta$  –157.61 (s, 1H). RP-UPLC  $t_{\text{R}} = 0.888$  min (method 2, purity 100%); LC-MS ESI,  $m/z$  502.1  $[\text{M-H}]^-$  (anal. calcd. for  $\text{C}_{22}\text{H}_{22}\text{FN}_5\text{O}_8$ ,  $m/z = 503.4$ ).  $[\alpha]_{\text{D}}^{20} = -118.5^\circ$  (c 0.24, MeOH).

**(2R,4S,4aS)-11-fluoro-2,4-dimethyl-8-(((S)-2-oxooxazolidin-4-yl)methoxy)-1,2,4,4a-tetrahydro-2'H,6H-spiro[isoxazolo[4,5-g][1,4]oxazino[4,3-a]quinoline-5,5'-pyrimidine]-2',4',6'(1'H,3'H)-trione (29).**—Prepared

following the preparation of **8** using **48v** (281 mg, 0.64 mmol) and pyrimidine-2,4,6(1*H*, 3*H*, 5*H*)-trione (91 mg, 0.71 mmol). Chiral column chromatography using hexane:EtOAc (55:45, isocratic, 15mL/min, Daicel IA column). Off-white solid (32 mg, 10%).  $^1\text{H}$  NMR (300 MHz, DMSO- $d_6$ )  $\delta$  7.93 (s, 1H), 7.07 (s, 1H), 4.50 – 4.42 (m, 1H), 4.41 – 4.29 (m, 2H), 4.29 – 4.18 (m, 2H), 4.12 – 4.02 (m, 1H), 3.98 – 3.90 (m, 1H), 3.85 – 3.72 (m, 1H), 3.71 – 3.59 (m, 2H), 3.17 – 3.04 (m, 1H), 2.95 – 2.85 (m, 1H), 1.14 (d,  $J = 6.1$  Hz, 3H), 0.89 (d,  $J = 6.2$  Hz, 3H). RP-UPLC  $t_{\text{R}} = 0.887$  min (method 2, purity 100%); LC-MS ESI,  $m/z$  502.1  $[\text{M-H}]^-$  (anal. calcd. for  $\text{C}_{22}\text{H}_{22}\text{FN}_5\text{O}_8$ ,  $m/z = 503.4$ ).  $[\alpha]_{\text{D}}^{20} = -113.3^\circ$  (c 0.23, MeOH).

**(2R,4S,4aS)-11-fluoro-2,4-dimethyl-8-(((S)-5-oxopyrrolidin-3-yl)methoxy)-1,2,4,4a-tetrahydro-2'H,6H-spiro[isoxazolo[4,5-g][1,4]oxazino[4,3-a]quinoline-5,5'-pyrimidine]-2',4',6'(1'H,3'H)-trione (30).**—Prepared

following the preparation of **8** using **48w** (282 mg, 0.65 mmol) and pyrimidine-2,4,6(1*H*, 3*H*, 5*H*)-trione (91 mg, 0.71 mmol). Chiral column chromatography using hexane:EtOH:DCM (60:30:10, isocratic, 15mL/min, Daicel IA column). Off-white solid (70 mg, 22%).  $^1\text{H}$  NMR (300 MHz, DMSO- $d_6$ )  $\delta$  7.00 (s, 1H), 4.29 (d,  $J = 6.3$  Hz, 2H), 4.07 – 3.96 (m, 1H), 3.94 – 3.83 (m, 1H), 3.82 – 3.66 (m, 1H), 3.66 – 3.54 (m, 1H), 3.52 – 3.39 (m, 1H), 3.39 – 3.28 (m, 1H), 3.19 – 3.10 (m, 1H), 3.09 – 2.82 (m, 3H), 2.47 – 2.34 (m, 1H), 2.17 – 2.05 (m, 1H), 1.10 (d,  $J = 6.4$  Hz, 3H), 0.85 (d,  $J = 6.3$  Hz, 3H).  $^{13}\text{C}$  NMR (151 MHz, DMSO- $d_6$ )  $\delta$  177.94, 171.94, 168.41, 166.24, 153.01 (d,  $J = 13.0$  Hz), 150.52, 135.63, 134.12 (d,  $J = 241.3$  Hz),

122.98, 114.24, 105.59, 72.71, 72.48, 72.23, 64.86, 56.53, 53.32, 44.53, 41.91, 33.33, 33.15, 18.28, 18.17. RP-UPLC  $t_R$  = 0.894 min (method 2, purity 100%); LC-MS ESI,  $m/z$  500.1 [M-H]<sup>-</sup> (anal. calcd. for C<sub>23</sub>H<sub>24</sub>FN<sub>5</sub>O<sub>7</sub>,  $m/z$  = 501.5).  $[\alpha]_D^{20}$  = -152.2° (c 0.23, MeOH).

**(2R,4S,4aS)-11-fluoro-2,4-dimethyl-8-((R)-5-oxopyrrolidin-3-yl)methoxy)-1,2,4,4a-tetrahydro-2'H,6H-spiro[isoxazolo[4,5-g][1,4]oxazino[4,3-a]quinoline-5,5'-pyrimidine]-2',4',6'(1'H,3'H)-trione (31).**—Prepared following the preparation of **8** using **48x** (224 mg, 0.51 mmol) and pyrimidine-2,4,6(1*H*, 3*H*, 5*H*)-trione (72 mg, 0.57 mmol). Chiral column chromatography using hexane:EtOH:MTBE:DCM (40:10:30:20, isocratic, 15mL/min, Daicel IA column). Off-white solid (34 mg, 13%). <sup>1</sup>H NMR (600 MHz, DMSO-*d*<sub>6</sub>) δ 7.55 (s, 1H), 7.06 (d, *J* = 1.2 Hz, 1H), 4.36 – 4.28 (m, 2H), 4.08 – 4.00 (m, 1H), 3.94 – 3.88 (m, 1H), 3.79 – 3.71 (m, 1H), 3.68 – 3.61 (m, 1H), 3.51 – 3.46 (m, 1H), 3.43 – 3.37 (m, 1H), 3.13 – 3.03 (m, 2H), 2.95 – 2.84 (m, 2H), 2.34 – 2.27 (m, 1H), 2.10 – 2.03 (m, 1H), 1.11 (d, *J* = 6.2 Hz, 3H), 0.85 (d, *J* = 6.3 Hz, 3H). <sup>13</sup>C NMR (151 MHz, DMSO-*d*<sub>6</sub>) δ 176.12, 171.84, 168.53, 166.26, 153.13 (d, *J* = 12.5 Hz), 150.55, 135.71, 134.24 (d, *J* = 239.9 Hz), 123.38, 114.28, 105.67, 72.57, 72.45, 72.13, 64.92, 56.81 (d, *J* = 9.2 Hz), 53.46, 44.29, 39.07, 33.71, 33.41, 18.64, 18.60. RP-UPLC  $t_R$  = 0.889 min (method 2, purity 100%); LC-MS ESI,  $m/z$  500.2 [M-H]<sup>-</sup> (anal. calcd. for C<sub>23</sub>H<sub>24</sub>FN<sub>5</sub>O<sub>7</sub>,  $m/z$  = 501.5).  $[\alpha]_D^{20}$  = -170.8° (c 0.21, MeOH).

**(2R,4S,4aS)-11-fluoro-2,4-dimethyl-8-(2-((S)-5-oxopyrrolidin-2-yl)ethoxy)-1,2,4,4a-tetrahydro-2'H,6H-spiro[isoxazolo[4,5-g][1,4]oxazino[4,3-a]quinoline-5,5'-pyrimidine]-2',4',6'(1'H,3'H)-trione (32).**—Prepared following the preparation of **8** using **48y** (359 mg, 0.80 mmol) and pyrimidine-2,4,6(1*H*, 3*H*, 5*H*)-trione (113 mg, 0.88 mmol). Chiral column chromatography using hexane:EtOH:DCM (55:35:15, isocratic, 15mL/min, Daicel IA column). Beige solid (38 mg, 9%). <sup>1</sup>H NMR (300 MHz, DMSO-*d*<sub>6</sub>) δ 11.61 (s, 2H), 7.80 (s, 1H), 7.10 (s, 1H), 4.48 – 4.34 (m, 2H), 4.12 – 4.00 (m, 1H), 3.98 – 3.89 (m, 1H), 3.85 – 3.60 (m, 3H), 3.60 – 3.50 (m, 1H), 3.17 – 3.02 (m, 1H), 2.97 – 2.87 (m, 1H), 2.24 – 2.09 (m, 3H), 2.03 – 1.87 (m, 2H), 1.79 – 1.64 (m, 1H), 1.14 (d, *J* = 6.1 Hz, 3H), 0.89 (d, *J* = 6.3 Hz, 3H). <sup>13</sup>C NMR (101 MHz, DMSO-*d*<sub>6</sub>) δ 177.03, 171.42, 168.11, 166.19, 153.12 (d, *J* = 12.5 Hz), 149.98, 135.64, 134.31 (d, *J* = 240.5 Hz), 123.16, 114.34, 105.95, 72.54, 72.15, 68.18, 64.93, 56.85 (d, *J* = 10.5 Hz), 53.58, 51.12, 39.06, 35.99, 30.29, 27.25, 18.67, 18.60. RP-UPLC  $t_R$  = 0.954 min (method 2, purity 100%); LC-MS ESI,  $m/z$  514.1 [M-H]<sup>-</sup> (anal. calcd. for C<sub>24</sub>H<sub>26</sub>FN<sub>5</sub>O<sub>7</sub>,  $m/z$  = 515.5).  $[\alpha]_D^{20}$  = -165.3° (c 0.27, MeOH).

**(2R,4S,4aS)-11-fluoro-2,4-dimethyl-8-((5-methyl-1,3,4-oxadiazol-2-yl)methoxy)-1,2,4,4a-tetrahydro-2'H,6H-spiro[isoxazolo[4,5-g][1,4]oxazino[4,3-a]quinoline-5,5'-pyrimidine]-2',4',6'(1'H,3'H)-trione (33).**—Prepared following the preparation of **8** using **48z** (77 mg, 0.177 mmol) and pyrimidine-2,4,6(1*H*, 3*H*, 5*H*)-trione (25 mg, 0.194 mmol). Chiral column chromatography using hexane:EtOH:DCM (56:40:4, isocratic, 15mL/min, Daicel IC column). Off-white solid (65 mg, 73%). <sup>1</sup>H NMR (400 MHz, DMSO-*d*<sub>6</sub>) δ 11.62 (br s, 2H), 7.13 (s, 1H), 5.66 (s, 2H), 4.14 – 4.04 (m, 1H), 3.99 – 3.89 (m, 1H), 3.85 – 3.74 (m, 1H), 3.73 – 3.61 (m, 1H), 3.60 – 3.52 (m, 1H), 3.16 – 3.06 (m, 1H), 2.97



– 2.89 (m, 1H), 2.54 (s, 3H), 1.14 (d,  $J = 6.2$  Hz, 3H), 0.90 (d,  $J = 6.3$  Hz, 3H).  $^{13}\text{C}$  NMR (101 MHz, DMSO- $d_6$ )  $\delta$  171.39, 168.13, 165.40, 165.33, 161.88, 153.51 (d,  $J = 13.2$  Hz), 149.98, 135.97, 134.20 (d,  $J = 240.0$  Hz), 123.70, 114.23, 105.10, 72.55, 72.16, 64.95, 61.68, 56.83 (d,  $J = 8.9$  Hz), 53.50, 39.01, 18.66, 18.58, 10.93.  $^{19}\text{F}$  NMR (377 MHz, DMSO- $d_6$ )  $\delta$  –157.50. RP-UPLC  $t_{\text{R}} = 0.983$  min (method 2, purity 99%); LC-MS ESI,  $m/z$  499.1  $[\text{M-H}]^-$  (anal. calcd. for  $\text{C}_{22}\text{H}_{21}\text{FN}_6\text{O}_7$ ,  $m/z = 500.4$ ).  $[\alpha]_{\text{D}}^{20} = -203^\circ$  (c 0.29, MeOH).

**(2R,4S,4aS)-11-fluoro-2,4-dimethyl-8-((S)-4-methyl-2-oxooxazolidin-3-yl)-2,3,4,4a-tetrahydro-1H,2'H,6H-spiro[isoxazolo[4,5-g]pyrazino[1,2-a]quinoline-5,5'-pyrimidine]-2',4',6'(1'H,3'H)-trione (34).**—

A mixture of **50a** (120 mg, 0.319 mmol) and pyrimidine-2,4,6(1H, 3H, 5H)-trione (41 mg, 0.319 mmol) in AcOH (2 mL) and water (0.5 mL) was stirred for 4 h at 80 °C. The solvents were removed, and the reaction mixture was precleaned by flash chromatography on silica gel, using a 4g column (over 16min) and a linear gradient 0–10% (DCM:MeOH). The major band was isolated and contained a mixture of isomers. The mixture of isomers was separated using reverse phase preparative HPLC [(10 mM ammonium acetate buffer containing 0.4% acetic acid in water):(10 mM ammonium acetate buffer containing 0.4% acetic acid in methanol), gradient, 20–60%, 15mL/min, C18 column). Compound **34** was isolated as a white solid (15 mg, 3.0%).  $^1\text{H}$  NMR (300 MHz, DMSO- $d_6$ )  $\delta$  7.55 (s, 1H), 4.65 (m, 2H), 4.19 (dd,  $J = 7.6, 4.2$  Hz, 1H), 4.01 (d,  $J = 12.0$  Hz, 1H), 3.83 (d,  $J = 9.1$  Hz, 1H), 3.56 (d,  $J = 14.5$  Hz, 1H), 3.05 – 2.80 (m, 4H), 1.41 (d,  $J = 5.7$  Hz, 3H), 1.02 (d,  $J = 5.5$  Hz, 3H), 0.78 (d,  $J = 6.4$  Hz, 3H).  $^{13}\text{C}$  NMR (151 MHz, DMSO- $d_6$ )  $\delta$  171.79, 168.31, 154.46, 153.93 (d,  $J = 12.8$  Hz), 152.58, 150.06, 135.90, 133.71 (d,  $J = 235.6$  Hz), 123.24, 118.24, 106.99, 70.70, 66.34, 53.65, 53.30, 52.00, 51.02, 40.91, 39.06, 21.50, 19.00, 18.01. RP-UPLC  $t_{\text{R}} = 2.61$  min (method 1, purity 100%); LC-MS ESI,  $m/z$  487.2  $[\text{M+H}]^+$  (anal. calcd. for  $\text{C}_{22}\text{H}_{23}\text{FN}_6\text{O}_6$ ,  $m/z = 486.5$ ).  $[\alpha]_{\text{D}}^{20} = -55^\circ$  (c 0.5, MeOH).

**(2R,4S,4aS)-11-fluoro-3-hydroxy-2,4-dimethyl-8-((S)-4-methyl-2-oxooxazolidin-3-yl)-2,3,4,4a-tetrahydro-1H,2'H,6H-spiro[isoxazolo[4,5-g]pyrazino[1,2-a]quinoline-5,5'-pyrimidine]-2',4',6'(1'H,3'H)-trione (35).**—

A mixture of **50b** (400 mg, 1.02 mmol) and pyrimidine-2,4,6(1H, 3H, 5H)-trione (131 mg, 1.02 mmol) in ethanol (3 mL) was stirred for 2 h at 80 °C. The solvents were removed, and the reaction mixture was precleaned by flash chromatography on silica gel, using a 4g column (over 16min) and a linear gradient 0–10% (DCM:MeOH). The major band was isolated and contained a mixture of isomers. The mixture was separated using reverse phase preparative HPLC [(10 mM ammonium acetate buffer containing 0.4% acetic acid in water):(10 mM ammonium acetate buffer containing 0.4% acetic acid in methanol), gradient, 20–60%, 15mL/min, C18 column). Compound **35** was isolated as a white solid (30 mg, 6.0 % yield).  $^1\text{H}$  NMR (300 MHz, DMSO- $d_6$ )  $\delta$  11.76 (s, 1H), 11.42 (s, 1H), 8.04 (s, 1H), 7.58 (s, 1H), 4.73–4.62 (m, 2H), 4.23 – 4.15 (m, 1H), 4.03–4.00 (m, 2H), 3.59 (d,  $J = 16.0$  Hz, 1H), 3.15 (d,  $J = 17.3$  Hz, 1H), 2.91 (d,  $J = 14.5$  Hz, 1H), 2.74–2.70 (m, 2H), 1.42 (d,  $J = 5.7$  Hz, 3H), 1.12 (d,  $J = 6.0$  Hz, 3H), 0.88 (d,  $J = 6.2$  Hz, 3H).  $^{13}\text{C}$  NMR (151 MHz, DMSO- $d_6$ )  $\delta$  171.51, 168.34, 154.52, 153.88 (d,  $J = 12.9$  Hz), 152.56, 149.93, 134.86 (d,  $J = 239.5$  Hz), 129.81, 123.16, 118.34, 107.29, 70.64, 64.07, 62.83, 61.56, 54.91, 54.04, 53.00, 39.05,

17.76, 17.18, 16.17. RP-UPLC  $t_R$  = 3.403 min (method 1, purity 100%); LC-MS ESI,  $m/z$  503.1 [M+H]<sup>+</sup> (anal. calcd. for C<sub>22</sub>H<sub>23</sub>FN<sub>6</sub>O<sub>7</sub>,  $m/z$  = 502.5).  $[\alpha]_D^{20}$  = -63° (c 1.0, MeOH).

**(2R,4S,4aS)-3-acetyl-11-fluoro-2,4-dimethyl-8-((S)-4-methyl-2-oxooxazolidin-3-yl)-2,3,4,4a-tetrahydro-1H,2'H,6H-spiro[isoxazolo[4,5-g]pyrazino[1,2-a]quinoline-5,5'-pyrimidine]-2',4',6'(1'H,3'H)-trione (36).**—Prepared as described for **35** using **50c** (220 mg, 0.526 mmol) and pyrimidine-2,4,6(1H, 3H, 5H)-trione (67 mg, 0.526 mmol). Flash column chromatography using CH<sub>2</sub>Cl<sub>2</sub>:MeOH (90:10). The mixture of isomers were separated using reverse phase preparative HPLC [(10 mM ammonium acetate buffer containing 0.4% acetic acid in water):(10 mM ammonium acetate buffer containing 0.4% acetic acid in methanol), gradient, 20–60%, 15mL/min, C18 column). Compound **36** was isolated as a white solid (40 mg, 14%). <sup>1</sup>H NMR (300 MHz, MeOD+CDCl<sub>3</sub>) δ 7.73 (s, 1H), 5.04 (d,  $J$  = 7.5 Hz, 1H), 4.79 – 4.66 (m, 2H), 4.19 (q,  $J$  = 3.1 Hz, 1H), 4.11 – 4.07 (m, 1H), 3.98 – 3.90 (m, 2H), 3.74 (t,  $J$  = 11.6 Hz, 1H), 3.51 (d,  $J$  = 16.6 Hz, 1H), 3.24 (d,  $J$  = 16.7 Hz, 1H), 2.06 (s, 3H), 1.53 (d,  $J$  = 6.0 Hz, 3H), 1.48 (d,  $J$  = 7.2 Hz, 3H), 1.31 (d,  $J$  = 6.1 Hz, 3H). <sup>13</sup>C NMR (101 MHz, MeOD+CDCl<sub>3</sub>) δ 171.80 (2C), 154.79, 153.02 (d,  $J$  = 12.9 Hz), 152.20, 149.34, 136.13, 135.64, 133.72, 120.65, 118.80, 109.23, 70.53 (2C), 65.82, 53.15 (2C), 50.20 (2C), 37.22 (2C), 20.60, 17.55 (2C). RP-UPLC  $t_R$  = 0.762 min (method 2, purity 100%); LC-MS ESI,  $m/z$  529.2 [M+H]<sup>+</sup> (anal. calcd. for C<sub>24</sub>H<sub>25</sub>FN<sub>6</sub>O<sub>7</sub>,  $m/z$  = 528.4).  $[\alpha]_D^{20}$  = -63° (c 1.0, MeOH).

**2-((2R,4S,4aS)-11-fluoro-2,4-dimethyl-8-((S)-4-methyl-2-oxooxazolidin-3-yl)-2',4',6'-trioxo-1,1',2,3',4,4a,4',6'-octahydro-2'H,3H,6H-spiro[isoxazolo[4,5-g]pyrazino[1,2-a]quinoline-5,5'-pyrimidin]-3-yl)acetonitrile (37).**—Prepared as described for **35** using **50d** (350 mg, 0.843 mmol) and pyrimidine-2,4,6(1H, 3H, 5H)-trione (108 mg, 0.843 mmol). Flash column chromatography using CH<sub>2</sub>Cl<sub>2</sub>:MeOH (90:10). The mixture of isomers were separated using reverse phase preparative HPLC [(10 mM ammonium acetate buffer containing 0.4% acetic acid in water):(10 mM ammonium acetate buffer containing 0.4% acetic acid in methanol), gradient, 20–60%, 15mL/min, C18 column). Compound **37** was isolated as a major component (*Note: minor diastereomer was observed but was not isolated*). White solid (23 mg, 5.0%). <sup>1</sup>H NMR (300 MHz, DMSO-*d*<sub>6</sub>) δ 11.81 (s, 1H), 11.48 (s, 1H), 7.61 (s, 1H), 4.74 – 4.62 (m, 2H), 4.22 – 4.16 (m, 1H), 4.13 (d,  $J$  = 9.1 Hz, 1H), 4.04 – 3.97 (m, 3H), 3.63 (d,  $J$  = 14.3 Hz, 1H), 3.18 (t,  $J$  = 12.2 Hz, 1H), 2.93 (d,  $J$  = 14.3 Hz, 1H), 2.73–2.68 (m, 2H), 1.42 (d,  $J$  = 5.7 Hz, 3H), 1.12 (d,  $J$  = 6.1 Hz, 3H), 0.84 (d,  $J$  = 6.4 Hz, 3H). <sup>13</sup>C NMR (151 MHz, DMSO-*d*<sub>6</sub>) δ 171.41, 168.36, 154.53, 153.84 (d,  $J$  = 12.5 Hz), 152.59, 149.85, 135.21, 133.92 (d,  $J$  = 239.7 Hz), 123.22, 118.39, 115.57, 107.64, 70.65, 64.80, 56.65 (d,  $J$  = 8.0 Hz), 56.11, 54.80 (2C), 53.01, 38.99, 37.63, 17.73, 17.28, 16.44. RP-UPLC  $t_R$  = 0.913 min (method 2, purity 96%); LC-MS ESI,  $m/z$  526.0 [M+H]<sup>+</sup> (anal. calcd. for C<sub>24</sub>H<sub>24</sub>FN<sub>7</sub>O<sub>6</sub>,  $m/z$  = 525.5).  $[\alpha]_D^{20}$  = -62° (c 1.0, DMSO).

**(2R,4S,4aS)-11-fluoro-2,4-dimethyl-8-((S)-4-methyl-2-oxooxazolidin-3-yl)-2',4',6'-trioxo-1,1',2,3',4,4a,4',6'-octahydro-2'H,3H,6H-spiro[isoxazolo[4,5-g]pyrazino[1,2-a]quinoline-5,5'-pyrimidine]-3-carbonitrile (38).**—Cyanic bromide (65 mg, 0.617 mmol) and K<sub>2</sub>CO<sub>3</sub> (85 mg, 0.617 mmol) were added to a non-separated mixture of **34+34E**

(200 mg, 0.411 mmol) in acetone (20 mL) and resulting reaction mixture was stirred at 25 °C for 16 h. Then the solvent was removed under reduced pressure and residue was taken up in EtOAc (20 mL) and washed with water (2×10 mL). The organic phase was isolated, dried over Na<sub>2</sub>SO<sub>4</sub>, filtered and solvent removed under reduced pressure. The mixture of isomers were separated using reverse phase preparative HPLC [(10 mM ammonium acetate buffer containing 0.4% acetic acid in water):(10 mM ammonium acetate buffer containing 0.4% acetic acid in methanol), gradient, 20–60%, 15mL/min, C18 column). Compound **38** was isolated as a major component (*Note: minor diastereomer was observed but was not isolated*). White solid (30 mg, 14%). <sup>1</sup>H NMR (300 MHz, DMSO-*d*<sub>6</sub>) δ 11.83 (s, 1H), 11.55 (s, 1H), 7.64 (s, 1H), 4.75 – 4.61 (m, 2H), 4.22 – 4.16 (m, 1H), 4.12 – 4.06 (m, 2H), 3.67 (d, *J* = 14.3 Hz, 1H), 3.49 (t, *J* = 9.0 Hz, 1H), 3.41 (dd, *J* = 9.3, 6.8 Hz, 1H), 3.22 (d, *J* = 13.1 Hz, 1H), 3.00 (d, *J* = 14.3 Hz, 1H), 1.42 (d, *J* = 5.9 Hz, 3H), 1.30 (d, *J* = 6.5 Hz, 3H), 1.04 (d, *J* = 6.7 Hz, 3H). RP-UPLC *t*<sub>R</sub> = 4.02 min (method 1, purity 99%); LC-MS ESI, *m/z* 512.2 [M+H]<sup>+</sup> (anal. calcd. for C<sub>23</sub>H<sub>22</sub>FN<sub>7</sub>O<sub>6</sub>, *m/z* = 511.2). [α]<sub>D</sub><sup>20</sup> = –75° (c 0.4, MeOH).

**11-fluoro-2,4-dimethyl-2',4',6'-trioxo-8-(1H-1,2,4-triazol-1-yl)-1',2,3',4,4a,4',6'-octahydro-2'H,3H,6H-spiro[isoxazolo[4,5-g]pyrazino[1,2-a]quinoline-5,5'-pyrimidine]-3-carbonitrile (39).**—To a solution of **54a** (190 mg,

0.470 mmol) in 2mL (EtOH:2M HCl, 10:1), pyrimidine-2,4,6(1H, 3H, 5H)-trione (66 mg, 0.510 mmol) was added. The solution instantly turned an orange colour. The reaction mixture was heated at 80°C for 16 h. The reaction was cooled, and solvent removed to afford an orange-yellow residue. The crude residue was pre-cleaned using normal phase chromatography, by dry loading onto flash silica and purification was performed by flash chromatography using 0–10% (MeOH in DCM). The major fraction was isolated, solvent removed to afford the product as a mixture of isomers Attempts to dissolve the mixture proved difficult and thus HPLC chiral separation was not performed. The racemic mix was found to be soluble in DMF and DMSO, two solvents which would have detrimental effects to chiral chromatography separation. The title compound was isolated as a mixture of isomers (125 mg, 53%) as a pale brown solid. <sup>1</sup>H NMR (300 MHz, DMSO-*d*<sub>6</sub>) δ 11.91 (s, 1H), 11.56 (s, 1H), 9.44 (s, 1H), 8.52 (s, 1H), 7.66 (s, 1H), 4.19 – 4.06 (m, 2H), 3.82 (d, *J* = 14.2 Hz, 1H), 3.60 – 3.39 (m, 2H), 3.01 (d, *J* = 14.3 Hz, 1H), 1.32 (d, *J* = 6.4 Hz, 3H), 1.06 (d, *J* = 5.6 Hz, 3H). *1 proton masked under water peak*. <sup>19</sup>F NMR (377 MHz, DMSO-*d*<sub>6</sub>) δ –156.30. RP-UPLC *t*<sub>R</sub> = 1.029 min (method 2, purity 94%); LC-MS ESI, *m/z* 378.1 [M-H]<sup>–</sup> (anal. calcd. for C<sub>21</sub>H<sub>18</sub>FN<sub>9</sub>O<sub>4</sub>, *m/z* = 379.1).

**(2R,4S,4aS)-11-fluoro-8-((S)-3-hydroxypyrrolidin-1-yl)-2,4-dimethyl-2',4',6'-trioxo-1',2,3',4,4a,4',6'-octahydro-2'H,3H,6H-spiro[isoxazolo[4,5-g]pyrazino[1,2-a]quinoline-5,5'-pyrimidine]-3-carbonitrile (40).**—Prepared

following the preparation of **8** using **54b** (433 mg, 1.00 mmol) and pyrimidine-2,4,6(1H, 3H, 5H)-trione (141 mg, 1.01 mmol). Chiral column chromatography using hexane:EtOH:DCM (60:30:10, isocratic, 15mL/min, Daicel IA column). Off-white solid (132 mg, 27%). <sup>1</sup>H NMR (300 MHz, DMSO-*d*<sub>6</sub>) δ 11.88 (s, 1H), 11.51 (s, 1H), 7.37 (s, 1H), 4.41 (d, *J* = 4.7 Hz, 1H), 4.06 (dd, *J* = 17.0, 11.7 Hz, 2H), 3.61 – 3.31 (m, 7H), 3.30 – 3.07 (m, 1H), 2.98 (d, *J* = 14.1 Hz, 1H), 2.16 – 1.79 (m, 2H), 1.29 (d, *J* = 6.4 Hz, 3H), 1.04 (d, *J* = 6.7 Hz, 3H). <sup>13</sup>C NMR (101 MHz, MeOD) δ 172.21, 169.40, 160.01, 150.97, 137.96, 135.88, 135.57, 122.44,

117.33, 114.94, 111.12, 71.74, 65.06, 57.93, 56.51, 55.97, 47.86, 41.15, 35.04, 30.86, 24.41, 16.77, 16.44. RP-UPLC  $t_R$  = 2.763 min (method 1, purity 71%); LC-MS ESI,  $m/z$  496.1 [M-H]<sup>-</sup> (anal. calcd. for C<sub>23</sub>H<sub>24</sub>FN<sub>7</sub>O<sub>5</sub>,  $m/z$  = 497.5).  $[\alpha]_D^{20}$  = -115° (c 0.26, MeOH).

**(2R,4S,4aS)-11-fluoro-8-((R)-3-hydroxypyrrolidin-1-yl)-2,4-dimethyl-2',4',6'-trioxo-1,1',2,3',4,4a,4',6'-octahydro-2'H,3H,6H-spiro[isoxazolo[4,5-g]pyrazino[1,2-a]quinoline-5,5'-pyrimidine]-3-carbonitrile (41).**—Prepared following the preparation of **8** using **54c** (236 mg, 0.549 mmol) and pyrimidine-2,4,6(1H, 3H, 5H)-trione (77 mg, 0.604 mmol). Isomers were separated using reverse phase preparative HPLC [(10 mM ammonium acetate buffer containing 0.4% acetic acid in water): (10 mM ammonium acetate buffer containing 0.4% acetic acid in methanol), gradient, 20–60%, 15mL/min, C18 column). Compound **41** was isolated as a major component. (*Note: minor diastereomer was observed but was not isolated*). White solid (141 mg, 52%). <sup>1</sup>H NMR (300 MHz, DMSO-*d*<sub>6</sub>) δ 11.88 (d, *J* = 1.6 Hz, 1H), 11.51 (t, *J* = 1.7 Hz, 1H), 7.43 – 7.32 (m, 1H), 4.54 – 4.29 (m, 1H), 4.15 – 3.96 (m, 2H), 3.69 – 3.30 (m, 7H), 3.25 – 3.13 (m, 1H), 2.98 (d, *J* = 14.1 Hz, 1H), 2.11 – 1.83 (m, 2H), 1.29 (d, *J* = 6.4 Hz, 3H), 1.04 (d, *J* = 6.7 Hz, 3H). RP-UPLC  $t_R$  = 2.394 min (method 1, purity 100%); LC-MS ESI,  $m/z$  495.8 [M-H]<sup>-</sup> (anal. calcd. for C<sub>23</sub>H<sub>24</sub>FN<sub>7</sub>O<sub>5</sub>,  $m/z$  = 497.5).  $[\alpha]_D^{20}$  = -45° (c 0.24, MeOH).

**(2R,4S,4aS)-11-fluoro-2,4-dimethyl-2',4',6'-trioxo-8-(((S)-5-oxopyrrolidin-2-yl)methoxy)-1,1',2,3',4,4a,4',6'-octahydro-2'H,3H,6H-spiro[isoxazolo[4,5-g]pyrazino[1,2-a]quinoline-5,5'-pyrimidine]-3-carbonitrile (42).**—Prepared following the preparation of **8** using **54d** (312 mg, 0.679 mmol) and pyrimidine-2,4,6(1H, 3H, 5H)-trione (96 mg, 0.747 mmol). Chiral column chromatography using hexane:EtOH:IPA (45:35:20, isocratic, 15mL/min, Daicel IA column). Off-white solid (35 mg, 9.3%). <sup>1</sup>H NMR (600 MHz, DMSO-*d*<sub>6</sub>) δ 7.85 (s, 1H), 7.12 (d, *J* = 1.2 Hz, 1H), 4.26 (ddd, *J* = 42.2, 10.3, 4.7 Hz, 2H), 4.09 (d, *J* = 9.3 Hz, 1H), 4.03 – 3.98 (m, 1H), 3.95 (dd, *J* = 8.3, 4.4 Hz, 1H), 3.52 (d, *J* = 14.2 Hz, 1H), 3.48 – 3.41 (m, 1H), 3.41 – 3.36 (m, 1H), 3.22 – 3.16 (m, 1H), 2.90 (dd, *J* = 14.2, 1.5 Hz, 1H), 2.29 – 2.21 (m, 1H), 2.21 – 2.09 (m, 2H), 1.91 – 1.85 (m, 1H), 1.26 (d, *J* = 6.5 Hz, 3H), 1.00 (d, *J* = 6.7 Hz, 3H). <sup>13</sup>C NMR (151 MHz, DMSO-*d*<sub>6</sub>) δ 177.38, 171.88, 169.04, 166.32, 152.96 (d, *J* = 12.3 Hz), 151.13, 135.63, 134.55 (d, *J* = 240.8 Hz), 123.81, 114.38, 113.69, 106.47, 73.22, 63.51, 55.88 (d, *J* = 7.2 Hz), 54.98, 54.36, 54.20, 52.56, 39.06, 30.07, 23.13, 16.28, 16.23. RP-UPLC  $t_R$  = 0.888 min (method 2, purity 100%); LC-MS ESI,  $m/z$  524.2 [M-H]<sup>-</sup> (anal. calcd. for C<sub>24</sub>H<sub>24</sub>FN<sub>7</sub>O<sub>6</sub>,  $m/z$  = 525.5).  $[\alpha]_D^{20}$  = -122° (c 0.23, MeOH).

**(2S,4R,4aR)-11-fluoro-2,4-dimethyl-8-(((S)-5-oxopyrrolidin-2-yl)methoxy)-2,3,4,4a-tetrahydro-1H,2'H,6H-spiro[isoxazolo[4,5-g]pyrido[1,2-a]quinoline-5,5'-pyrimidine]-2',4',6'(1'H,3'H)-trione (43).**—Prepared following the preparation of **8** using **54e** (371 mg, 0.855 mmol) and pyrimidine-2,4,6(1H, 3H, 5H)-trione (120 mg, 0.941 mmol). Chiral column chromatography using hexane:EtOH:EtOAc (65:10:25, isocratic, 15mL/min, Daicel IC column). White solid (52 mg, 12%). <sup>1</sup>H NMR (300 MHz, DMSO-*d*<sub>6</sub>) δ 7.87 (s, 1H), 7.07 (s, 1H), 4.28 (qd, *J* = 10.4, 4.7 Hz, 2H), 4.06 – 3.88 (m, 2H), 3.78 (d, *J* = 9.9 Hz, 1H), 3.54 (d, *J* = 13.7 Hz, 1H), 2.95 – 2.82 (m, 2H), 2.35 – 2.09 (m, 3H), 1.99 – 1.70 (m, 4H), 0.90 (d, *J* = 6.4 Hz, 3H),

0.64 (d,  $J = 6.4$  Hz, 3H).  $^{13}\text{C}$  NMR (151 MHz,  $\text{DMSO-}d_6$ )  $\delta$  178.24, 172.76, 169.21, 167.20, 154.11 (d,  $J = 12.7$  Hz), 150.98, 137.69, 135.23 (d,  $J = 240.0$  Hz), 124.64, 114.99, 106.15, 74.02, 67.49, 59.43 (d,  $J = 8.9$  Hz), 55.49, 53.47, 44.32, 39.81, 33.75, 32.71, 30.96, 24.05, 20.02, 19.74. RP-UPLC  $t_{\text{R}} = 1.028$  min (method 2, purity 100%); LC-MS ESI,  $m/z$  498.2  $[\text{M-H}]^-$  (anal. calcd. for  $\text{C}_{24}\text{H}_{26}\text{FN}_6\text{O}_6$ ,  $m/z = 499.5$ ).  $[\alpha]_{\text{D}}^{20} = -154^\circ$  (c 0.24, MeOH).

**(2R,4S,4aS)-11-fluoro-2,4-dimethyl-8-(5-methyl-1,3,4-oxadiazol-2-yl)-2',4',6'-trioxo-1,1',2,3',4,4a,4',6'-octahydro-2'H,3H,6H-spiro[isoxazolo[4,5-g]pyrazino[1,2-a]quinoline-5,5'-pyrimidine]-3-carbonitrile (44).**—A mixture

of **57** (350 mg, 0.963 mmol) and pyrimidine-2,4,6(1H, 3H, 5H)-trione (123 mg, 0.963 mmol) in ethanol (4 mL) was stirred for 20 h at 110 °C. The solvents were removed, and the reaction mixture was precleaned by flash chromatography on silica gel, using a 4g column (over 16min) and a linear gradient 0–10% (DCM:MeOH). The major band was isolated and contained a mixture of isomers. The mixture was separated using chiral chromatography hexane:MeOH (20:80), isocratic, 15mL/min, Daicel IC column. Compound **44** was isolated as a white solid (64 mg, 10%).  $^1\text{H}$  NMR (300 MHz,  $\text{DMSO-}d_6$ )  $\delta$  11.72 (s, 2H), 7.70 (s, 1H), 4.21 – 4.07 (m, 2H), 3.86 (d,  $J = 14.3$  Hz, 1H), 3.60 – 3.49 (m, 1H), 3.49 – 3.39 (m, 1H), 3.25 (s, 1H), 3.01 (d,  $J = 14.2$  Hz, 1H), 2.68 (s, 3H), 1.32 (d,  $J = 6.4$  Hz, 3H), 1.10 – 1.01 (m, 3H).  $^{13}\text{C}$  NMR (101 MHz,  $\text{DMSO-}d_6$ )  $\delta$  171.09, 168.41, 165.81, 156.67, 153.32 (d,  $J = 12.8$  Hz), 150.11, 144.98, 136.14, 134.19 (d,  $J = 241.8$  Hz), 126.32, 116.11, 113.58, 111.65, 63.59, 55.92 (d,  $J = 8.5$  Hz), 54.98, 54.36, 54.18, 38.74, 16.34, 16.25, 11.08.  $^{19}\text{F}$  NMR (377 MHz,  $\text{DMSO-}d_6$ )  $\delta$  –155.40. RP-UPLC  $t_{\text{R}} = 0.981$  min (method 2, purity 100%); LC-MS ESI,  $m/z$  493.1  $[\text{M-H}]^-$  (anal. calcd. for  $\text{C}_{22}\text{H}_{19}\text{FN}_8\text{O}_5$ ,  $m/z = 494.4$ ).  $[\alpha]_{\text{D}}^{20} = -148^\circ$  (c 0.11, MeOH).

**(2R,3S,4S,4aR)-11-fluoro-3-hydroxy-2,4-dimethyl-8-(5-methyl-1,3,4-oxadiazol-2-yl)-2,3,4,4a-tetrahydro-1H,2'H,6H-spiro[isoxazolo[4,5-g]pyrido[1,2-a]quinoline-5,5'-pyrimidine]-2',4',6'(1'H,3'H)-trione (45).**—Prepared following

the preparation of **8** using **58** (200 mg, 0.534 mmol) and pyrimidine-2,4,6(1H, 3H, 5H)-trione (68 mg, 0.534 mmol). Chiral column chromatography using hexane:EtOH:EtOAc (70:14:16, isocratic, 15mL/min, Daicel IC column). Light yellow solid (27 mg, 10%).  $^1\text{H}$  NMR (300 MHz,  $\text{DMSO-}d_6$ )  $\delta$  11.62 (brs, 2H), 7.60 (s, 1H), 4.73 (d,  $J = 7.6$  Hz, 1H), 3.98 – 3.93 (m, 2H), 3.74 (d,  $J = 14.3$  Hz, 1H), 3.01 (t,  $J = 13.1$  Hz, 1H), 2.91 (d,  $J = 14.2$  Hz, 1H), 2.75 (q,  $J = 9.24$  Hz, 1H), 2.68 (s, 3H), 1.72 – 1.63 (m, 2H), 1.01 (d,  $J = 6.4$  Hz, 3H), 0.76 (d,  $J = 6.6$  Hz, 3H).  $^{13}\text{C}$  NMR (101 MHz,  $\text{DMSO-}d_6$ )  $\delta$  171.82, 168.46, 165.72, 156.77, 153.54 (d,  $J = 12.6$  Hz), 150.13, 144.78, 137.02, 133.89 (d,  $J = 241.63$  Hz), 126.64, 115.72, 110.49, 78.92, 64.95, 55.86 (d,  $J = 8.8$  Hz), 54.54, 40.90, 38.77, 15.58, 14.78, 11.07. *Note: one of the peak is for two carbons.*  $^{19}\text{F}$  NMR (377 MHz,  $\text{DMSO-}d_6$ )  $\delta$  –157.66. RP-UPLC  $t_{\text{R}} = 0.939$  min (method 2, purity 99%); LC-MS ESI,  $m/z$  485.1  $[\text{M+H}]^+$  (anal. calcd. for  $\text{C}_{22}\text{H}_{21}\text{FN}_6\text{O}_6$ ,  $m/z = 484.4$ ).  $[\alpha]_{\text{D}}^{20} = -190^\circ$  (c 0.19, THF).

## Supplementary Material

Refer to Web version on PubMed Central for supplementary material.

## ACKNOWLEDGMENT

The *Mtb* DNA gyrase assay was carried out by Inspiralis, Ltd. of Norfolk, United Kingdom with the experimental method described in the Supplementary Information. The authors wish to acknowledge Tando Ntsabo of H3D for the routine MIC screening; Dr Dale Taylor, Mr Virgil Verhoog and Ms Sumaya Salie for cytotoxicity data; Dr Mathew Njoroge, Dr Nina Lawrence, Ms Nesia Barnes, Mr Warren Oliphant, and Mr Ronald Olkers for logD and solubility determinations; Marianna de Kock and Claudia Spies, SAMRC and Stellenbosch University, South Africa for excellent technical assistance in generating MICs against clinical TB isolates. Lina Castro, Aaron Korkegian and Anu Kumar from Infectious Disease Research Institute for technical assistance and support.

### Funding Sources

The project was funded through Global Health Grants (Number OPP1066878 and OPP1024038) received from the Bill and Melinda Gates Foundation, the Division of Intramural Research of the NIAID/NIH and the Strategic Health Innovation Partnerships (SHIP) unit of the South African Medical Research Council (SAMRC). Additional support from the University of Cape Town and the South African Research Chairs Initiative of the Department of Science and Technology, administered through the South African National Research Foundation, are gratefully acknowledged (K.C.). N.O. was funded was supported by the U.S. Veterans Administration Merit Review award 101Bx002198 and the National Institutes of Health (R01 GM126363)

## ABBREVIATIONS

<b>ADC</b>	albumin dextrose catalase
<b>ATc</b>	anhydrotetracycline
<b>DAD</b>	diode array detector
<b>FQ</b>	fluoroquinolone
<b>INH</b>	isoniazid
<b>MDR</b>	multidrug resistant
<b>MGIT</b>	mycobacteria growth indicator tube
<b>MIC</b>	minimum inhibitory concentration
<b>MoA</b>	mode-of-action
<b>MoI</b>	mode-of-inhibition
<b>Mtb</b>	<i>Mycobacterium tuberculosis</i>
<b>MW</b>	molecular weight
<b>NBTIs</b>	novel bacterial topoisomerase inhibitors
<b>NMR</b>	nuclear magnetic resonance
<b>PDA</b>	photodiode array
<b>QRDR</b>	quinoline resistance-determining region
<b>RIF</b>	rifampicin
<b>RR-TB</b>	rifampicin-resistant-TB
<b>SAR</b>	structure-activity relationship

<b>RMSD</b>	root mean square deviation
<b>SPT</b>	spiropyrimidinetrione
<b>T-reaction</b>	tertiary amino effect reaction
<b>TB</b>	tuberculosis
<b>TLC</b>	thin-layer chromatography
<b>TMS</b>	tetramethylsilane
<b>WT</b>	wild-type
<b>XDR</b>	extensively drug resistant

## REFERENCES

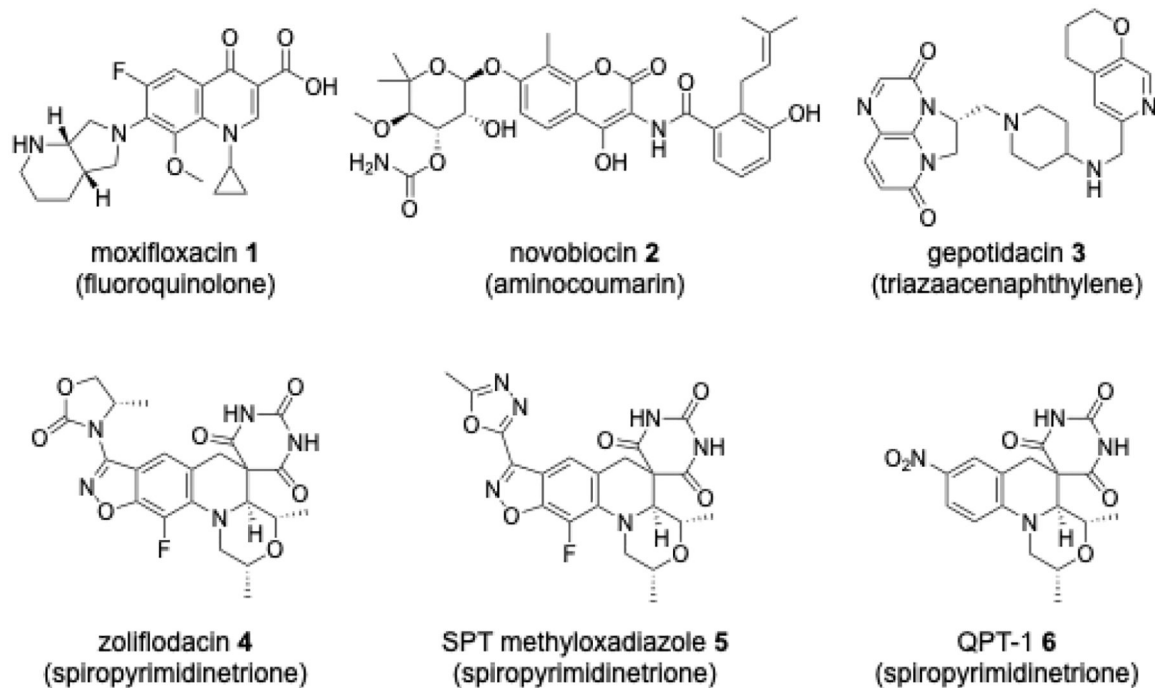
- (1). Tuberculosis: Key facts. <https://www.who.int/news-room/fact-sheets/detail/tuberculosis> (accessed February 14, 2022).
- (2). New TB drugs. <https://tbfacts.org/new-tb-drugs/> (accessed February 14, 2022).
- (3). Bandodkar B; Shandil RK; Bhat J; Balganesb TS, Two decades of TB drug discovery efforts—what have we learned? *Applied Sciences* 2020, 10, 5704.
- (4). Singh V; Chibale K, Strategies to combat multi-drug resistance in tuberculosis. *Acc. Chem. Res* 2021, 54, 2361–2376. [PubMed: 33886255]
- (5). Aldred KJ; Kerns RJ; Osheroff N, Mechanism of quinolone action and resistance. *Biochemistry* 2014, 53, 1565–1574. [PubMed: 24576155]
- (6). Gibson EG; Ashley RE; Kerns RJ; Osheroff N, Fluoroquinolone interactions with bacterial type II topoisomerases and target-mediated drug resistance. In *Antimicrobial Resistance in the Twenty-first Century*, Fong B; Shlaes D; Drlica K, Eds. Springer: New York, 2018; pp 507–529.
- (7). Bax BD; Murshudov G; Maxwell A; Germe T, DNA topoisomerase inhibitors: trapping a DNA-cleaving machine in motion. *J. Mol. Biol* 2019, 431, 3427–3449. [PubMed: 31301408]
- (8). Aubry A; Fisher LM; Jarlier V; Cambau E, First functional characterization of a singly expressed bacterial type II topoisomerase: the enzyme from *Mycobacterium tuberculosis*. *Biochem. Biophys. Res. Commun* 2006, 348, 158–165. [PubMed: 16876125]
- (9). Cole ST; Brosch R; Parkhill J; Garnier T; Churcher C; Harris D; Gordon SV; Eiglmeier K; Gas S; Barry CE; Tekaiia F; Badcock K; Basham D; Brown D; Chillingworth T; Connor R; Davies R; Devlin K; Feltwell T; Gentles S; Hamlin N; Holroyd S; Hornsby T; Jagels K; Krogh A; McLean J; Moule S; Murphy L; Oliver K; Osborne J; Quail MA; Rajandream MA; Rogers J; Rutter S; Seeger K; Skelton J; Squares R; Squares S; Sulston JE; Taylor K; Whitehead S; Barrell BG, Deciphering the biology of *Mycobacterium tuberculosis* from the complete genome sequence. *Nature* 1998, 393, 537–544. [PubMed: 9634230]
- (10). Basarab GS, Four Ways to Skin a Cat: Inhibition of Bacterial Topoisomerases Leading to the Clinic. In *Antibacterials: Volume I*, Fisher JF; Mobashery S; Miller MJ, Eds. Springer International Publishing: Cham: 2018; pp 165–188.
- (11). Moadebi S; Harder CK; Fitzgerald MJ; Elwood KR; Marra F, Fluoroquinolones for the treatment of pulmonary tuberculosis. *Drugs* 2007, 67, 2077–2099. [PubMed: 17883288]
- (12). Dawson R; Diacon AH; Everitt D; van Niekerk C; Donald PR; Burger DA; Schall R; Spigelman M; Conradie A; Eisenach K; Venter A; Ive P; Page-Shipp L; Variava E; Reither K; Ntinginya NE; Pym A; von Groote-Bidlingmaier F; Mendel CM, Efficiency and safety of the combination of moxifloxacin, pretomanid (PA-824), and pyrazinamide during the first 8 weeks of antituberculosis treatment: a phase 2b, open-label, partly randomised trial in patients with drug-susceptible or drug-resistant pulmonary tuberculosis. *Lancet* 2015, 385, 1738–1747. [PubMed: 25795076]

- (13). Bisacchi GS; Manchester JJ, A new-class antibacterial—Almost. Lessons in drug discovery and development: A critical analysis of more than 50 years of effort toward ATPase inhibitors of DNA gyrase and topoisomerase IV. *ACS Infectious Diseases* 2015, 1, 4–41. [PubMed: 27620144]
- (14). Kale RR; Kale MG; Waterson D; Raichurkar A; Hameed SP; Manjunatha MR; Kishore Reddy BK; Malolanarasimhan K; Shinde V; Koushik K; Jena LK; Menasinakai S; Humnabadkar V; Madhavapeddi P; Basavarajappa H; Sharma S; Nandishaiah R; Mahesh Kumar KN; Ganguly S; Ahuja V; Gaonkar S; Naveen Kumar CN; Ogg D; Boriack-Sjodin PA; Sambandamurthy VK; de Sousa SM; Ghorpade SR, Thiazolopyridone ureas as DNA gyrase B inhibitors: optimization of antitubercular activity and efficacy. *Bioorg. Med. Chem. Lett* 2014, 24, 870–879. [PubMed: 24405701]
- (15). Kale MG; Raichurkar A; Hameed PS; Waterson D; McKinney D; Manjunatha MR; Kranthi U; Koushik K; Jena LK; Shinde V; Rudrapatna S; Barde S; Humnabadkar V; Madhavapeddi P; Basavarajappa H; Ghosh A; Ramya VK; Guptha S; Sharma S; Vachaspati P; Kumar KNM; Giridhar J; Reddy J; Panduga V; Ganguly S; Ahuja V; Gaonkar S; Kumar CNN; Ogg D; Tucker JA; Boriack-Sjodin PA; de Sousa SM; Sambandamurthy VK; Ghorpade SR, Thiazolopyridine ureas as novel antitubercular agents acting through inhibition of DNA gyrase B. *J. Med. Chem* 2013, 56, 8834–8848. [PubMed: 24088190]
- (16). Locher CP; Jones SM; Hanzelka BL; Perola E; Shoen CM; Cynamon MH; Ngwane AH; Wiid IJ; van Helden PD; Betoudji F; Nuermberger EL; Thomson JA, A novel inhibitor of gyrase B is a potent drug candidate for treatment of tuberculosis and nontuberculosis mycobacterial infections. *Antimicrob. Agents Chemother* 2015, 59, 1455–1465. [PubMed: 25534737]
- (17). Gibson EG; Bax B; Chan PF; Osheroff N, Mechanistic and structural basis for the actions of the antibacterial gepotidacin against *Staphylococcus aureus* gyrase. *ACS Infect. Dis* 2019, 5, 570–581. [PubMed: 30757898]
- (18). O’Riordan W; Tiffany C; Scangarella-Oman N; Perry C; Hossain M; Ashton T; Dumont E, Efficacy, safety, and tolerability of gepotidacin (GSK2140944) in the treatment of patients with suspected or confirmed gram-positive acute bacterial skin and skin structure infections. *Antimicrob. Agents Chemother* 2017, 61, e02095–16. [PubMed: 28373199]
- (19). Hameed PS; Patil V; Solapure S; Sharma U; Madhavapeddi P; Raichurkar A; Chinnapattu M; Manjrekar P; Shanbhag G; Puttur J; Shinde V; Menasinakai S; Rudrapatana S; Achar V; Awasthy D; Nandishaiah R; Humnabadkar V; Ghosh A; Narayan C; Ramya VK; Kaur P; Sharma S; Werngren J; Hoffner S; Panduga V; Kumar CNN; Reddy J; Kumar Kn M; Ganguly S; Bharath S; Bheemaroo U; Mukherjee K; Arora U; Gaonkar S; Coulson M; Waterson D; Sambandamurthy VK; de Sousa SM, Novel N-linked aminopiperidine-based gyrase inhibitors with improved hERG and in vivo efficacy against *Mycobacterium tuberculosis*. *J. Med. Chem* 2014, 57, 4889–4905. [PubMed: 24809953]
- (20). Hameed PS; Manjrekar P; Raichurkar A; Shinde V; Puttur J; Shanbhag G; Chinnapattu M; Patil V; Rudrapatana S; Sharma S; Kumar CNN; Nandishaiah R; Madhavapeddi P; Sriram D; Solapure S; Sambandamurthy VK, Left-hand side exploration of novel bacterial topoisomerase inhibitors to improve selectivity against hERG binding. *ACS Med. Chem. Lett* 2015, 6, 741–746. [PubMed: 26191359]
- (21). Blanco D; Perez-Herran E; Cacho M; Ballell L; Castro J; González del Río R; Lavandera JL; Remuñán MJ; Richards C; Rullas J; Vázquez-Muñiz MJ; Woldu E; Zapatero-González MC; Angulo-Barturen I; Mendoza A; Barros D, *Mycobacterium tuberculosis* gyrase inhibitors as a new class of antitubercular drugs. *Antimicrob. Agents Chemother* 2015, 59, 1868–1875. [PubMed: 25583730]
- (22). Gibson EG; Blower TR; Cacho M; Bax B; Berger JM; Osheroff N, Mechanism of action of *Mycobacterium tuberculosis* gyrase Inhibitors: a novel class of gyrase poisons. *ACS Infect. Dis* 2018, 4, 1211–1222. [PubMed: 29746087]
- (23). Bradford PA; Miller AA; O’Donnell J; Mueller JP, Zoliflodacin: An oral spiropyrimidinetrione antibiotic for the treatment of *Neisseria gonorrhoeae*, including multi-drug-resistant isolates. *ACS Infect. Dis* 2020, 6, 1332–1345. [PubMed: 32329999]
- (24). Basarab GS; Ghorpade S; Gibhardt L; Muller R; Njoroge M; Peton N; Govender P; Massoudi LM; Robertson GT; Lenaerts AJ; Boshoff HIM; Joeris D; Parish T; Durand-Reville TF;

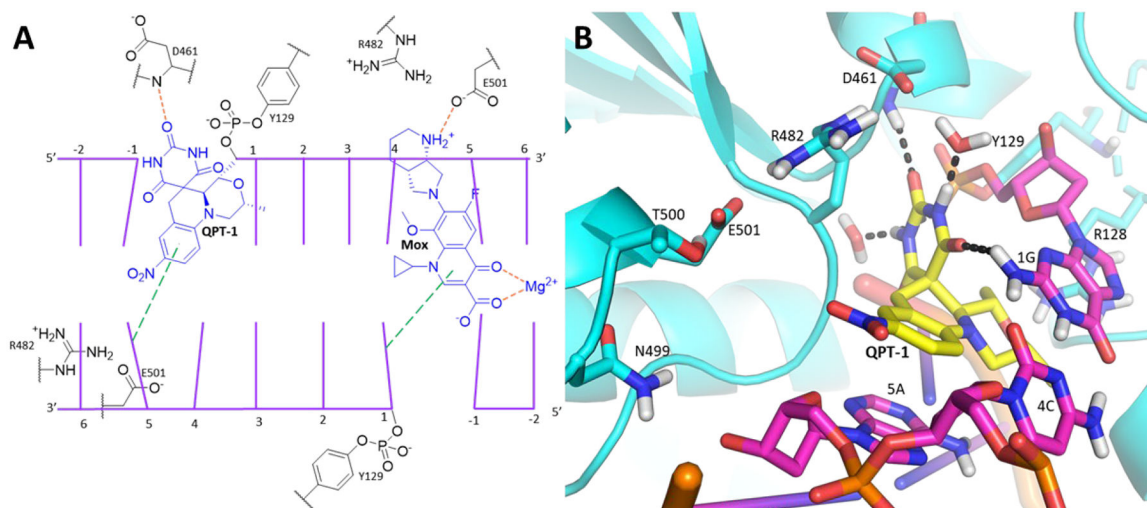


- Perros M; Singh V; Chibale K, Spiropyrimidinetriones: a class of DNA gyrase inhibitors with activity against *Mycobacterium tuberculosis* and without cross-resistance to fluoroquinolones. *Antimicrob. Agents Chemother* 2021, 66, e02192–21.
- (25). Eribo OA; du Plessis N; Ozturk M; Guler R; Walzl G; Chegou NN, The gut microbiome in tuberculosis susceptibility and treatment response: guilty or not guilty? *Cell. Mol* 2020, 77, 1497–1509.
- (26). Chan PF; Srikannathasan V; Huang J; Cui H; Fosberry AP; Gu M; Hann MM; Hibbs M; Homes P; Ingraham K; Pizzollo J; Shen C; Shillings AJ; Spitzfaden CE; Tanner R; Theobald AJ; Stavenger RA; Bax BD; Gwynn MN, Structural basis of DNA gyrase inhibition by antibacterial QPT-1, anticancer drug etoposide and moxifloxacin. *Nat. Commun* 2015, 6, 1–13.
- (27). Blower TR; Williamson BH; Kerns RJ; Berger JM, Crystal structure and stability of gyrase–fluoroquinolone cleaved complexes from *mycobacterium tuberculosis*. *Proc. Natl. Acad. Sci* 2016, 113, 1706–1713. [PubMed: 26792525]
- (28). Hooper DC; Jacoby GA, Mechanisms of drug resistance: quinolone resistance. *Ann. N. Y. Acad. Sci* 2015, 1354, 12–31. [PubMed: 26190223]
- (29). Avalos E; Catanzaro D; Catanzaro A; Ganiats T; Brodine S; Alcaraz J; Rodwell T, Frequency and geographic distribution of *gyrA* and *gyrB* mutations associated with fluoroquinolone resistance in clinical *Mycobacterium tuberculosis* isolates: a systematic review. *PLoS One* 2015, 10, e0120470. [PubMed: 25816236]
- (30). Srikannathasan V; Wohlkonig A; Shillings A; Singh O; Chan PF; Huang J; Gwynn MN; Fosberry AP; Homes P; Hibbs M; Theobald AJ; Spitzfaden C; Bax BD, Crystallization and initial crystallographic analysis of covalent DNA-cleavage complexes of *Staphylococcus aureus* DNA gyrase with QPT-1, moxifloxacin and etoposide. *Acta Cryst.* 2015, F71, 1242–1246.
- (31). Friesner RA; Banks JL; Murphy RB; Halgren TA; Klicic JJ; Mainz DT; Repasky MP; Knoll EH; Shelley M; Perry JK; Shaw DE; Francis P; Shenkin PS, Glide: a new approach for rapid, accurate docking and scoring. 1. method and assessment of docking accuracy. *J. Med. Chem* 2004, 47, 1739–1749. [PubMed: 15027865]
- (32). Halgren TA; Murphy RB; Friesner RA; Beard HS; Frye LL; Pollard WT; Banks JL, Glide: a new approach for rapid, accurate docking and scoring. 2. enrichment factors in database screening. *J. Med. Chem* 2004, 47, 1750–1759. [PubMed: 15027866]
- (33). Briones JF; Basarab GS, Expedient synthesis of tetrahydroquinoline-3-spirohydantoin derivatives via the lewis acid-catalyzed tert-amino effect reaction. *Chem. Comm* 2016, 52, 8541–8544. [PubMed: 27314439]
- (34). Bravian K; Basarab GS; Gowravaram MR; Hauck SI; Zhou F Fused, spirocyclic heteroaromatic compounds for the treatment of bacterial infections. *WO* 2010/043893 A1, 2010.
- (35). Bridges AJ; Lee A; Maduakor EC; Schwartz CE, Fluorine as an ortho-directing group in aromatic metalation: Generality of the reaction and the high position of fluorine in the Dir-Met potency scale. *Tetrahedron Lett.* 1992, 33, 7495–7498.
- (36). Basarab GS; Brassil P; Doig P; Galullo V; Haimes HB; Kern G; Kutschke A; McNulty J; Schuck VJA; Stone G; Gowravaram MR, Novel DNA gyrase inhibiting spiropyrimidinetriones with a benzisoxazole scaffold: SAR and in vivo characterization. *J. Med. Chem* 2014, 57, 9078–9095. [PubMed: 25286019]
- (37). Basarab GS; Doig P; Galullo V; Kern G; Kimzey A; Kutschke A; Newman JP; Morningstar M; Mueller J; Otterson L; Vishwanathan K; Zhou F; Gowravaram M, Discovery of novel DNA gyrase inhibiting spiropyrimidinetriones: benzisoxazole fusion with N-linked oxazolidinone substituents leading to a clinical candidate (ETX0914). *J. Med. Chem* 2015, 58, 6264–6282. [PubMed: 26158756]
- (38). Basarab GS; Gowravaram MR; Hauck SI; Zhou F Preparation of spiro[oxazino[4,3-*a*]isoxazolo[4,5-*g*]quinoline-*pyrimidine*]trione. Compounds and methods for treating bacterial infections. *US* 20140206677, 2014.
- (39). Ruble JC; Hurd AR; Johnson TA; Sherry DA; Barbachyn MR; Toogood PL; Bundy GL; Graber DR; Kamilar GM, Synthesis of (–)-PNU-286607 by asymmetric cyclization of alkylidene barbiturates. *J. Am. Chem. Soc* 2009, 131, 3991–3997. [PubMed: 19260642]

- (40). Basarab GS; Galullo V; DeGrace N; Hauck S; Joubran C; Wesolowski SS, Synthesis of a tetrahydronaphthyridine spiropyrimidinetrione DNA gyrase inhibiting antibacterial agent - differential substitution at all five carbon atoms of pyridine. *Org. Lett* 2014, 16, 6456–6459. [PubMed: 25458849]
- (41). Basarab GS; Kern GH; McNulty J; Mueller JP; Lawrence K; Vishwanathan K; Alm RA; Barvian K; Doig P; Galullo V; Gardner H; Gowravaram M; Huband M; Kimzey A; Morningstar M; Kutschke A; Lahiri SD; Perros M; Singh R; Schuck VJA; Tommasi R; Walkup G; Newman JV, Responding to the challenge of untreatable gonorrhea: ETX0914, a first-in-class agent with a distinct mechanism-of-action against bacterial type II topoisomerases. *Sci. Rep* 2015, 5, 11827–11840. [PubMed: 26168713]
- (42). Le Manach C; Dam J; Woodland JG; Kaur G; Khonde LP; Brunshwig C; Njoroge M; Wicht KJ; Horatschek A; Paquet T; Boyle GA; Gibbard L; Taylor D; Lawrence N; Yeo T; Mok S; Eastman RT; Dorjsuren D; Talley DC; Guo H; Simeonov A; Reader J; van der Watt M; Erlank E; Venter N; Zawada JW; Aswat A; Nardini L; Coetzer TL; Lauterbach SB; Bezuidenhout BC; Theron A; Mancama D; Koekemoer LL; Birkholtz L-M; Wittlin S; Delves M; Otilie S; Winzeler EA; von Geldern TW; Smith D; Fidock DA; Street LJ; Basarab GS; Duffy J; Chibale K, Identification and profiling of a novel diazaspiro[3.4]octane chemical series active against multiple stages of the human malaria parasite *Plasmodium falciparum* and optimization efforts. *J. Med. Chem* 2021, 64, 2291–2309. [PubMed: 33573376]
- (43). Zgurskaya HI; Rybenkov VV, Permeability barriers of gram-negative pathogens. *Ann. N. Y. Acad. Sci* 2019, 1459, 5–18. [PubMed: 31165502]
- (44). Schindler BD; Kaatz GW, Multidrug efflux pumps of gram-positive bacteria. *Drug Resist. Updat* 2016, 27, 1–13. [PubMed: 27449594]
- (45). Sharapova A; Ol'khovich M; Blokhina S; Zhironova E; Perlovich G, Solubility and partition behavior of moxifloxacin: experimental results and thermodynamics properties. *J. Mol. Liq* 2021, 339, 116814–116826.
- (46). Johnson EO; LaVerriere E; Office E; Stanley M; Meyer E; Kawate T; Gomez JE; Audette RE; Bandyopadhyay N; Betancourt N; Delano K; Da Silva I; Davis J; Gallo C; Gardner M; Golas AJ; Guinn KM; Kennedy S; Korn R; McConnell JA; Moss CE; Murphy KC; Nietupski RM; Papavinasasundaram KG; Pinkham JT; Pino PA; Proulx MK; Ruecker N; Song N; Thompson M; Trujillo C; Wakabayashi S; Wallach JB; Watson C; Ioerger TR; Lander ES; Hubbard BK; Serrano-Wu MH; Ehrt S; Fitzgerald M; Rubin EJ; Sasseti CM; Schnappinger D; Hung DT, Large-scale chemical-genetics yields new *M. tuberculosis* inhibitor classes. *Nature* 2019, 571, 72–78. [PubMed: 31217586]
- (47). Aldred KJ; McPherson SA; Wang P; Kerns RJ; Graves DE; Turnbough CL Jr.; Osheroff N, Drug interactions with *Bacillus anthracis* topoisomerase IV: biochemical basis for quinolone action and resistance. *Biochemistry* 2012, 51, 370–81. [PubMed: 22126453]
- (48). Iacobino A; Piccaro G; Pardini M; Fattorini L; Giannoni F, Moxifloxacin activates the SOS response in *Mycobacterium tuberculosis* in a dose- and time-dependent manner. *Microorganisms* 2021, 9, 255. [PubMed: 33513836]
- (49). Aldred KJ; Blower TR; Kerns RJ; Berger JM; Osheroff N, Fluoroquinolone interactions with *mycobacterium tuberculosis* gyrase: enhancing drug activity against wild-type and resistant gyrase. *Proc. Natl. Acad. Sci* 2016, 113, E839–E846. [PubMed: 26792518]
- (50). Singh V; Donini S; Pacitto A; Sala C; Hartkoorn RC; Dhar N; Keri G; Ascher DB; Mondésert G; Vocat A; Lupien A; Sommer R; Vermet H; Lagrange S; Buechler J; Warner DF; McKinney JD; Pato J; Cole ST; Blundell TL; Rizzi M; Mizrahi V, The inosine monophosphate dehydrogenase, GuaB2, is a vulnerable new bactericidal drug target for tuberculosis. *ACS Infect. Dis* 2017, 3, 5–17. [PubMed: 27726334]
- (51). Schrödinger Release2021–1: Maestro, Schrödinger, LLC: New York, NY, 2021.
- (52). Sastry GM; Adzhigirey M; Day T; Annabhimoju R; Sherman W, Protein and ligand preparation: parameters, protocols, and influence on virtual screening enrichments. *J. Comput. Aided. Mol. Des* 2013, 27, 221–34. [PubMed: 23579614]
- (53). Jacobson MP; Friesner RA; Xiang Z; Honig B, On the role of the crystal environment in determining protein side-chain conformations. *J. Mol. Biol* 2002, 320, 597–608. [PubMed: 12096912]

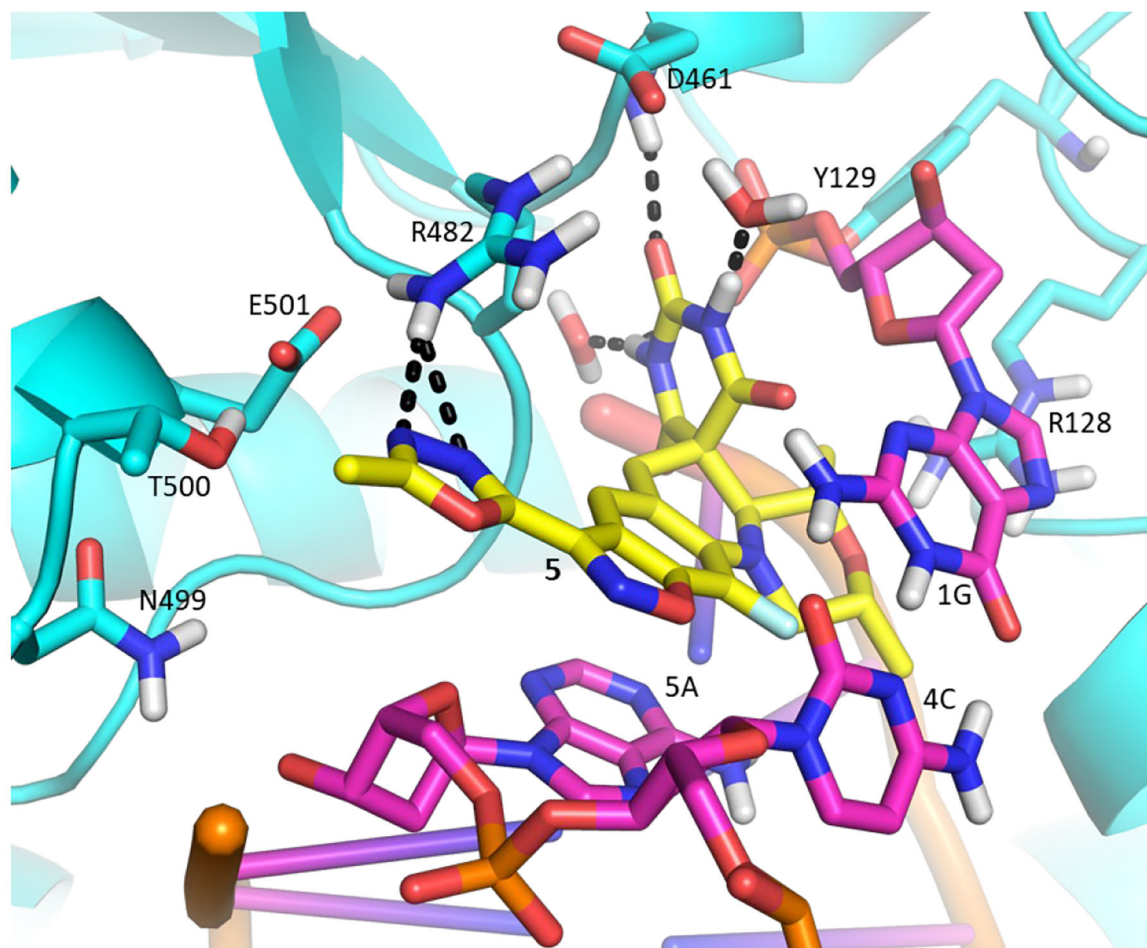


**Figure 1.**  
Known inhibitors of gyrase and Topoisomerase IV - compound class in parentheses.

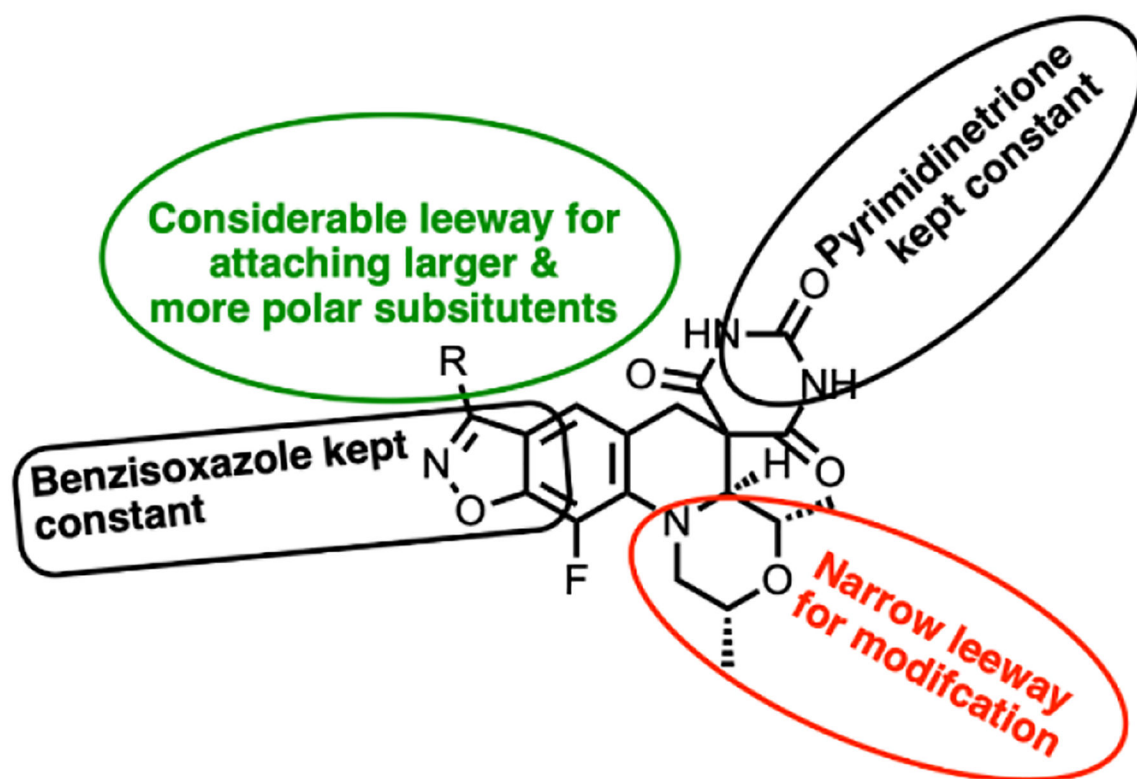


**Figure 2.**

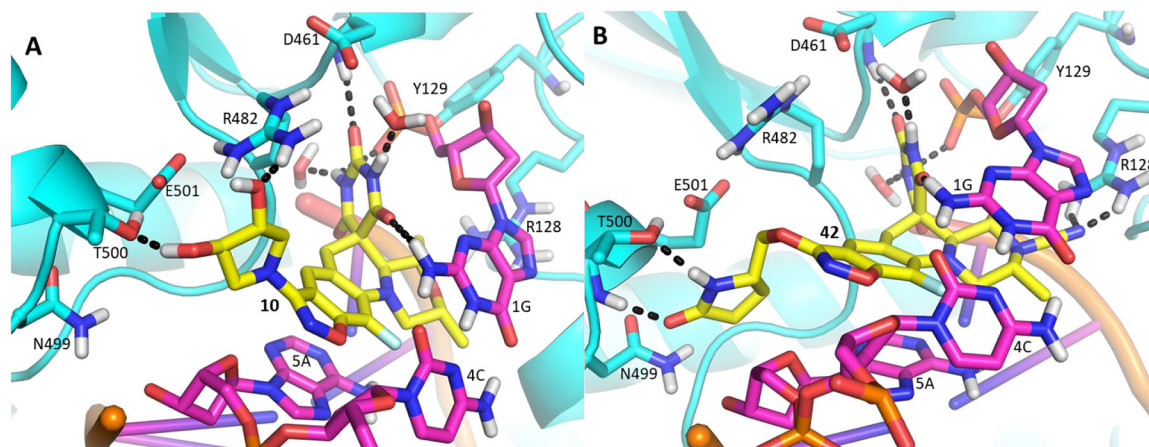
(A) A hybrid illustration of the double-stranded DNA break on complementary strands four bases apart with each break creating a FQ/SPT binding site, one showing QPT-1 and the other moxifloxacin. (B) Energy minimized structure of QPT-1 (yellow carbons) translocated into the *Mtb* gyrase binding site.



**Figure 3.** Model of **5** (yellow carbons) docked into *Mtb* gyrase making the same contacts as the modelled QPT-1 and showing an additional H-bond contact between the methyloxadiazole and R482.

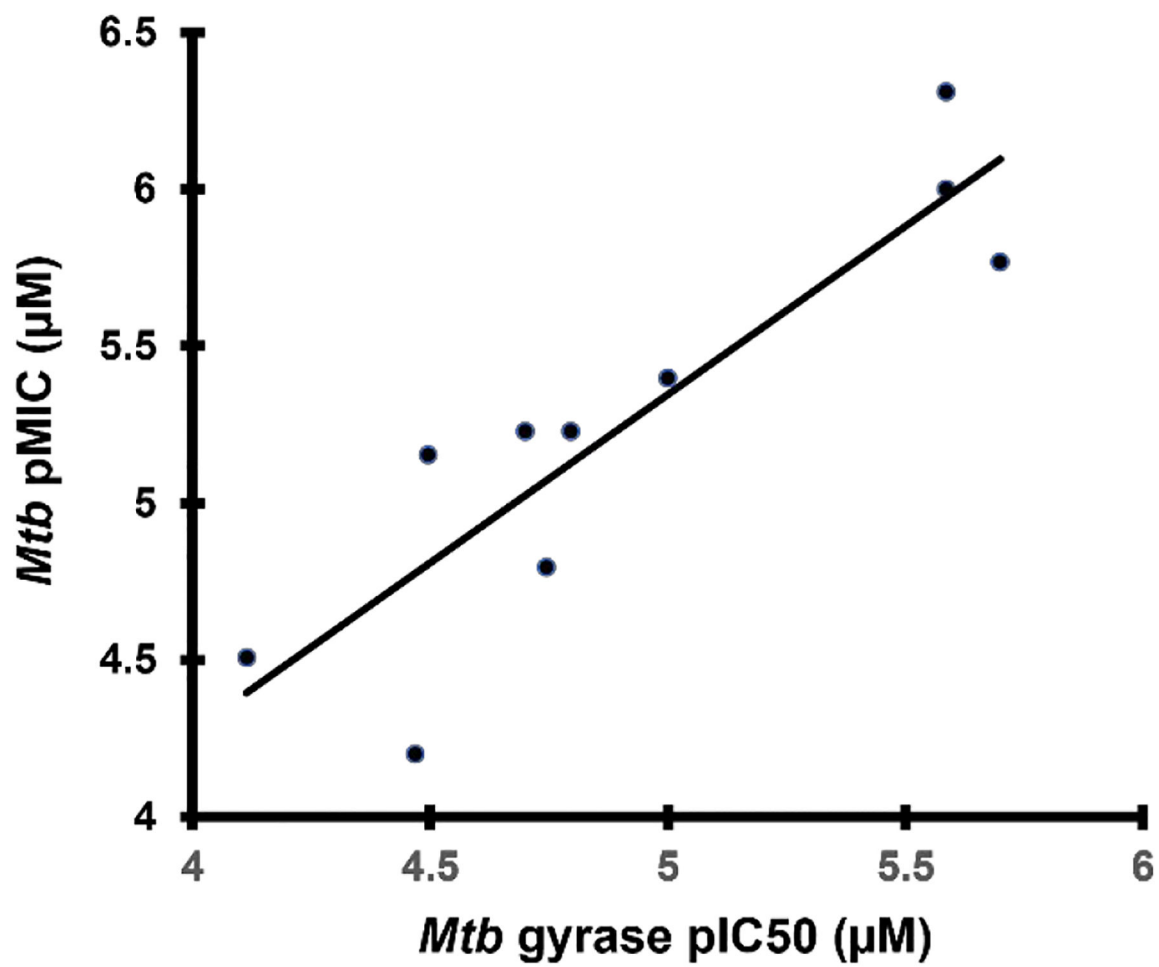


**Figure 4.**  
SAR explorations.



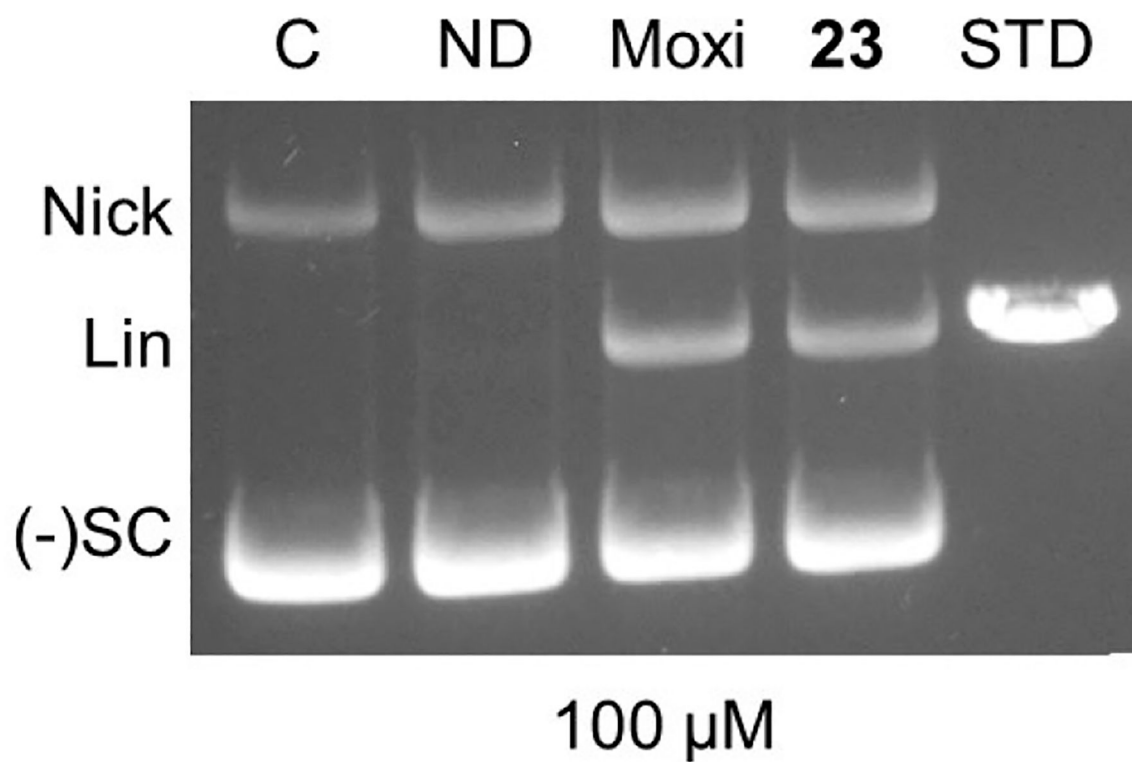
**Figure 5.**

(A) Model of **10** (yellow) with the dihydroxypyrrolidine forming H-bond interactions with the sidechain functionality of T500 and R482; (B) Model of **42** (yellow) with the CN forming H-bond with the guanidine of R128 and the pyrrolidinone forming H-bonds with the backbone NH and hydroxyl of T500.



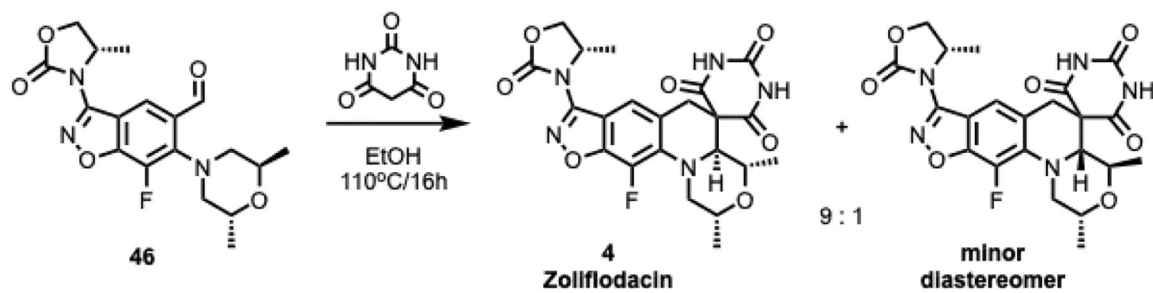
**Figure 6.**  
Compound MIC versus gyrase inhibitory potency.



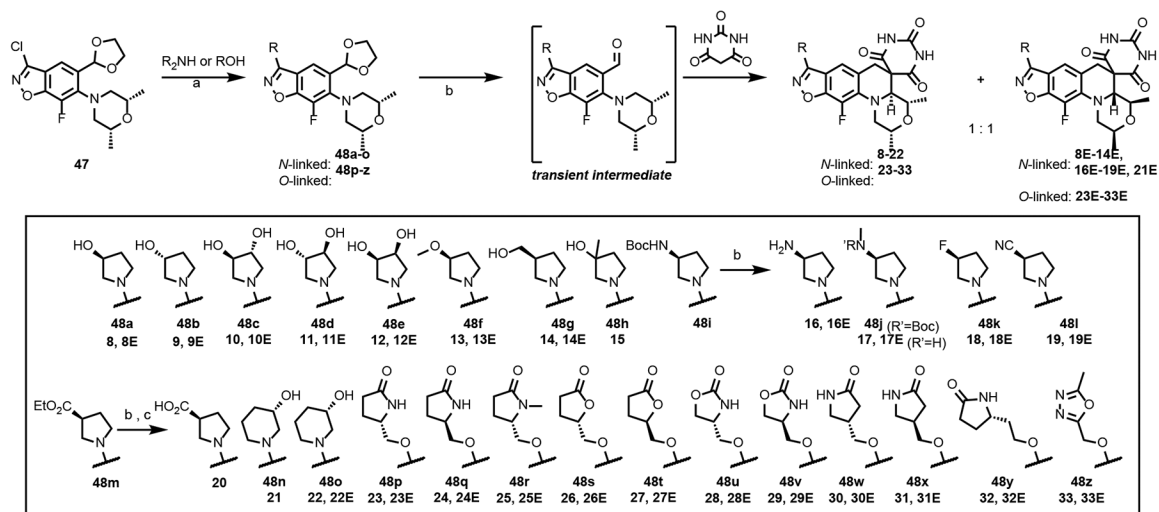


**Figure 7.**

Stabilization of doubly cleaved DNA complex for gyrase by **23** and moxifloxacin each at 100  $\mu$ M. Lanes from left to right are 1) negatively supercoiled DNA control, 2) *Mtb* gyrase + DNA with no drug, 3) *Mtb* gyrase + DNA + moxifloxacin, 4) *Mtb* gyrase + DNA + **23**, 5) Linear DNA standard. Nick = nicked DNA (single-stranded DNA break), Lin = linear DNA (double-stranded DNA break), (-)SC = negatively supercoiled pBR2322 DNA.

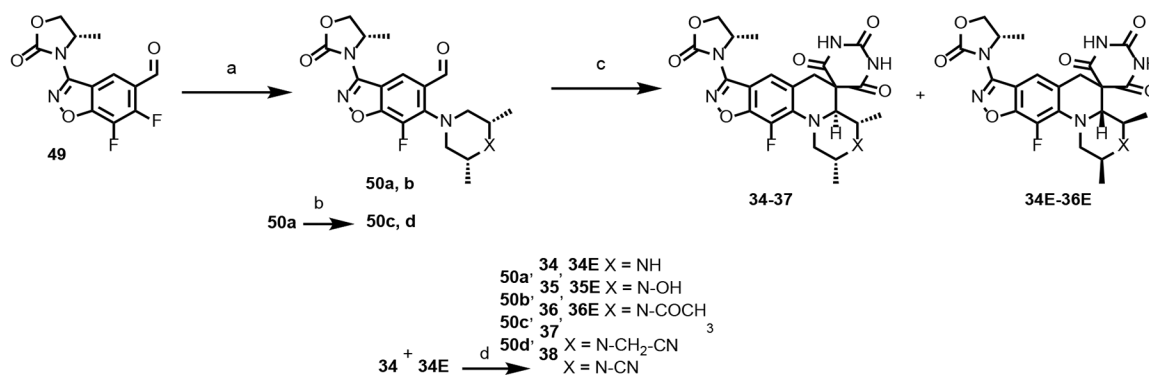
**Scheme 1.**

Synthesis of **1** via tertiary amino effect reaction (T-reaction) – chiral enablement

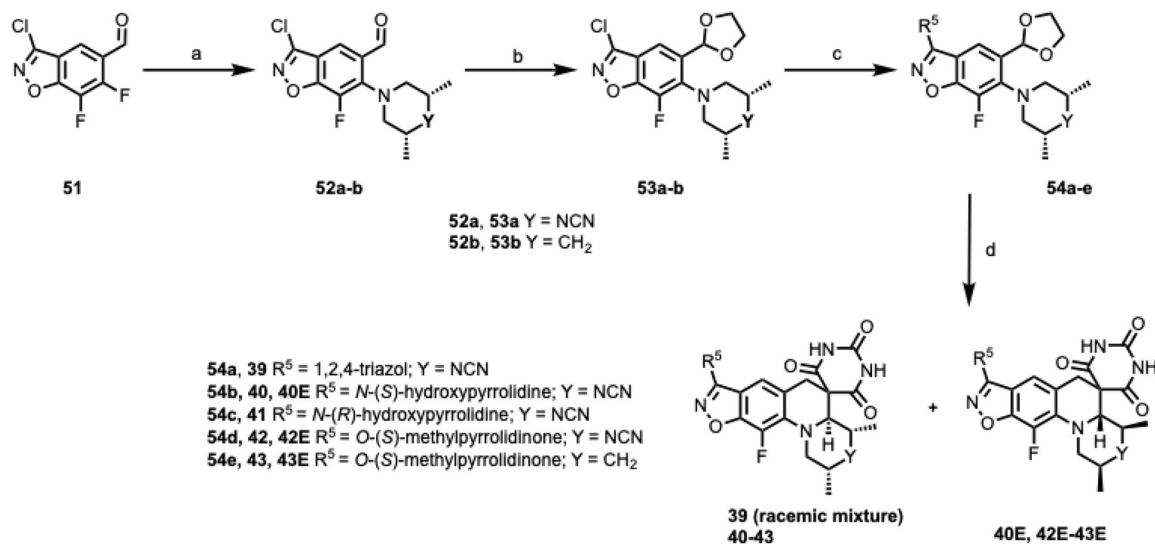


**Scheme 2.**  
 Synthesis of Compounds 8–33.

Reagents and conditions: (a) *For cyclic amines*: DBU, CH<sub>3</sub>CN, 90 °C, 16 h, 30–95%; *For alcohols*: NaH, DMF, 0–30°C, 1 h, 24–95%; (b) EtOH/2M HCl (10:1), 80 °C, 16 h, 3–65%, (c) LiOH, 1,4-dioxane: H<sub>2</sub>O (3:1), 30°C, 1 h, 36%.

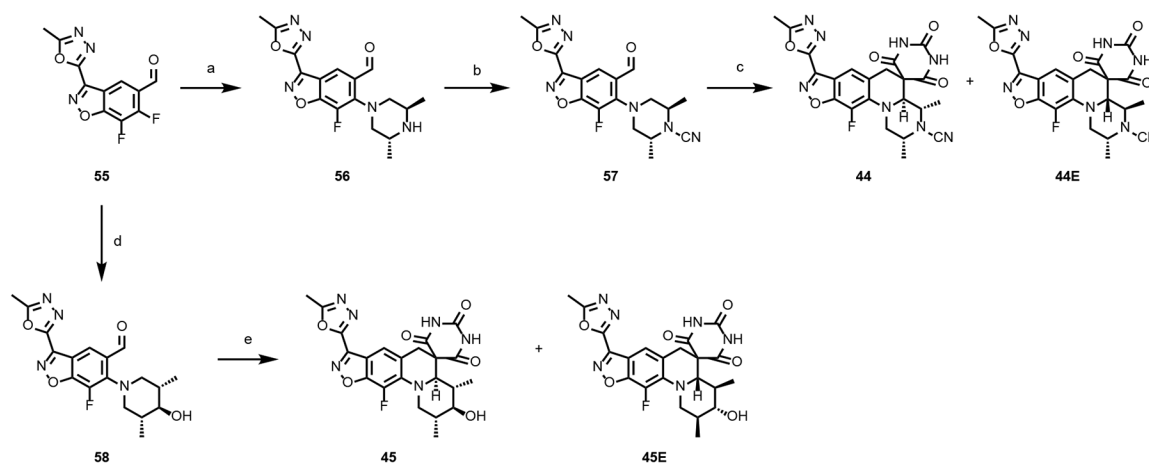
**Scheme 3.****Synthesis of Compounds 34–38.**

Reagents and conditions: (a) amine [*meso*-2,6-dimethylpiperazine (for **50a**) or *meso*-2,6-dimethylpiperazin-1-ol hydrochloride **S3** (for **50b**)], K<sub>2</sub>CO<sub>3</sub>, CH<sub>3</sub>CN, 80°C (MW), 1–2 h or Et<sub>3</sub>N, DMSO, 90–110°C, 2 h, 41–86%; (b) (Ac)<sub>2</sub>O, pyridine, CH<sub>2</sub>Cl<sub>2</sub>, 25°C, 24 h, 80% (for **50c**) or BrCH<sub>2</sub>CN, K<sub>2</sub>CO<sub>3</sub>, acetone, 25°C, 16 h, 68% (for **50d**) (c) barbituric acid, AcOH:H<sub>2</sub>O (4:1) or EtOH, 80°C, 2 h, 2–23%; (d) Br-CN, K<sub>2</sub>CO<sub>3</sub>, acetone, 25°C, 16 h, 14%.

**Scheme 4.**

Synthesis of compounds **39–43**.

Reagents and conditions: (a) *meso*-2,6-dimethylpiperazine-1-carbonitrile hydrochloride (**S5**) for **52a** or *meso*-3,5-dimethylpiperidine for **52b**, K<sub>2</sub>CO<sub>3</sub>, CH<sub>3</sub>CN, 80–110 °C, 1–16 h, 26–81%; (b) ethylene glycol, *p*-TSA, toluene, 130 °C, 16 h, 57–87%; (c) 1*H*-1,2,4-triazol for **54a**, [(*S*)-3-hydroxypyrrolidine for **54b**, (*R*)-3-hydroxypyrrolidine for **54c**, [(*S*)-5-(hydroxymethyl)pyrrolidin-2-one for **54d** and **54e**, DBU in CH<sub>3</sub>CN (for *N*-linked analogues) or NaH in DMF (for *O*-linked analogues), 30–110 °C, 1–16 h, 69–95%; (d) barbituric acid, EtOH:2M HCl (10:1), 80 °C, 16 h, 10–27%.

**Scheme 5:**

Synthesis of compounds **44** and **45**.

Reagents and conditions: (a) (2*R*,6*R*)-2,6-dimethylpiperazine dihydrochloride,  $K_2CO_3$ ,  $CH_3CN$ :water (20:1), 90 °C, 13 h, 92%; (b) Br-CN,  $K_2CO_3$ , acetone, 27 °C, 9 h, 77%; (c) barbituric acid, EtOH, 110 °C, 20 h, 4–10%; (d) (*meso*-3*S*,4*r*,5*R*)-3,5-dimethylpiperidin-4-ol hydrochloride,  $K_2CO_3$ ,  $CH_3CN$ :water (10:1), 90 °C, 1 h, 89%; (e) barbituric acid, EtOH, 80 °C, 16 h, 10–18%.

**Table 1.**

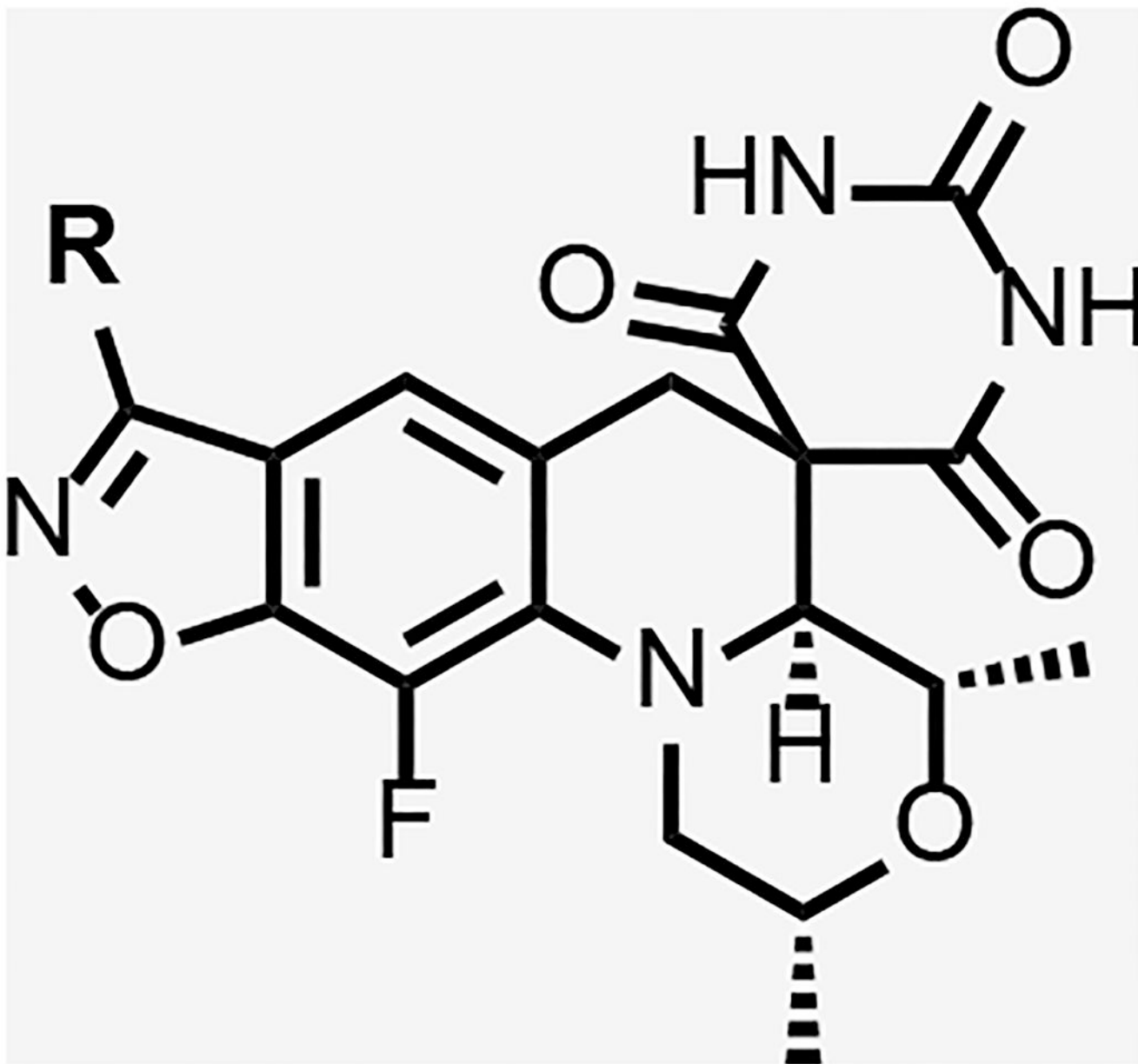
Author Manuscript

Author Manuscript

Author Manuscript

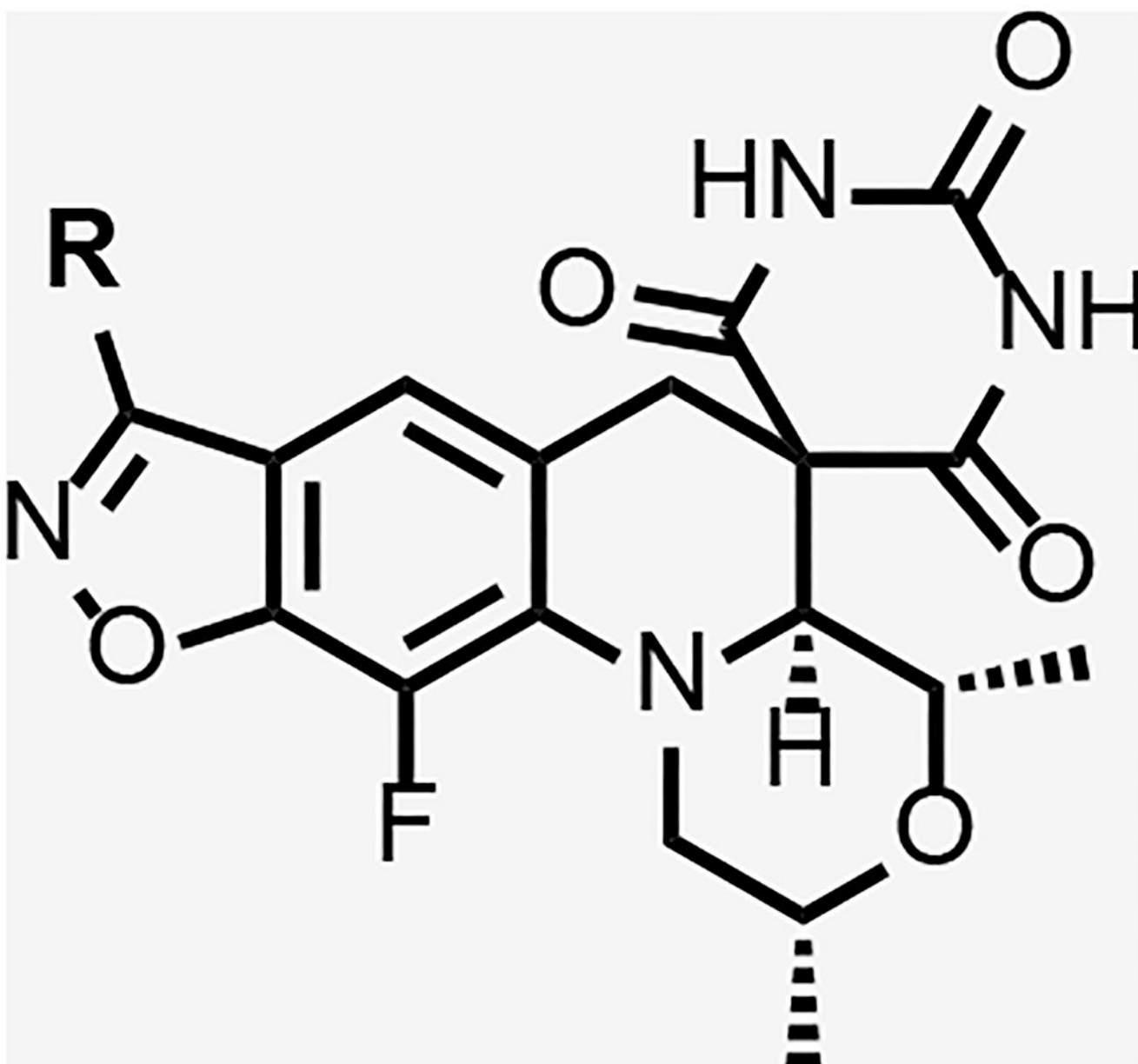
Author Manuscript

## Data for reference compounds

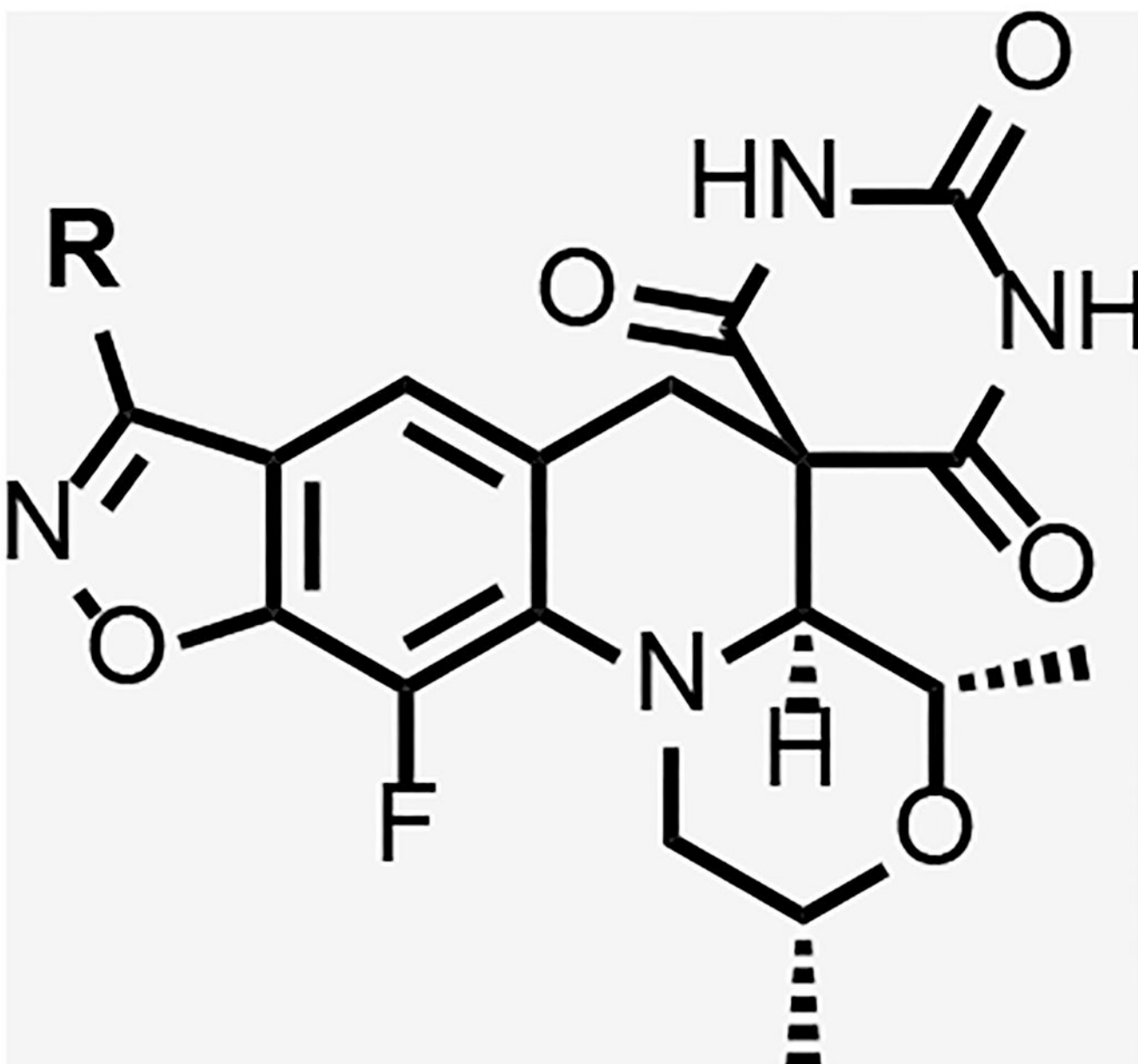


Compound	R	Solubility ( $\mu\text{M}$ )	logD	<i>Mtb</i> gyrase IC <sub>50</sub> ( $\mu\text{M}$ )	<i>Sau</i> gyrase IC <sub>50</sub> ( $\mu\text{M}$ )	<i>Mtb</i> <sup>a</sup> MIC ( $\mu\text{M}$ )	<i>Sau</i> <sup>b</sup> MIC ( $\mu\text{M}$ )	<i>Ecol</i> <sup>f</sup> MIC ( $\mu\text{M}$ )	HepG2 IC <sub>50</sub> ( $\mu\text{M}$ )
Zoliflodacin 4		160	2.0	32	4.3	7.0	0.35	1.4	>50

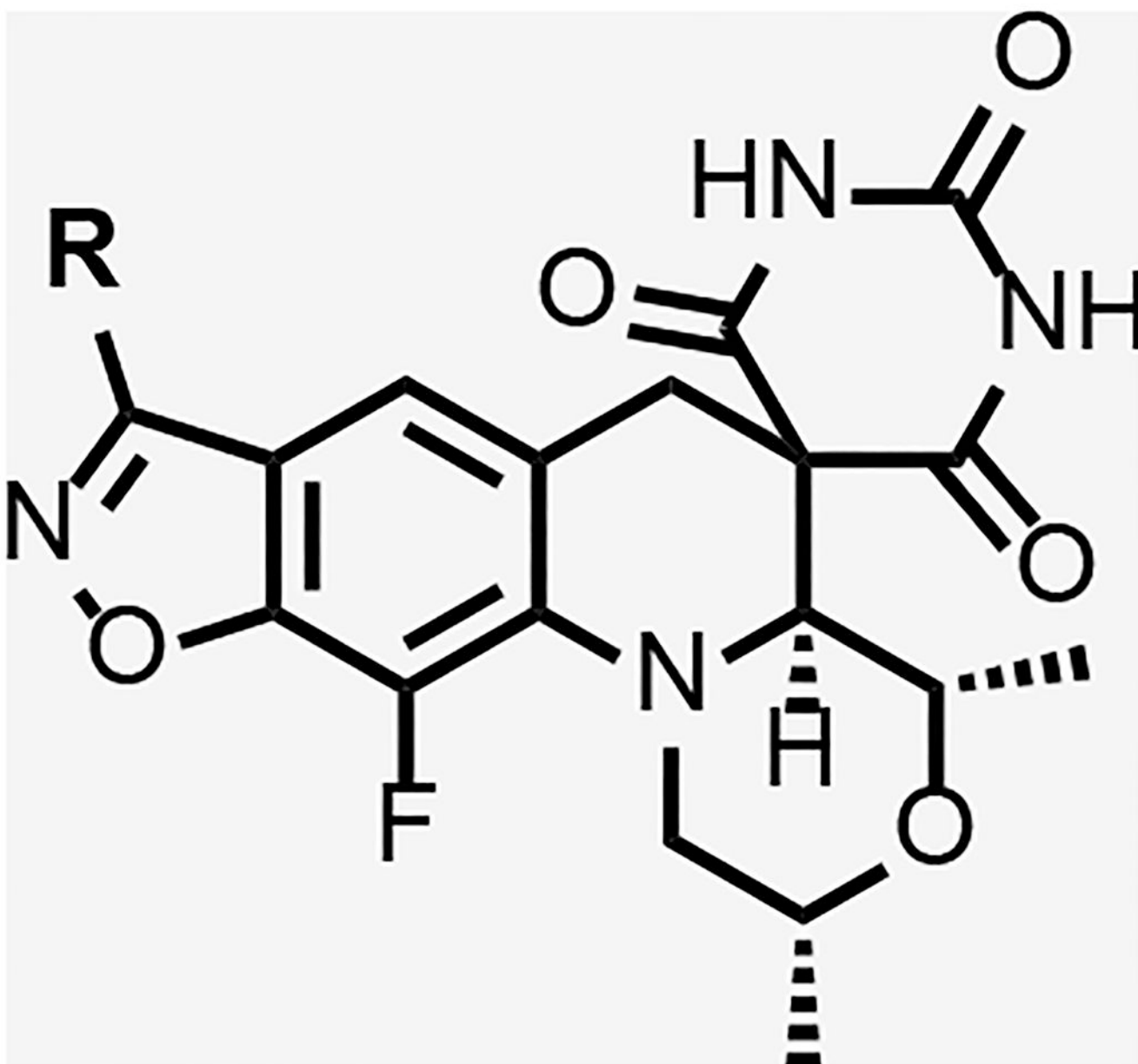




Compound	R	Solubility ( $\mu\text{M}$ )	logD	<i>Mtb</i> gyrase IC <sub>50</sub> ( $\mu\text{M}$ )	<i>Sau</i> gyrase IC <sub>50</sub> ( $\mu\text{M}$ )	<i>Mtb</i> <sup>a</sup> MIC ( $\mu\text{M}$ )	<i>Sau</i> <sup>b</sup> MIC ( $\mu\text{M}$ )	<i>Ecol</i> <sup>f</sup> MIC ( $\mu\text{M}$ )	HepG2 IC <sub>50</sub> ( $\mu\text{M}$ )
Methyl-oxadiazole 5		140	2.3	2	ND	1.7	0.45	31	>300



Compound	R	Solubility ( $\mu\text{M}$ )	logD	<i>Mtb</i> gyrase IC <sub>50</sub> ( $\mu\text{M}$ )	<i>Sau</i> gyrase IC <sub>50</sub> ( $\mu\text{M}$ )	<i>Mtb</i> <sup>a</sup> MIC ( $\mu\text{M}$ )	<i>Sau</i> <sup>b</sup> MIC ( $\mu\text{M}$ )	<i>Ecol</i> <sup>c</sup> MIC ( $\mu\text{M}$ )	HepG2 IC <sub>50</sub> ( $\mu\text{M}$ )
Triazole 7		115	1.6	18	1.7	2.0	0.24	2.0	26



Compound	R	Solubility ( $\mu\text{M}$ )	logD	<i>Mtb</i> gyrase IC <sub>50</sub> ( $\mu\text{M}$ )	<i>Sau</i> gyrase IC <sub>50</sub> ( $\mu\text{M}$ )	<i>Mtb</i> <sup>a</sup> MIC ( $\mu\text{M}$ )	<i>Sau</i> <sup>b</sup> MIC ( $\mu\text{M}$ )	<i>Ecol</i> <sup>c</sup> MIC ( $\mu\text{M}$ )	HepG2 IC <sub>50</sub> ( $\mu\text{M}$ )
Moxifloxacin		>200 <sup>45</sup>	0.3 <sup>45</sup>	10	6.8	0.17	0.14	0.14	>50

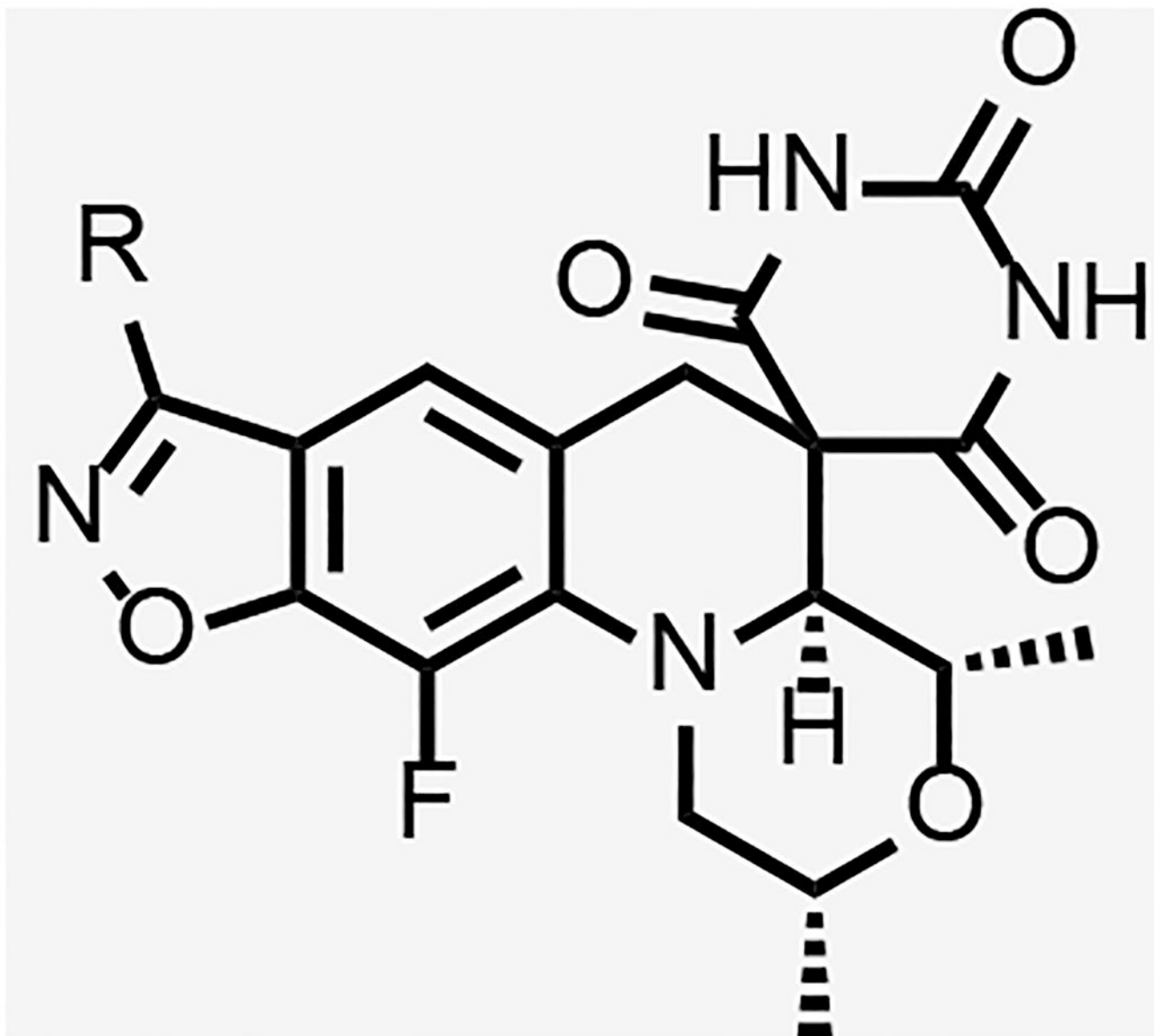
<sup>a</sup> *M. tuberculosis* H37Rv;

<sup>b</sup> *S. aureus* ATTC 25923

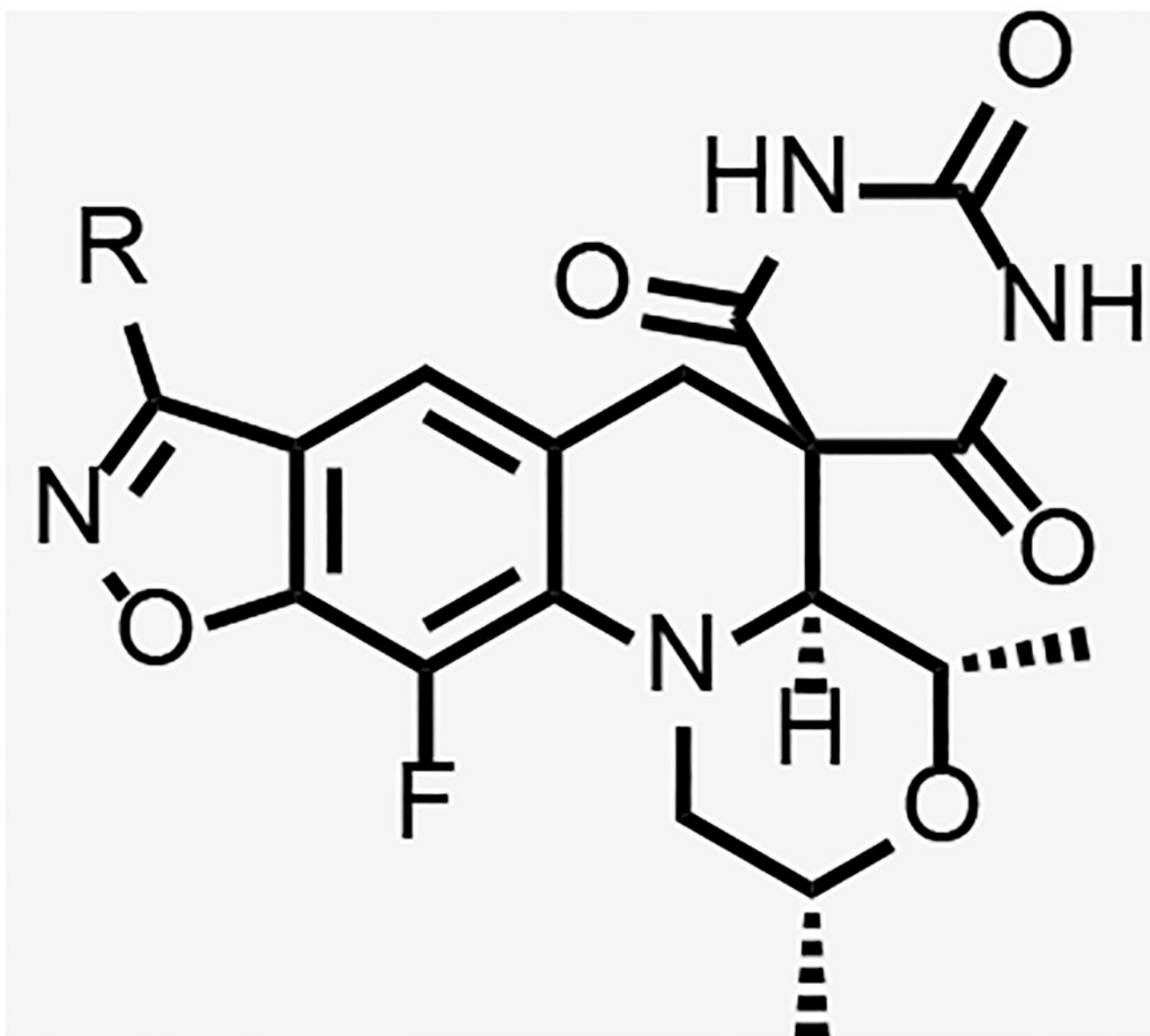
<sup>c</sup> *E. coli* ATTC 25922

Table 2.

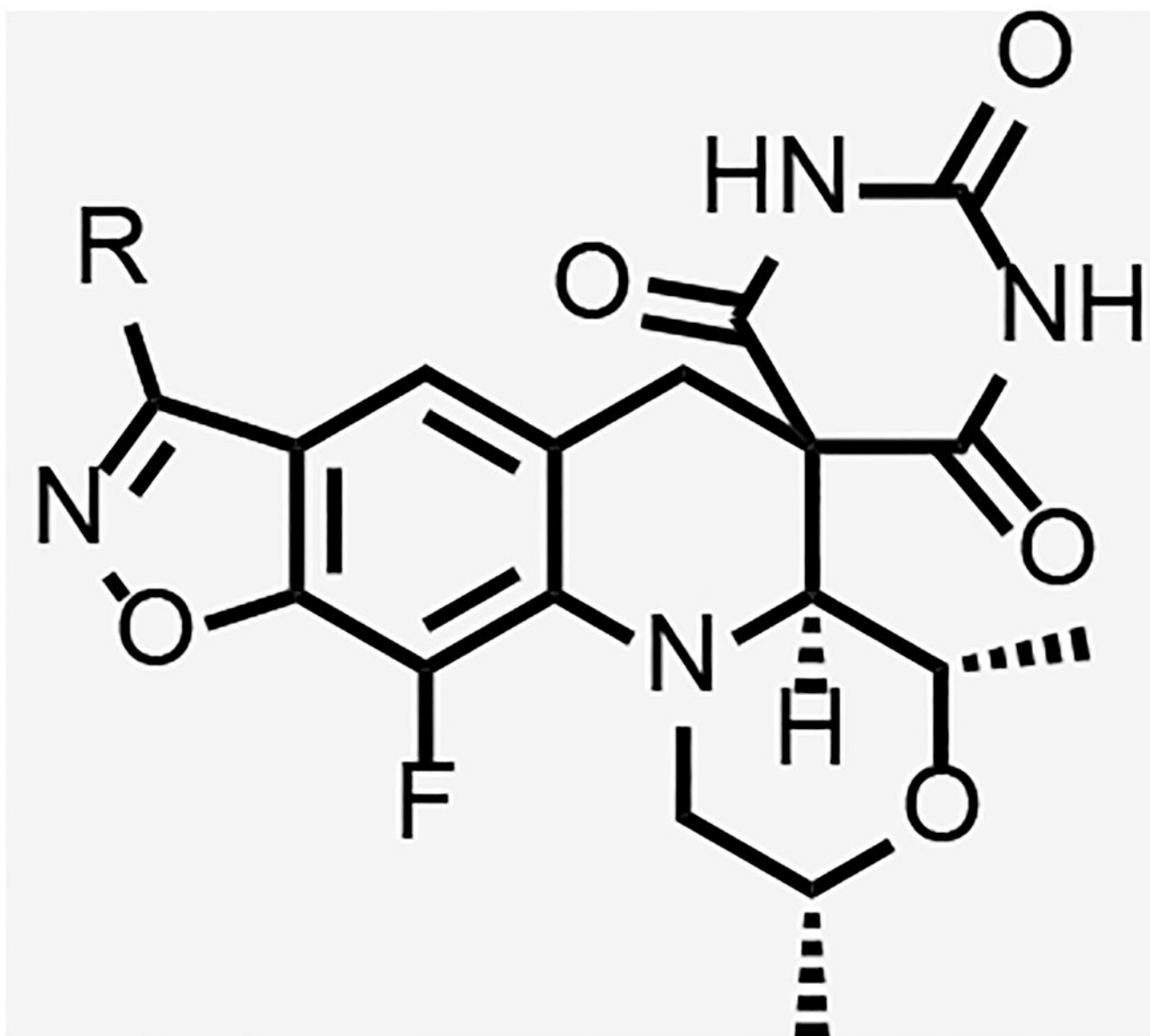
Data for SPTs with pyrrolidine and piperidine benzisoxazole substituents



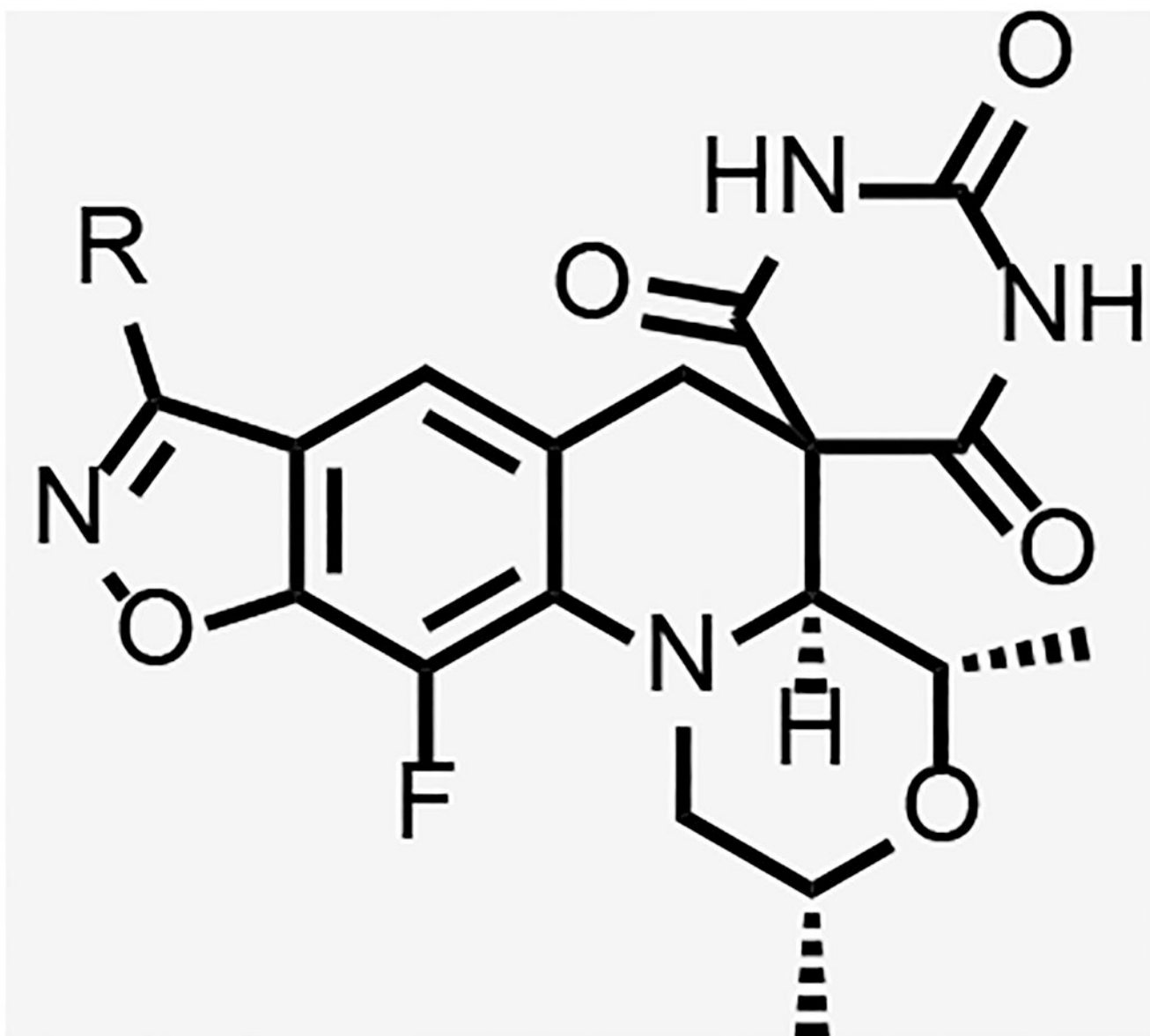
Compound	R	Solubility ( $\mu\text{M}$ )	logD	<i>Mtb</i> gyrase IC <sub>50</sub> ( $\mu\text{M}$ )	<i>Sau</i> gyrase IC <sub>50</sub> ( $\mu\text{M}$ )	<i>Mtb</i> <sup>a</sup> MIC ( $\mu\text{M}$ )	<i>Sau</i> <sup>b</sup> MIC ( $\mu\text{M}$ )	<i>Ecol</i> <sup>c</sup> MIC ( $\mu\text{M}$ )	HepG2 IC <sub>50</sub> ( $\mu\text{M}$ )
8		190	1.4	20	6.9	5.9	64	>125	>50



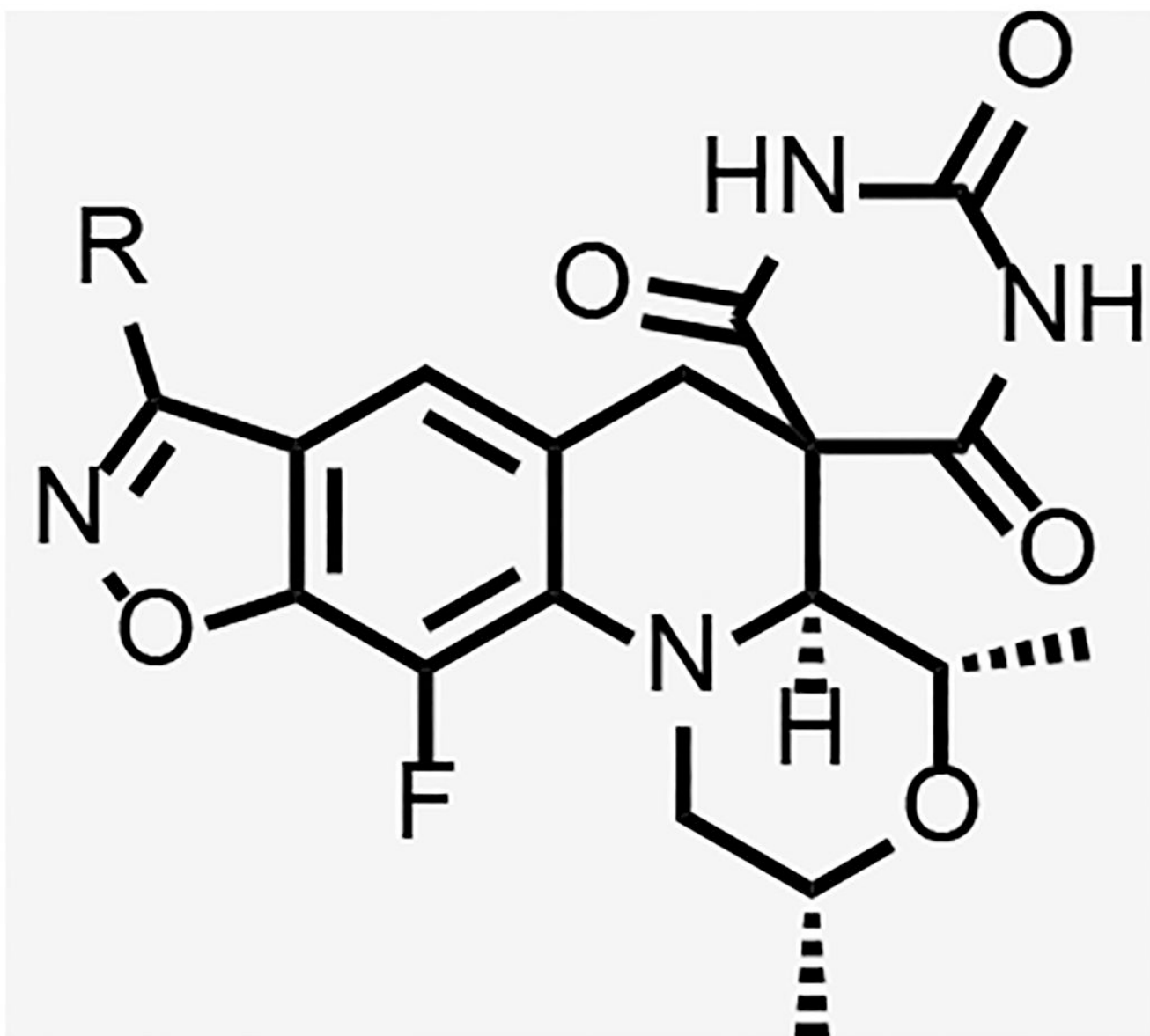
Compound	R	Solubility ( $\mu\text{M}$ )	logD	<i>Mtb</i> gyrase IC <sub>50</sub> ( $\mu\text{M}$ )	<i>Sau</i> gyrase IC <sub>50</sub> ( $\mu\text{M}$ )	<i>Mtb</i> <sup>a</sup> MIC ( $\mu\text{M}$ )	<i>Sau</i> <sup>b</sup> MIC ( $\mu\text{M}$ )	<i>Ecol</i> <sup>c</sup> MIC ( $\mu\text{M}$ )	HepG2 IC <sub>50</sub> ( $\mu\text{M}$ )
9		>200	1.4	-	-	3.9	64	>125	>50



Compound	R	Solubility ( $\mu\text{M}$ )	logD	<i>Mtb</i> gyrase IC <sub>50</sub> ( $\mu\text{M}$ )	<i>Sau</i> gyrase IC <sub>50</sub> ( $\mu\text{M}$ )	<i>Mtb</i> <sup>a</sup> MIC ( $\mu\text{M}$ )	<i>Sau</i> <sup>b</sup> MIC ( $\mu\text{M}$ )	<i>Ecol</i> <sup>c</sup> MIC ( $\mu\text{M}$ )	HepG2 IC <sub>50</sub> ( $\mu\text{M}$ )
10		>200	1.2	16	6.6	5.9	>125	>125	>50

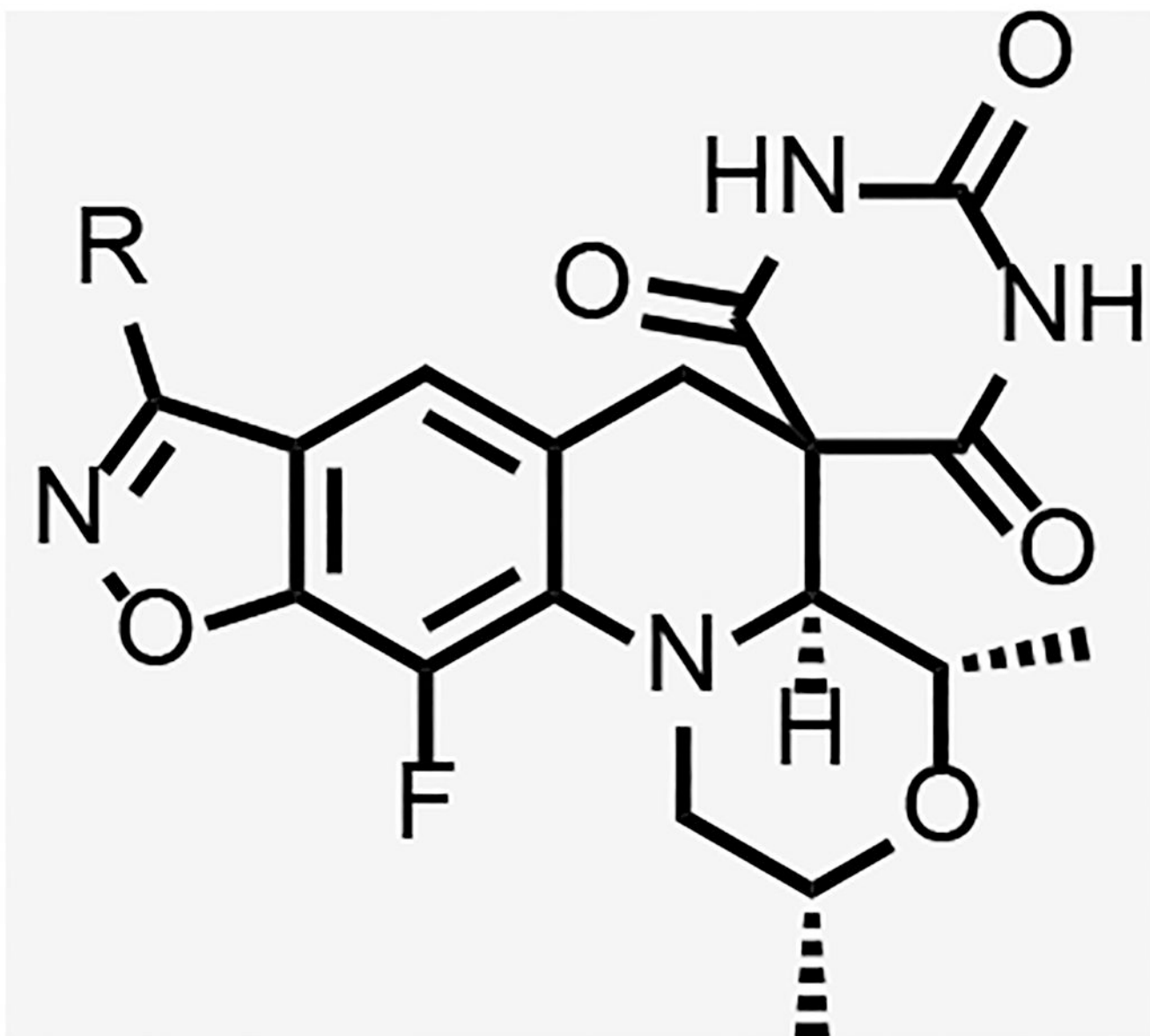


Compound	R	Solubility ( $\mu\text{M}$ )	logD	<i>Mtb</i> gyrase IC <sub>50</sub> ( $\mu\text{M}$ )	<i>Sau</i> gyrase IC <sub>50</sub> ( $\mu\text{M}$ )	<i>Mtb</i> <sup>a</sup> MIC ( $\mu\text{M}$ )	<i>Sau</i> <sup>b</sup> MIC ( $\mu\text{M}$ )	<i>Ecol</i> <sup>c</sup> MIC ( $\mu\text{M}$ )	HepG2 IC <sub>50</sub> ( $\mu\text{M}$ )
11		190	0.89	-	-	31	>125	>125	-

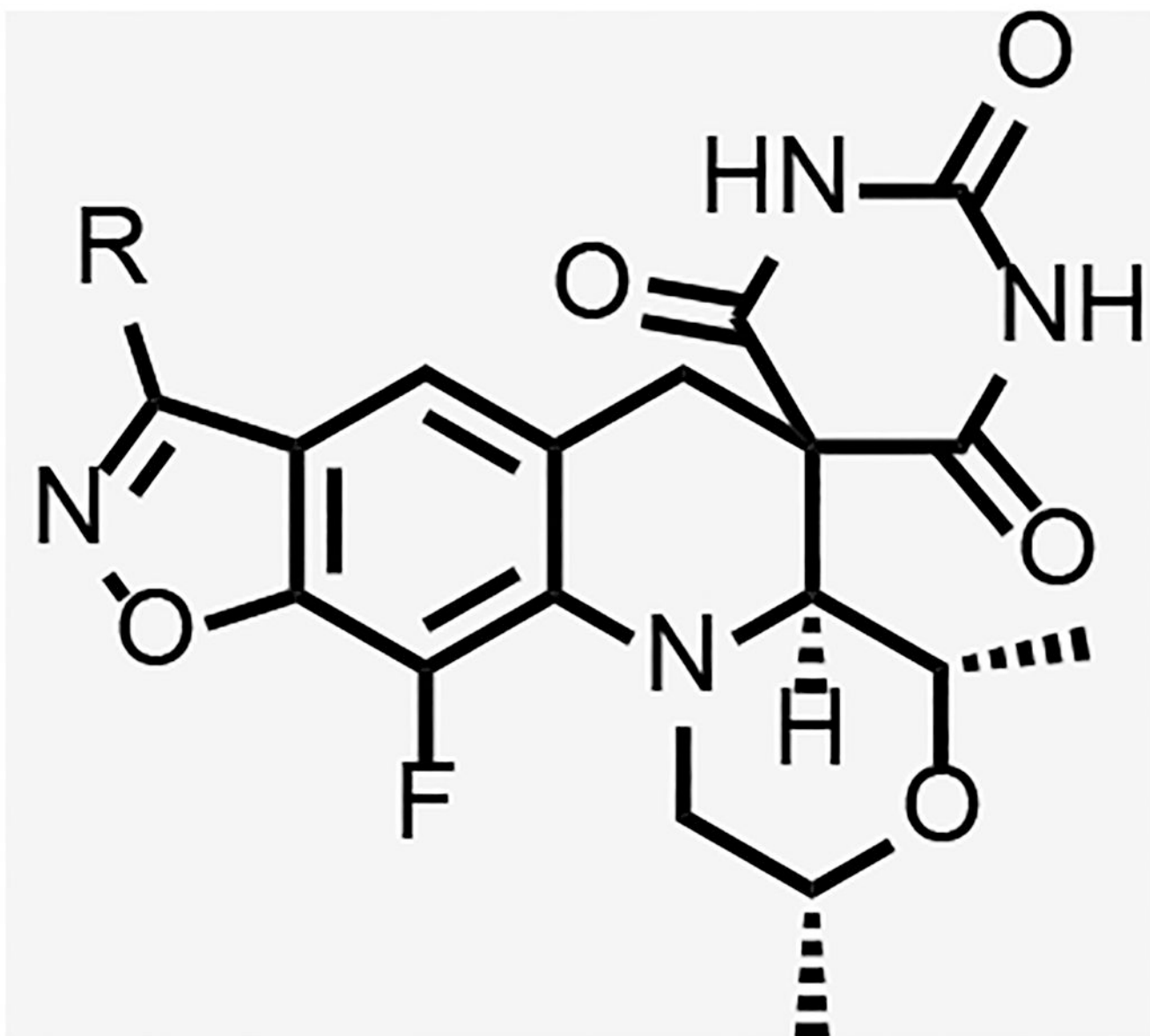


Compound	R	Solubility ( $\mu\text{M}$ )	logD	<i>Mtb</i> gyrase IC <sub>50</sub> ( $\mu\text{M}$ )	<i>Sau</i> gyrase IC <sub>50</sub> ( $\mu\text{M}$ )	<i>Mtb</i> <sup>a</sup> MIC ( $\mu\text{M}$ )	<i>Sau</i> <sup>b</sup> MIC ( $\mu\text{M}$ )	<i>Ecol</i> <sup>c</sup> MIC ( $\mu\text{M}$ )	HepG2 IC <sub>50</sub> ( $\mu\text{M}$ )
12		>200	0.76	-	-	16	>125	>125	>300

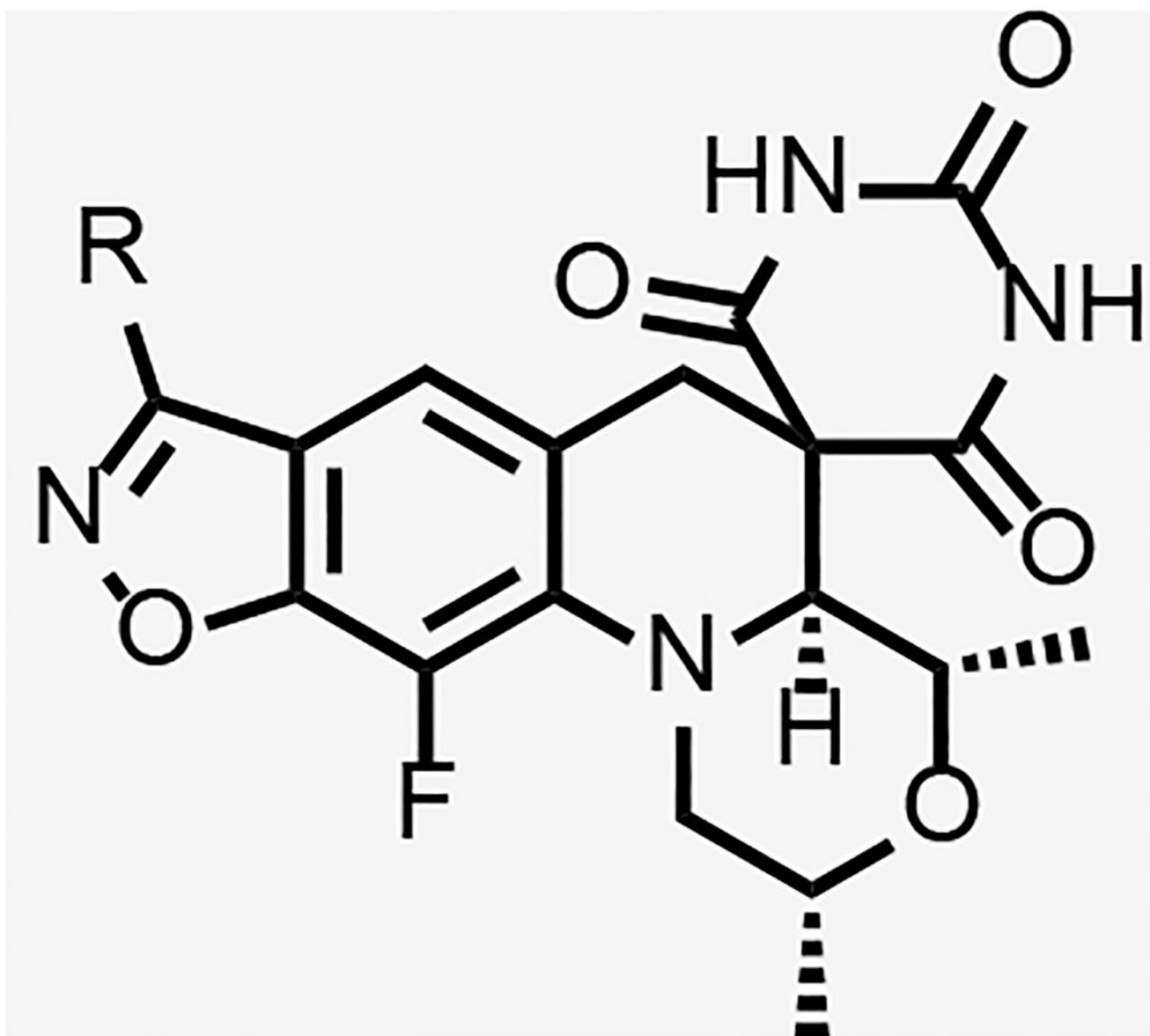




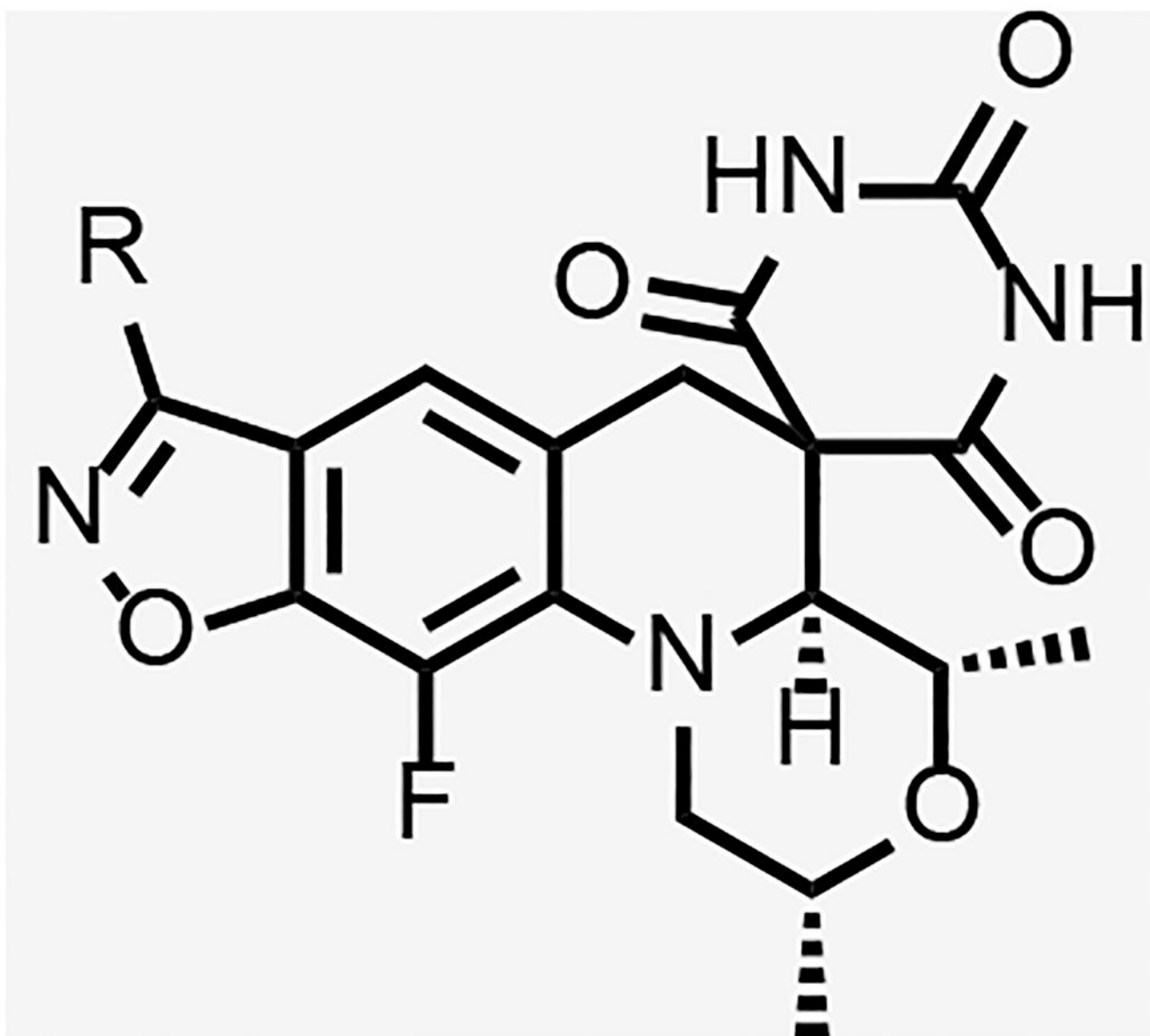
Compound	R	Solubility ( $\mu\text{M}$ )	logD	<i>Mtb</i> gyrase IC <sub>50</sub> ( $\mu\text{M}$ )	<i>Sau</i> gyrase IC <sub>50</sub> ( $\mu\text{M}$ )	<i>Mtb</i> <sup>a</sup> MIC ( $\mu\text{M}$ )	<i>Sau</i> <sup>b</sup> MIC ( $\mu\text{M}$ )	<i>Ecol</i> <sup>c</sup> MIC ( $\mu\text{M}$ )	HepG2 IC <sub>50</sub> ( $\mu\text{M}$ )
13		140	2.0	77	-	31	>125	>125	>300



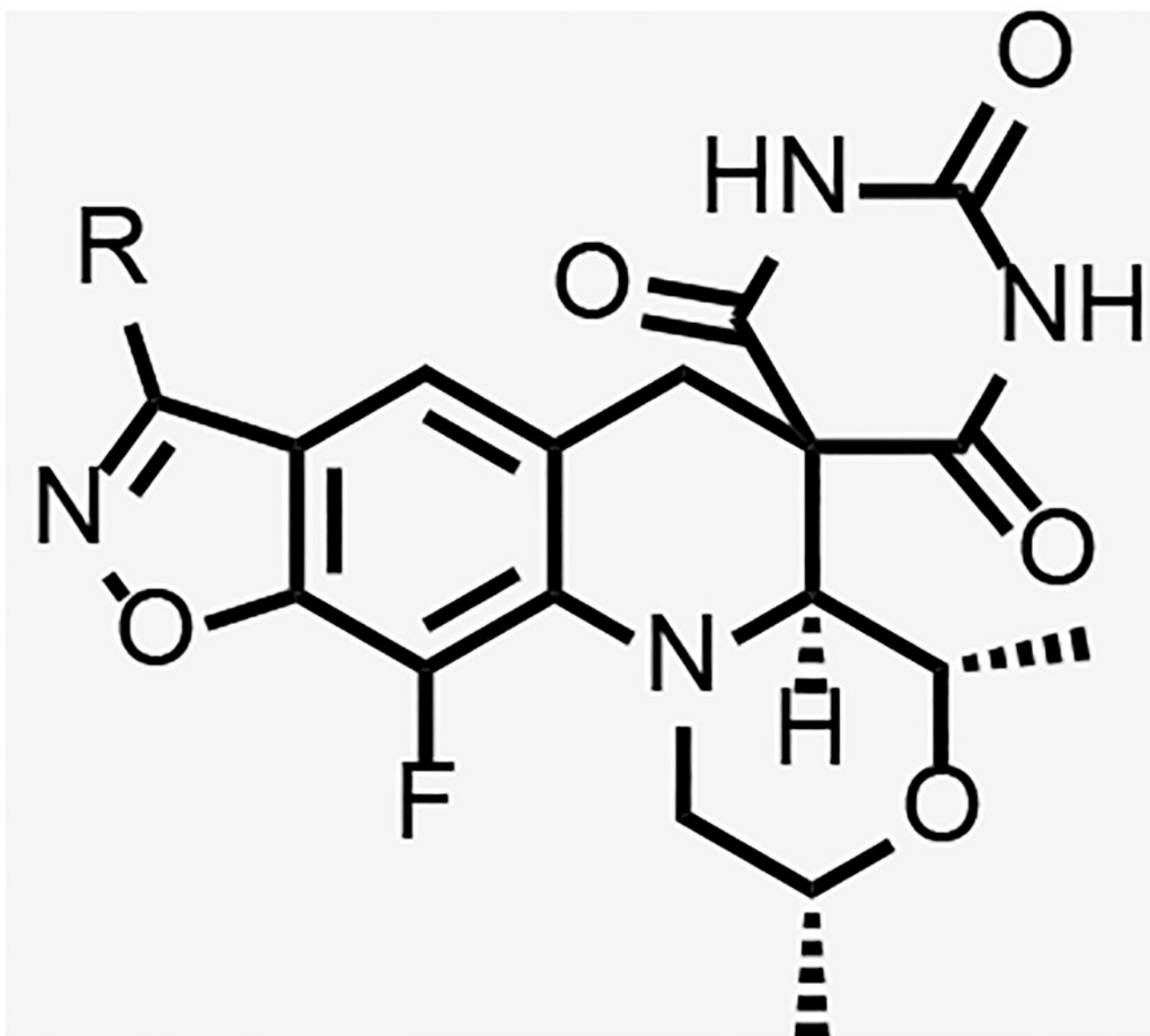
Compound	R	Solubility ( $\mu\text{M}$ )	logD	<i>Mtb</i> gyrase IC <sub>50</sub> ( $\mu\text{M}$ )	<i>Sau</i> gyrase IC <sub>50</sub> ( $\mu\text{M}$ )	<i>Mtb</i> <sup>a</sup> MIC ( $\mu\text{M}$ )	<i>Sau</i> <sup>b</sup> MIC ( $\mu\text{M}$ )	<i>Ecol</i> <sup>c</sup> MIC ( $\mu\text{M}$ )	HepG2 IC <sub>50</sub> ( $\mu\text{M}$ )
14		170	1.7	18	-	16	>125	>125	>300



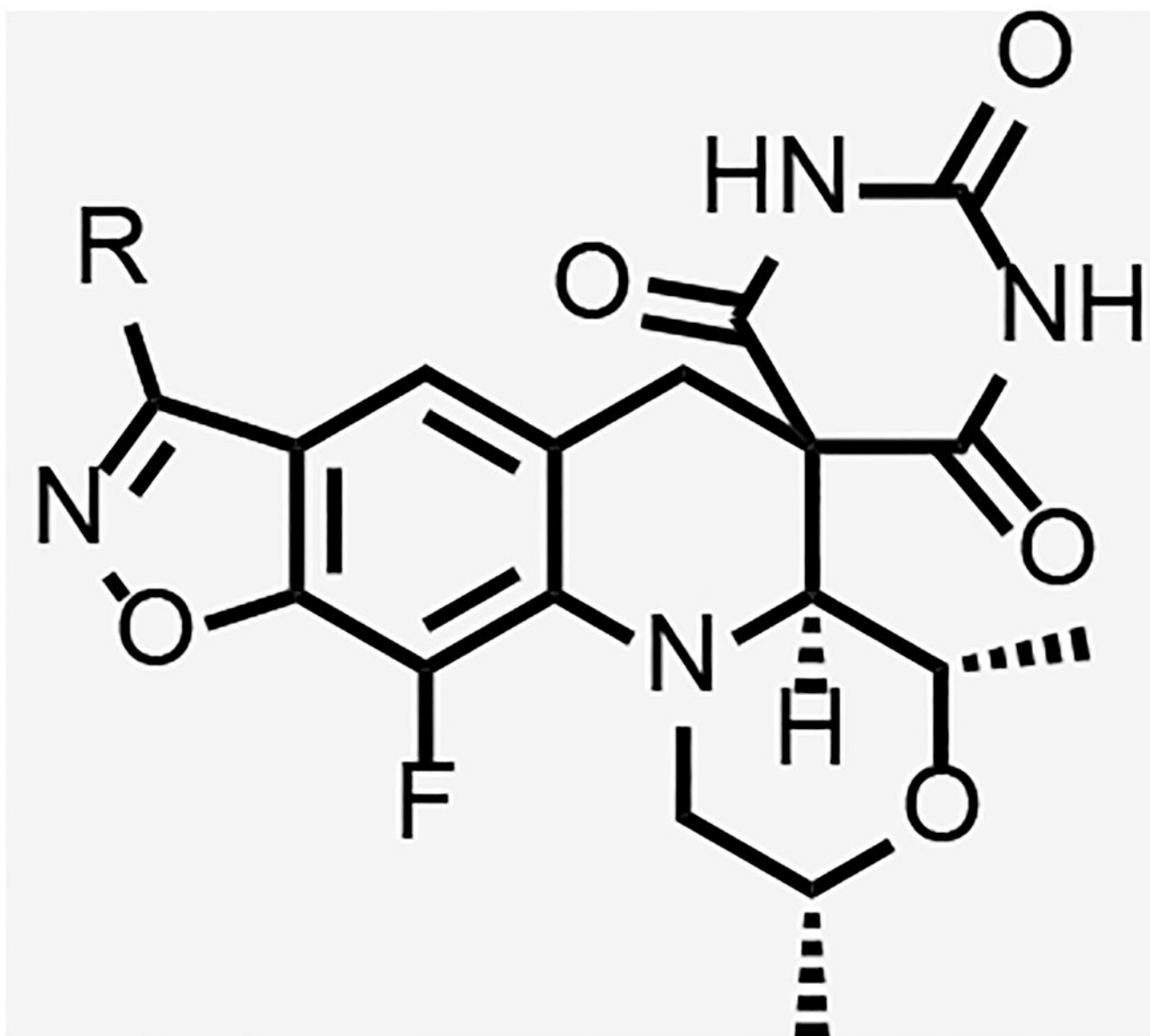
Compound	R	Solubility ( $\mu\text{M}$ )	logD	<i>Mtb</i> gyrase IC <sub>50</sub> ( $\mu\text{M}$ )	<i>Sau</i> gyrase IC <sub>50</sub> ( $\mu\text{M}$ )	<i>Mtb</i> <sup>a</sup> MIC ( $\mu\text{M}$ )	<i>Sau</i> <sup>b</sup> MIC ( $\mu\text{M}$ )	<i>Ecol</i> <sup>c</sup> MIC ( $\mu\text{M}$ )	HepG2 IC <sub>50</sub> ( $\mu\text{M}$ )
15		175	1.6	-	-	>250	>250	>250	>50



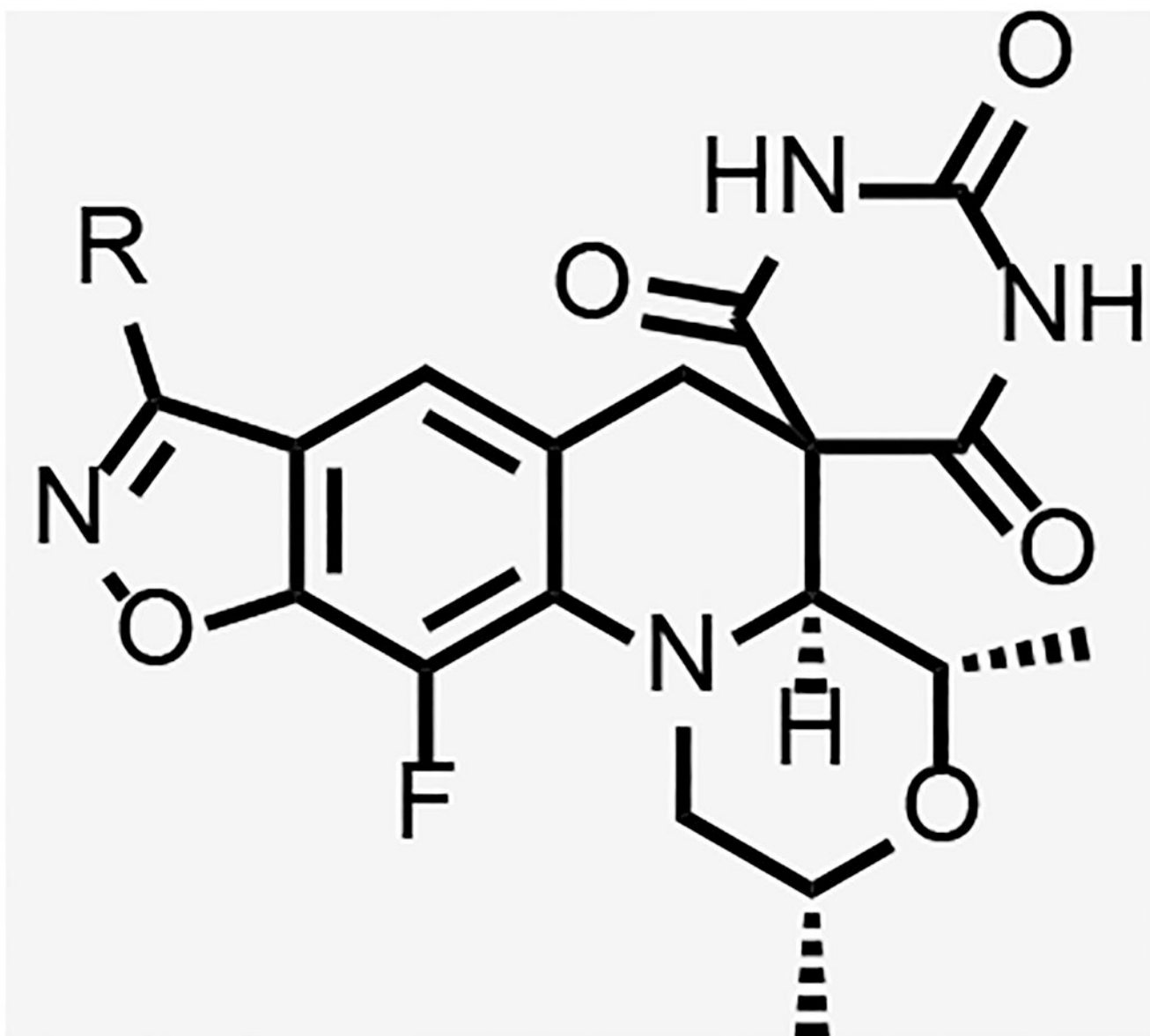
Compound	R	Solubility ( $\mu\text{M}$ )	logD	<i>Mtb</i> gyrase IC <sub>50</sub> ( $\mu\text{M}$ )	<i>Sau</i> gyrase IC <sub>50</sub> ( $\mu\text{M}$ )	<i>Mtb</i> <sup>a</sup> MIC ( $\mu\text{M}$ )	<i>Sau</i> <sup>b</sup> MIC ( $\mu\text{M}$ )	<i>Ecol</i> <sup>c</sup> MIC ( $\mu\text{M}$ )	HepG2 IC <sub>50</sub> ( $\mu\text{M}$ )
16		>200	0.16	34	-	63	125	125	>50



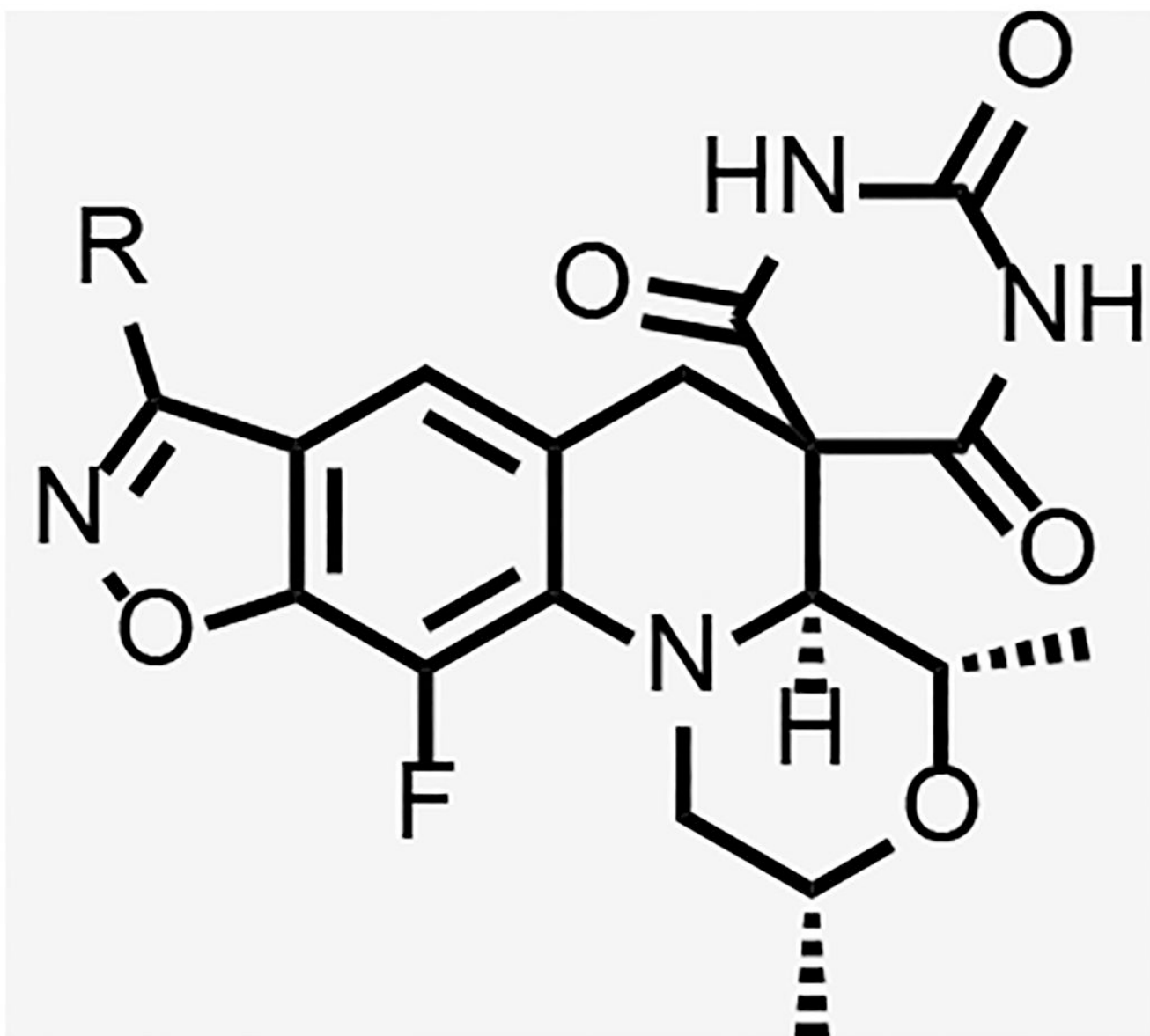
Compound	R	Solubility ( $\mu\text{M}$ )	logD	<i>Mtb</i> gyrase IC <sub>50</sub> ( $\mu\text{M}$ )	<i>Sau</i> gyrase IC <sub>50</sub> ( $\mu\text{M}$ )	<i>Mtb</i> <sup>a</sup> MIC ( $\mu\text{M}$ )	<i>Sau</i> <sup>b</sup> MIC ( $\mu\text{M}$ )	<i>Ecol</i> <sup>c</sup> MIC ( $\mu\text{M}$ )	HepG2 IC <sub>50</sub> ( $\mu\text{M}$ )
17		185	0.27	-	-	63	125	125	>300



Compound	R	Solubility ( $\mu\text{M}$ )	logD	<i>Mtb</i> gyrase IC <sub>50</sub> ( $\mu\text{M}$ )	<i>Sau</i> gyrase IC <sub>50</sub> ( $\mu\text{M}$ )	<i>Mtb</i> <sup>a</sup> MIC ( $\mu\text{M}$ )	<i>Sau</i> <sup>b</sup> MIC ( $\mu\text{M}$ )	<i>Ecol</i> <sup>c</sup> MIC ( $\mu\text{M}$ )	HepG2 IC <sub>50</sub> ( $\mu\text{M}$ )
18		5	2.2	-	-	4.0	2.0	31	>300

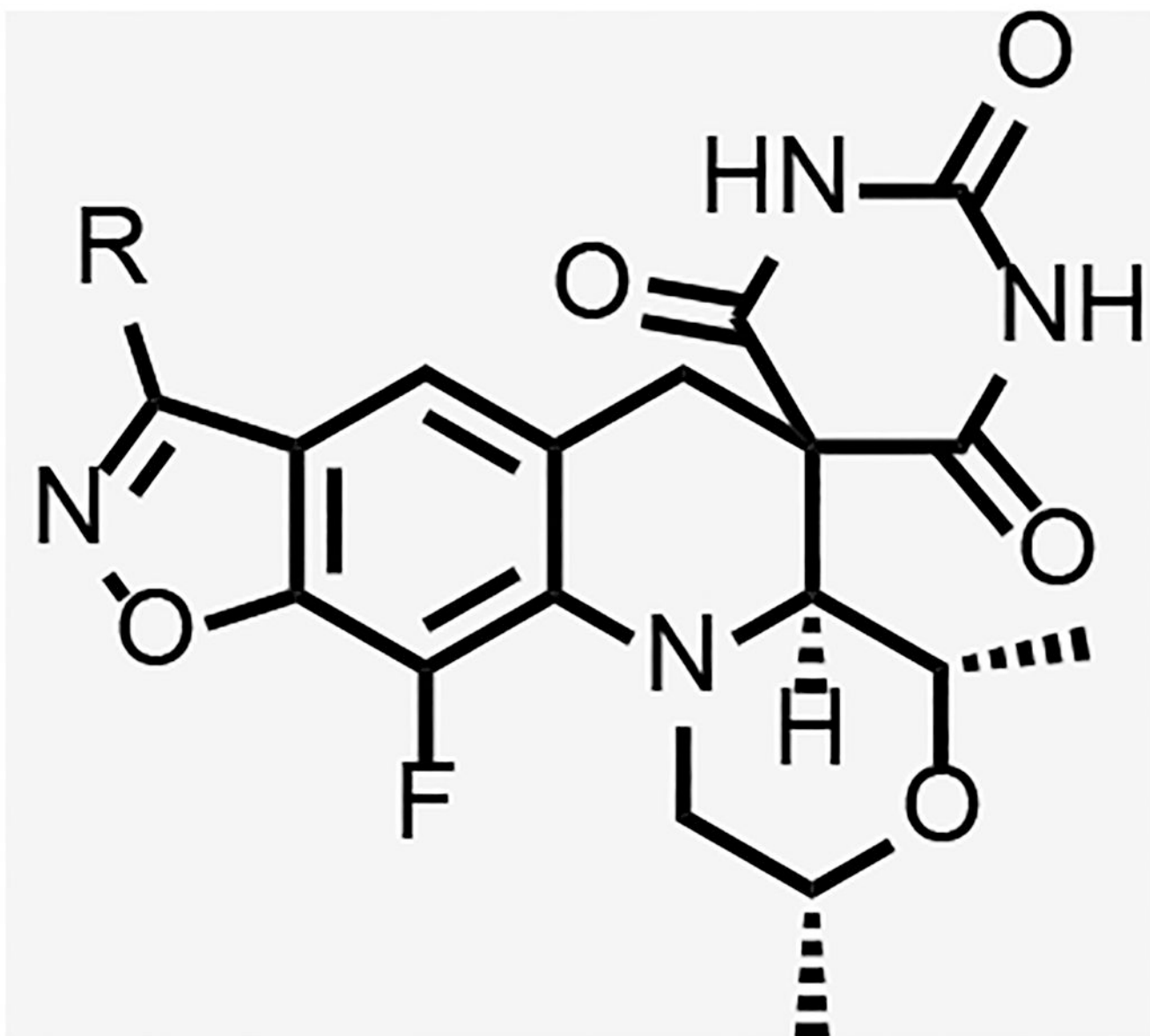


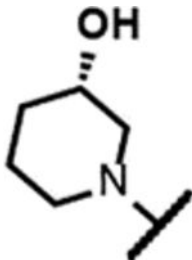
Compound	R	Solubility ( $\mu\text{M}$ )	logD	<i>Mtb</i> gyrase IC <sub>50</sub> ( $\mu\text{M}$ )	<i>Sau</i> gyrase IC <sub>50</sub> ( $\mu\text{M}$ )	<i>Mtb</i> <sup>a</sup> MIC ( $\mu\text{M}$ )	<i>Sau</i> <sup>b</sup> MIC ( $\mu\text{M}$ )	<i>Ecol</i> <sup>c</sup> MIC ( $\mu\text{M}$ )	HepG2 IC <sub>50</sub> ( $\mu\text{M}$ )
19		>200	1.7	10	-	4.0	>125	31	ND

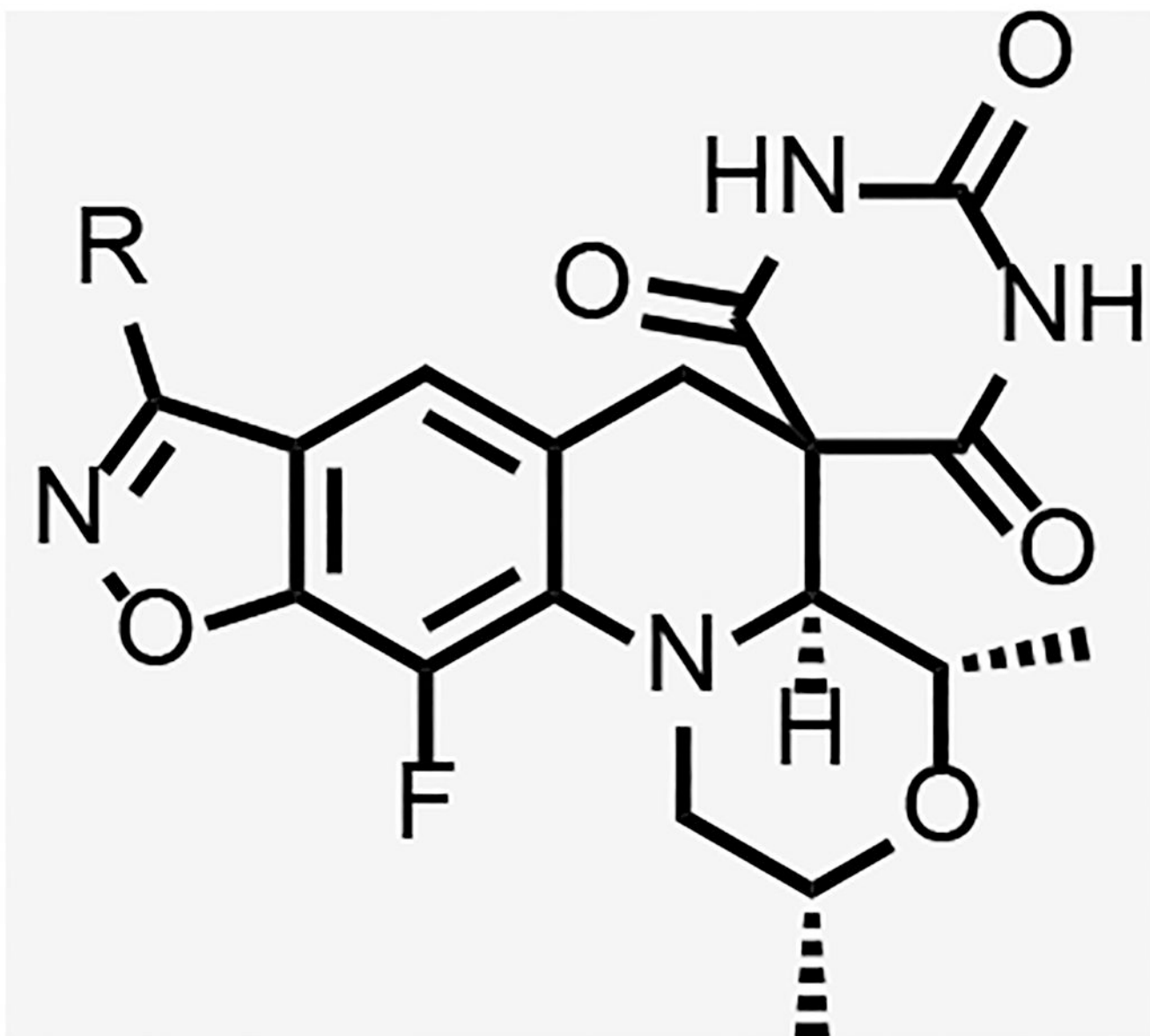


Compound	R	Solubility ( $\mu\text{M}$ )	logD	<i>Mtb</i> gyrase IC <sub>50</sub> ( $\mu\text{M}$ )	<i>Sau</i> gyrase IC <sub>50</sub> ( $\mu\text{M}$ )	<i>Mtb</i> <sup>a</sup> MIC ( $\mu\text{M}$ )	<i>Sau</i> <sup>b</sup> MIC ( $\mu\text{M}$ )	<i>Ecol</i> <sup>c</sup> MIC ( $\mu\text{M}$ )	HepG2 IC <sub>50</sub> ( $\mu\text{M}$ )
20		150	-	-	-	>125	>125	>125	ND





Compound	R	Solubility ( $\mu\text{M}$ )	logD	<i>Mtb</i> gyrase IC <sub>50</sub> ( $\mu\text{M}$ )	<i>Sau</i> gyrase IC <sub>50</sub> ( $\mu\text{M}$ )	<i>Mtb</i> <sup>a</sup> MIC ( $\mu\text{M}$ )	<i>Sau</i> <sup>b</sup> MIC ( $\mu\text{M}$ )	<i>Ecol</i> <sup>c</sup> MIC ( $\mu\text{M}$ )	HepG2 IC <sub>50</sub> ( $\mu\text{M}$ )
21		>200	1.9	-	-	16	94	>125	>50



Compound	R	Solubility ( $\mu\text{M}$ )	logD	<i>Mtb</i> gyrase IC <sub>50</sub> ( $\mu\text{M}$ )	<i>Sau</i> gyrase IC <sub>50</sub> ( $\mu\text{M}$ )	<i>Mtb</i> <sup>a</sup> MIC ( $\mu\text{M}$ )	<i>Sau</i> <sup>b</sup> MIC ( $\mu\text{M}$ )	<i>Ecol</i> <sup>c</sup> MIC ( $\mu\text{M}$ )	HepG2 IC <sub>50</sub> ( $\mu\text{M}$ )
22		>200	1.8	-	-	10	94	>125	>50

<sup>a</sup> *M. tuberculosis* H37Rv;

<sup>b</sup> *S. aureus* ATTC 25923

<sup>c</sup> *E. coli* ATTC 25922

Author Manuscript

Author Manuscript

Author Manuscript

Author Manuscript

**Table 3.**

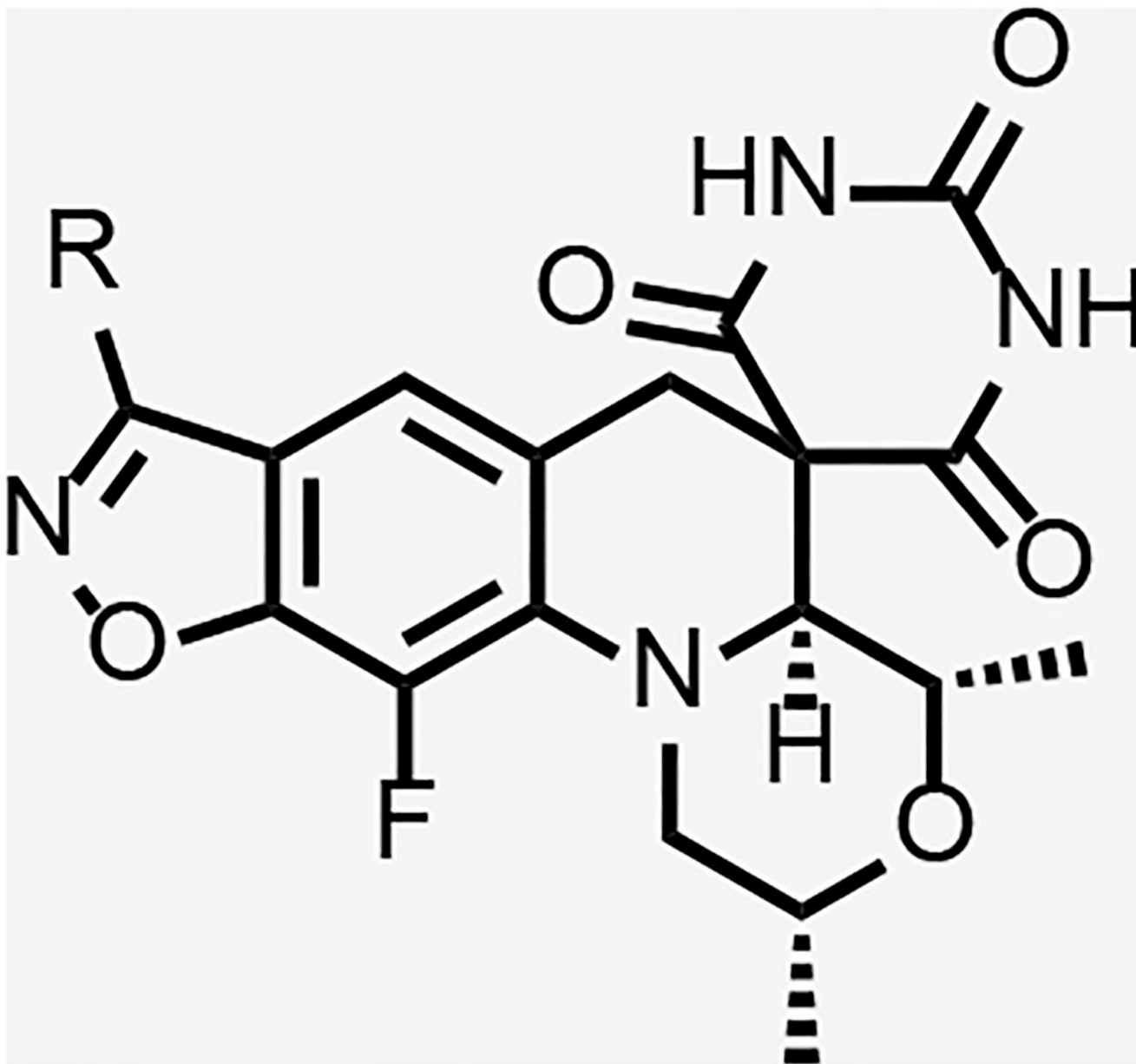
Author Manuscript

Author Manuscript

Author Manuscript

Author Manuscript

Data for SPTs with ether-linked benzisoxazole substituents



Compound	R	Solubility ( $\mu\text{M}$ )	logD	<i>Mtb</i> gyrase IC <sub>50</sub> ( $\mu\text{M}$ )	<i>Mtb</i> <sup>a</sup> MIC ( $\mu\text{M}$ )	<i>Sau</i> <sup>b</sup> MIC ( $\mu\text{M}$ )	<i>Ecol</i> <sup>c</sup> MIC ( $\mu\text{M}$ )	HepG2 IC <sub>50</sub> ( $\mu\text{M}$ )
23		185	1.4	2.6	1.0	>125	>125	>100

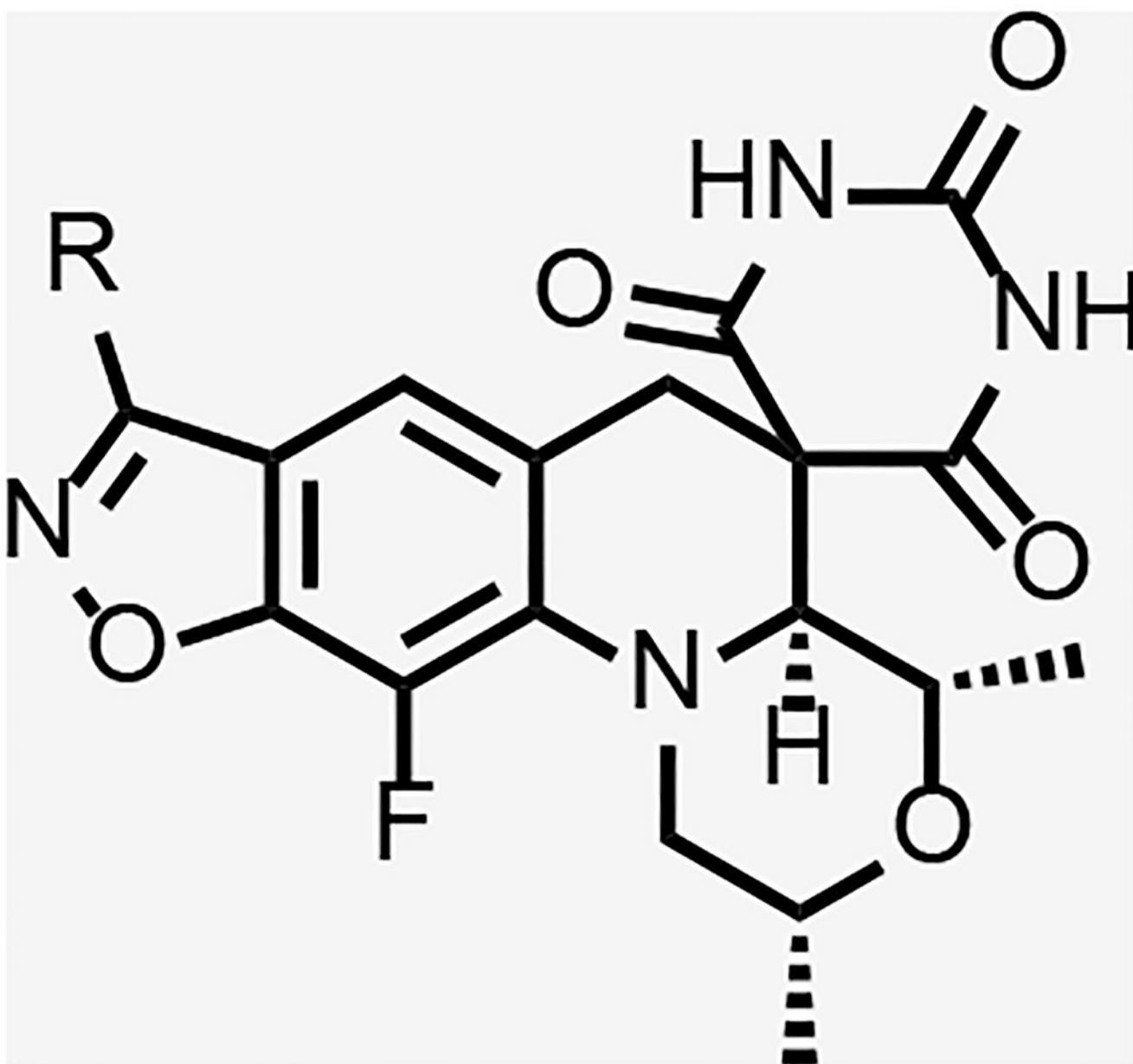




Author Manuscript

Author Manuscript

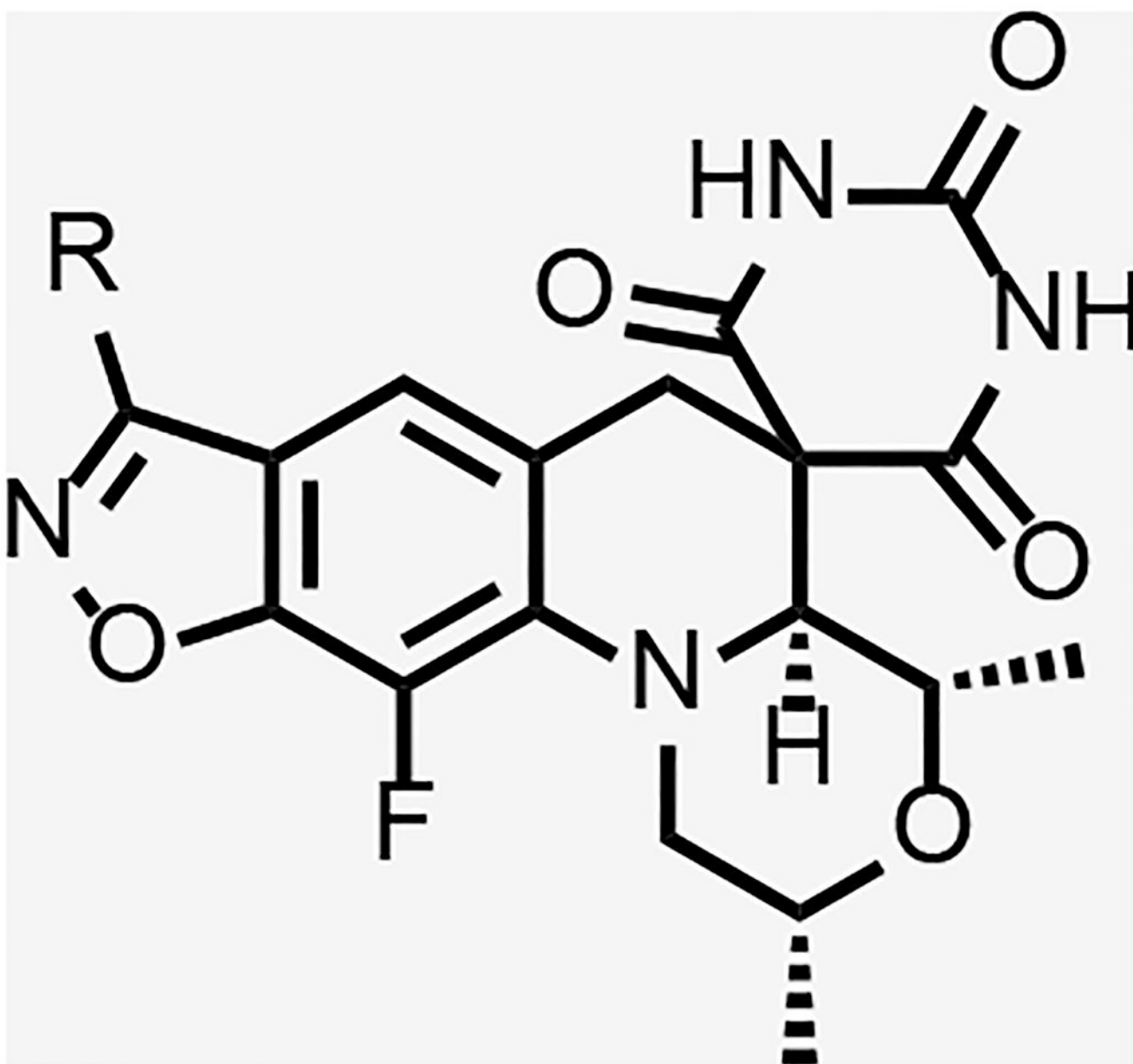
Author Manuscript



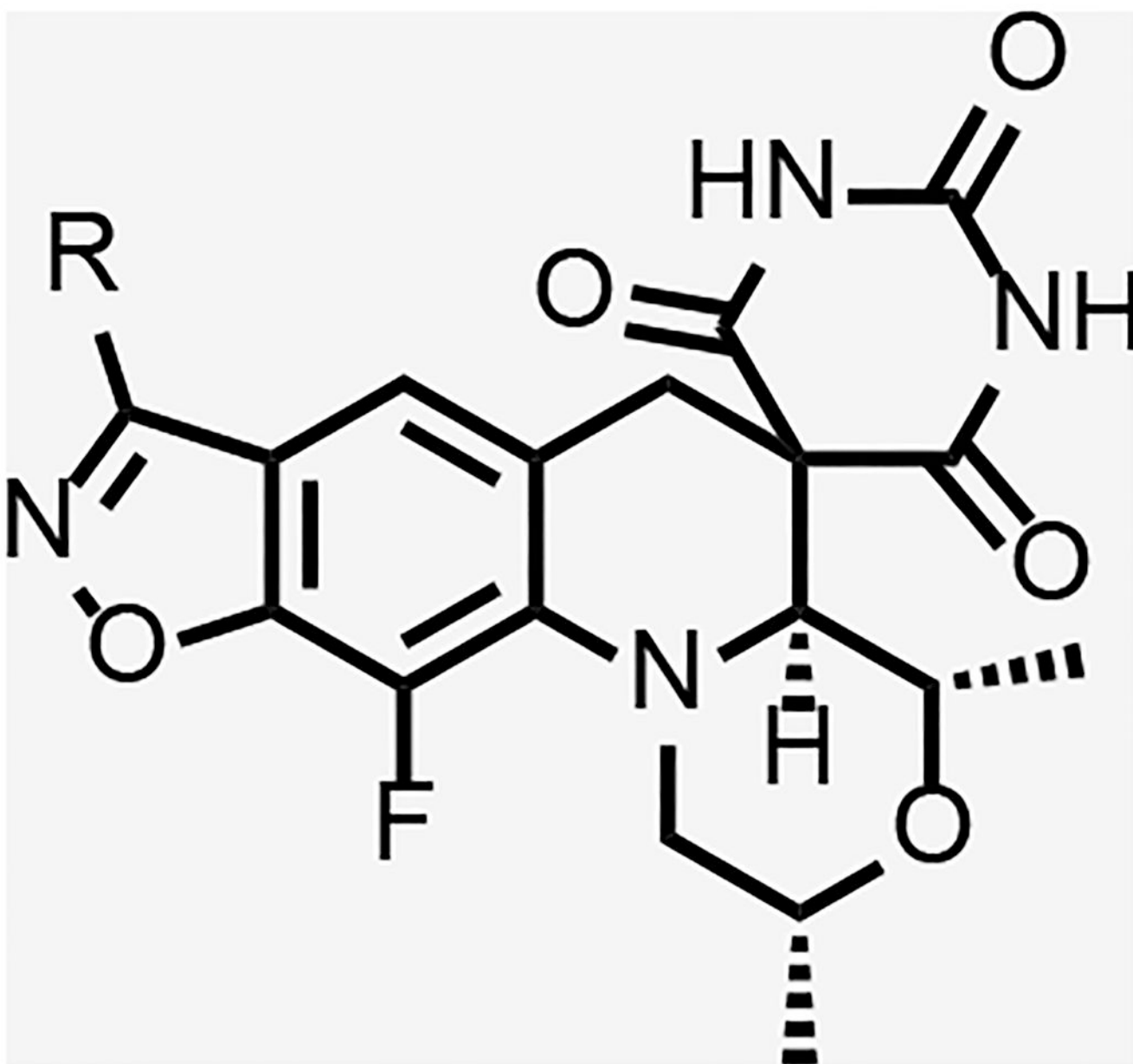
Compound	R	Solubility ( $\mu\text{M}$ )	logD	<i>Mtb</i> gyrase IC <sub>50</sub> ( $\mu\text{M}$ )	<i>Mtb</i> <sup>a</sup> MIC ( $\mu\text{M}$ )	<i>Sau</i> <sup>b</sup> MIC ( $\mu\text{M}$ )	<i>Ecol</i> <sup>c</sup> MIC ( $\mu\text{M}$ )	HepG2 IC <sub>50</sub> ( $\mu\text{M}$ )
26		170	1.6	-	2.0	3.9	>125	>300

Author Manuscript

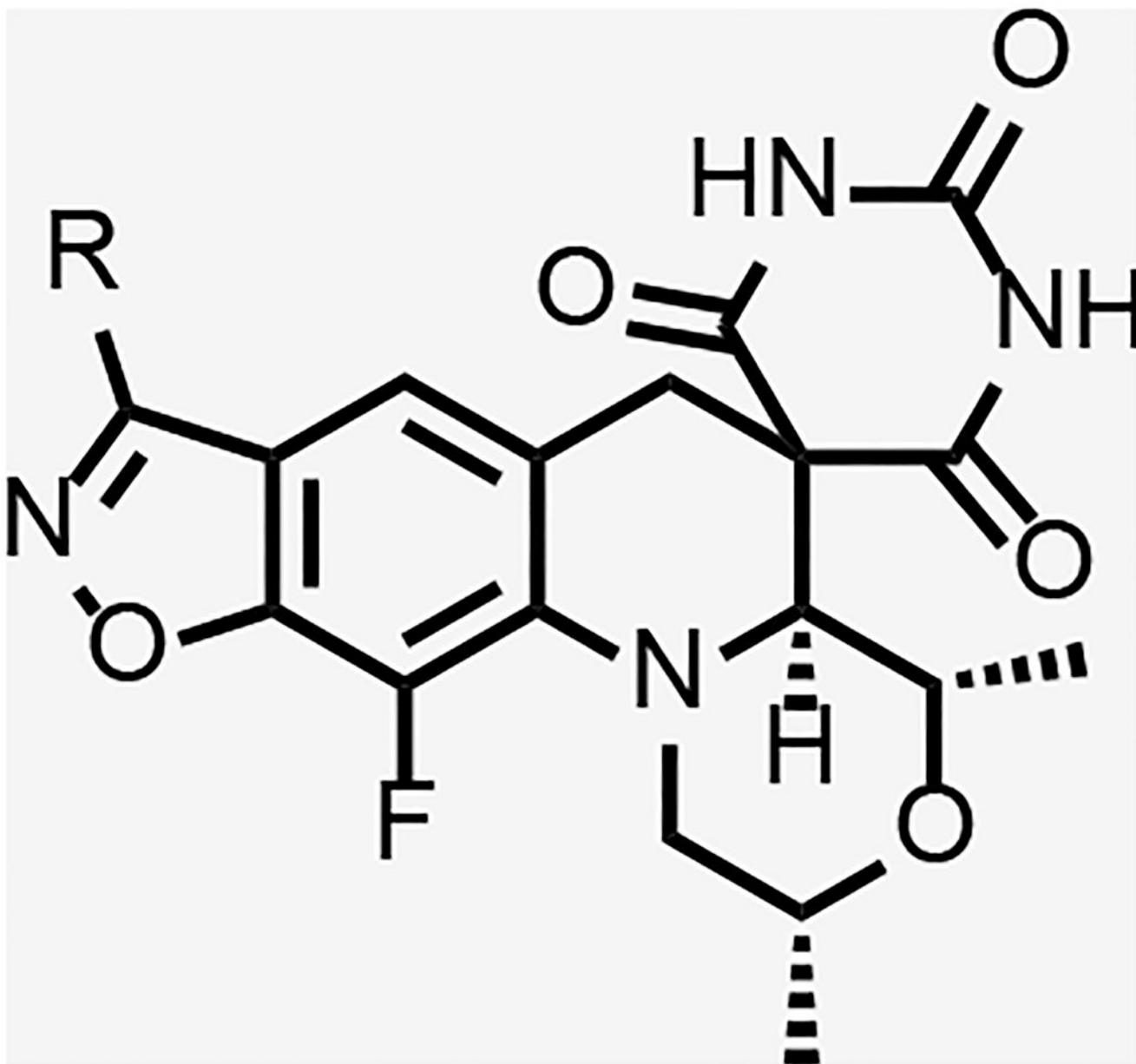




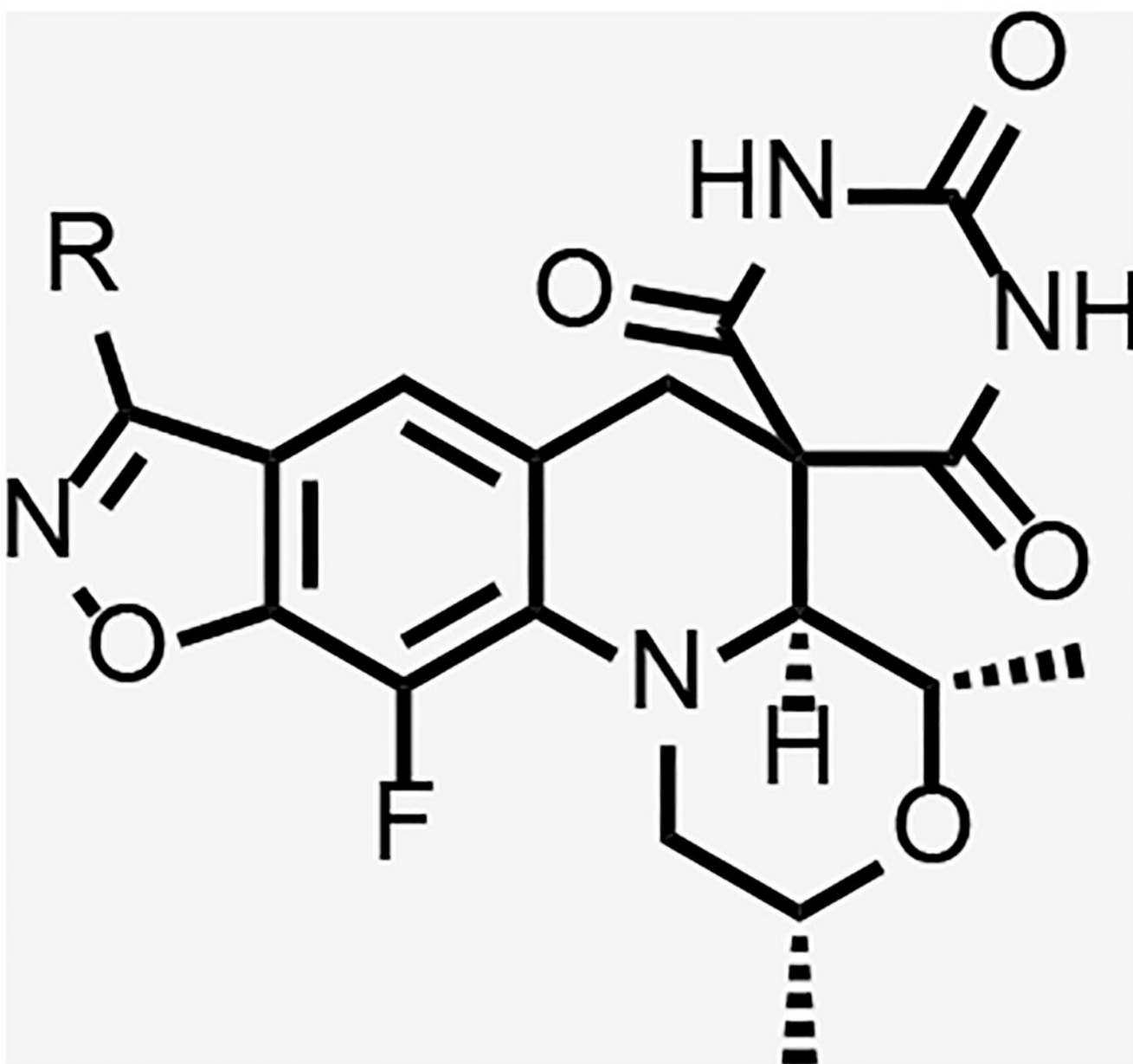
Compound	R	Solubility ( $\mu\text{M}$ )	logD	<i>Mtb</i> gyrase IC <sub>50</sub> ( $\mu\text{M}$ )	<i>Mtb</i> <sup>a</sup> MIC ( $\mu\text{M}$ )	<i>Sau</i> <sup>b</sup> MIC ( $\mu\text{M}$ )	<i>Ecol</i> <sup>c</sup> MIC ( $\mu\text{M}$ )	HepG2 IC <sub>50</sub> ( $\mu\text{M}$ )
27		155	1.5	-	3.9	>250	>250	>300



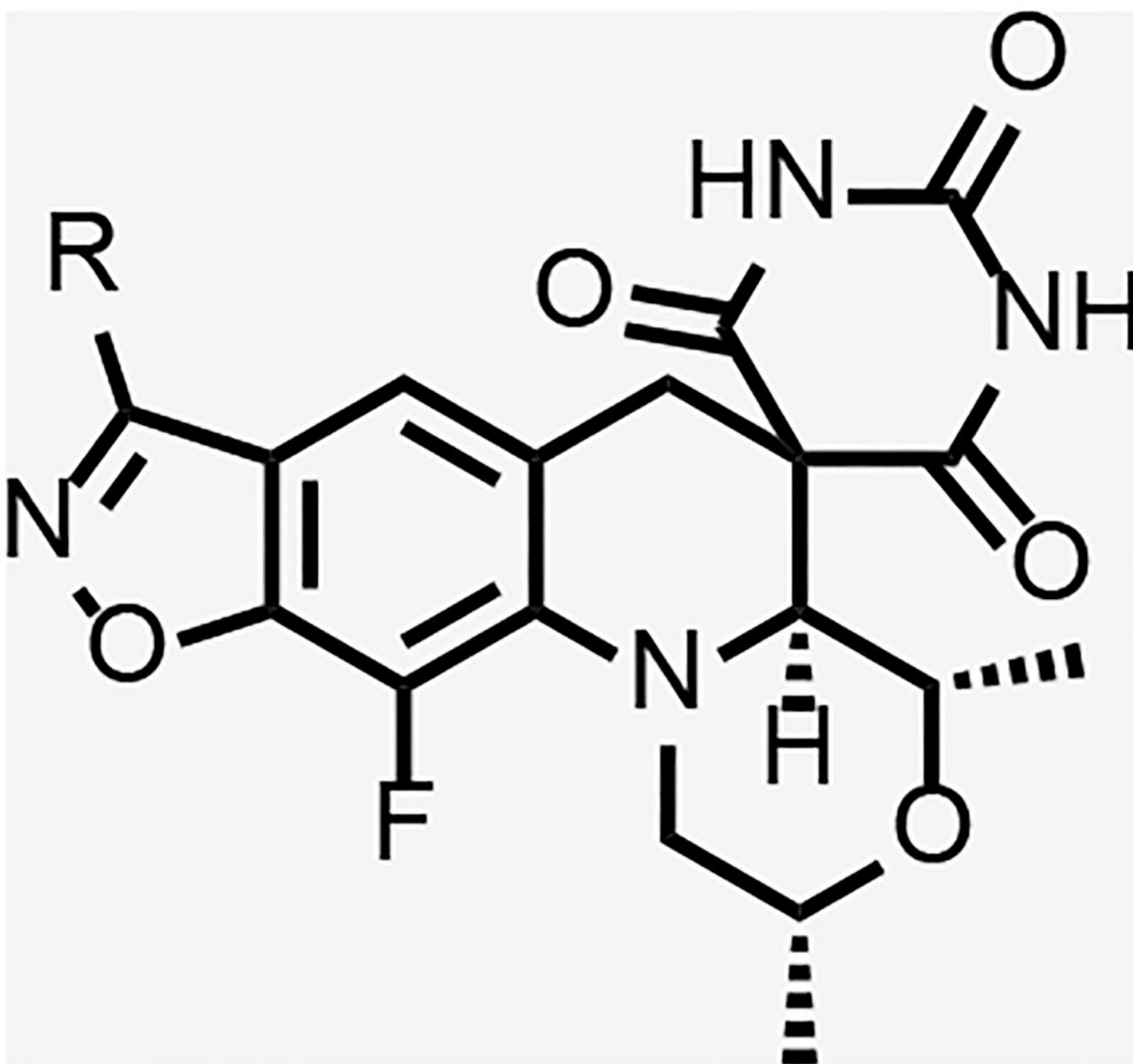
Compound	R	Solubility ( $\mu\text{M}$ )	logD	<i>Mtb</i> gyrase IC <sub>50</sub> ( $\mu\text{M}$ )	<i>Mtb</i> <sup>a</sup> MIC ( $\mu\text{M}$ )	<i>Sau</i> <sup>b</sup> MIC ( $\mu\text{M}$ )	<i>Ecol</i> <sup>c</sup> MIC ( $\mu\text{M}$ )	HepG2 IC <sub>50</sub> ( $\mu\text{M}$ )
28		180	1.3	-	2.0	63	>250	>300



Compound	R	Solubility ( $\mu\text{M}$ )	logD	<i>Mtb</i> gyrase IC <sub>50</sub> ( $\mu\text{M}$ )	<i>Mtb</i> <sup>a</sup> MIC ( $\mu\text{M}$ )	<i>Sau</i> <sup>b</sup> MIC ( $\mu\text{M}$ )	<i>Ecol</i> <sup>c</sup> MIC ( $\mu\text{M}$ )	HepG2 IC <sub>50</sub> ( $\mu\text{M}$ )
29		190	1.3	-	2.0	63	>250	>300



Compound	R	Solubility ( $\mu\text{M}$ )	logD	<i>Mtb</i> gyrase IC <sub>50</sub> ( $\mu\text{M}$ )	<i>Mtb</i> <sup>a</sup> MIC ( $\mu\text{M}$ )	<i>Sau</i> <sup>b</sup> MIC ( $\mu\text{M}$ )	<i>Ecol</i> <sup>c</sup> MIC ( $\mu\text{M}$ )	HepG2 IC <sub>50</sub> ( $\mu\text{M}$ )
30		190	1.3	-	2.0	>125	>250	>300

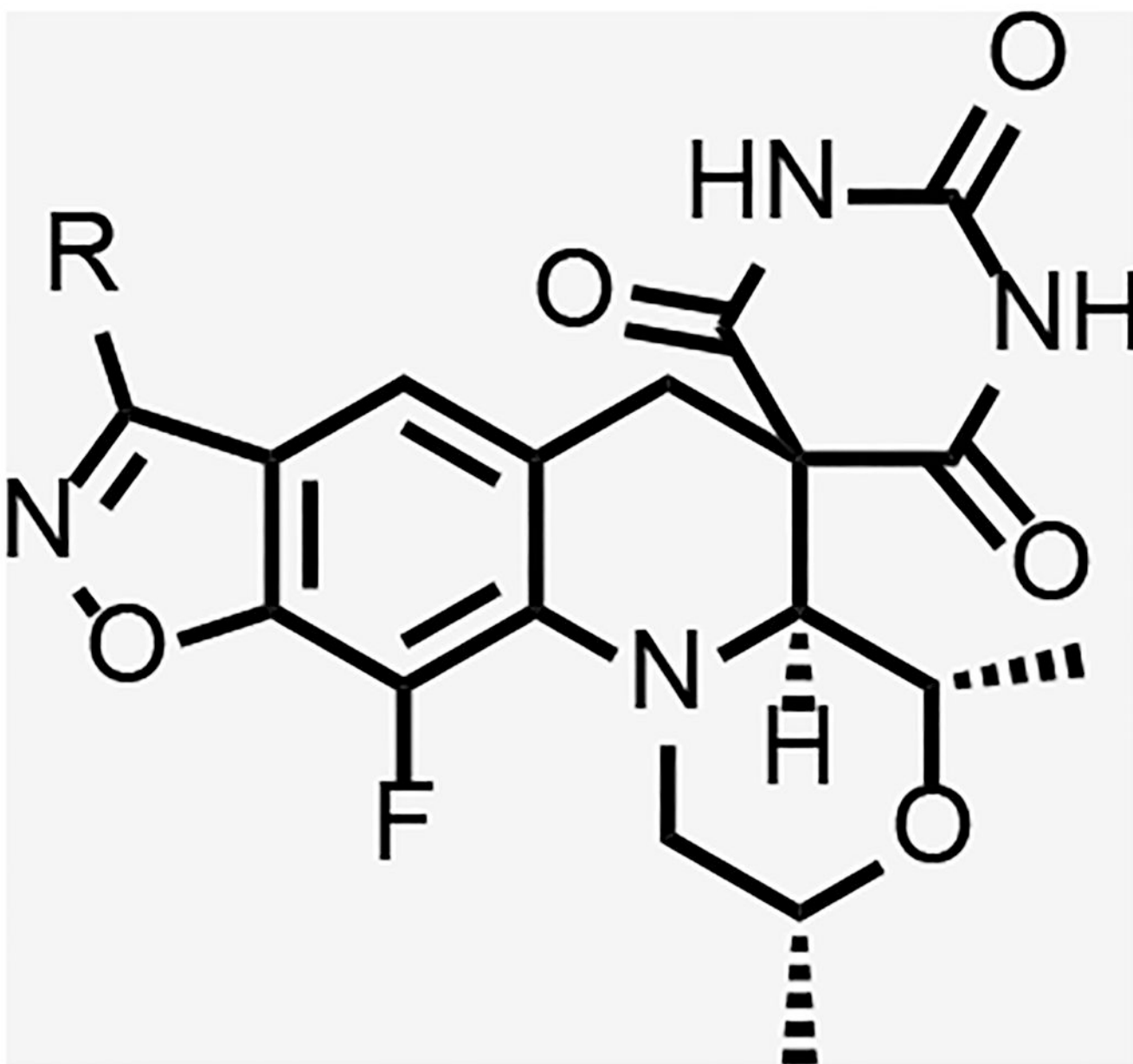


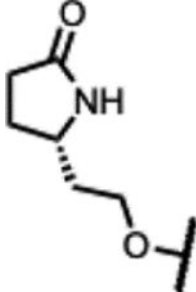
Compound	R	Solubility ( $\mu\text{M}$ )	logD	<i>Mtb</i> gyrase IC <sub>50</sub> ( $\mu\text{M}$ )	<i>Mtb</i> <sup>a</sup> MIC ( $\mu\text{M}$ )	<i>Sau</i> <sup>b</sup> MIC ( $\mu\text{M}$ )	<i>Ecol</i> <sup>c</sup> MIC ( $\mu\text{M}$ )	HepG2 IC <sub>50</sub> ( $\mu\text{M}$ )
31		200	1.4	-	2.0	31	63	>300

Author Manuscript

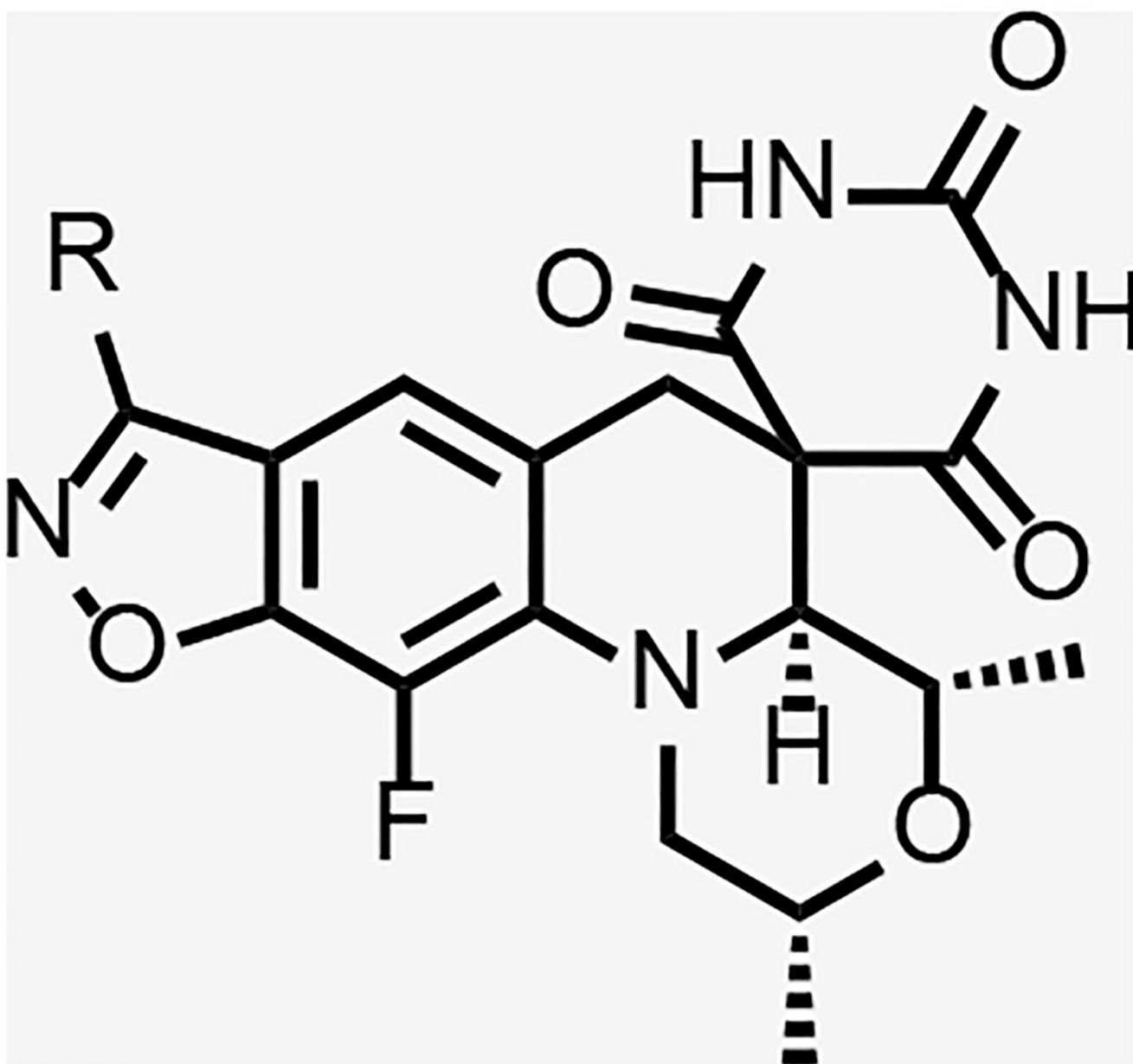
Author Manuscript

Author Manuscript



Compound	R	Solubility ( $\mu\text{M}$ )	logD	<i>Mtb</i> gyrase IC <sub>50</sub> ( $\mu\text{M}$ )	<i>Mtb</i> <sup>a</sup> MIC ( $\mu\text{M}$ )	<i>Sau</i> <sup>b</sup> MIC ( $\mu\text{M}$ )	<i>Ecol</i> <sup>c</sup> MIC ( $\mu\text{M}$ )	HepG2 IC <sub>50</sub> ( $\mu\text{M}$ )
32		190	1.7	-	3.9	31	>125	>300

Author Manuscript



Compound	R	Solubility ( $\mu\text{M}$ )	logD	<i>Mtb</i> gyrase IC <sub>50</sub> ( $\mu\text{M}$ )	<i>Mtb</i> <sup>a</sup> MIC ( $\mu\text{M}$ )	<i>Sau</i> <sup>b</sup> MIC ( $\mu\text{M}$ )	<i>Ecol</i> <sup>c</sup> MIC ( $\mu\text{M}$ )	HepG2 IC <sub>50</sub> ( $\mu\text{M}$ )
33		190	1.6	-	63	>125	>125	>300

<sup>a</sup> *M. tuberculosis* H37Rv;

<sup>b</sup> *S. aureus* ATTC 25923

<sup>c</sup> *E. coli* ATTC 25922

Author Manuscript

Author Manuscript

Author Manuscript

Author Manuscript



**Table 4.**

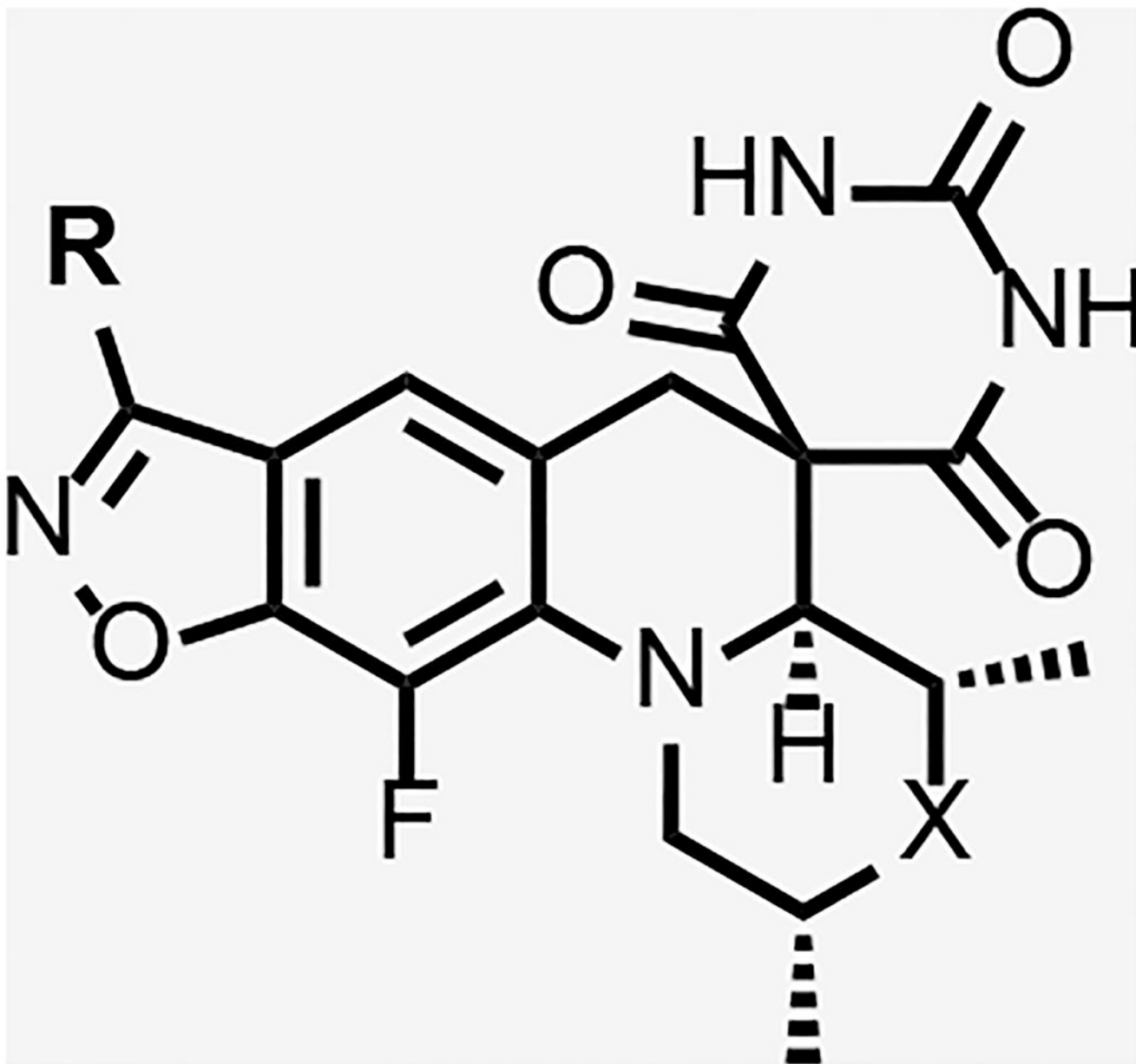
Author Manuscript

Author Manuscript

Author Manuscript

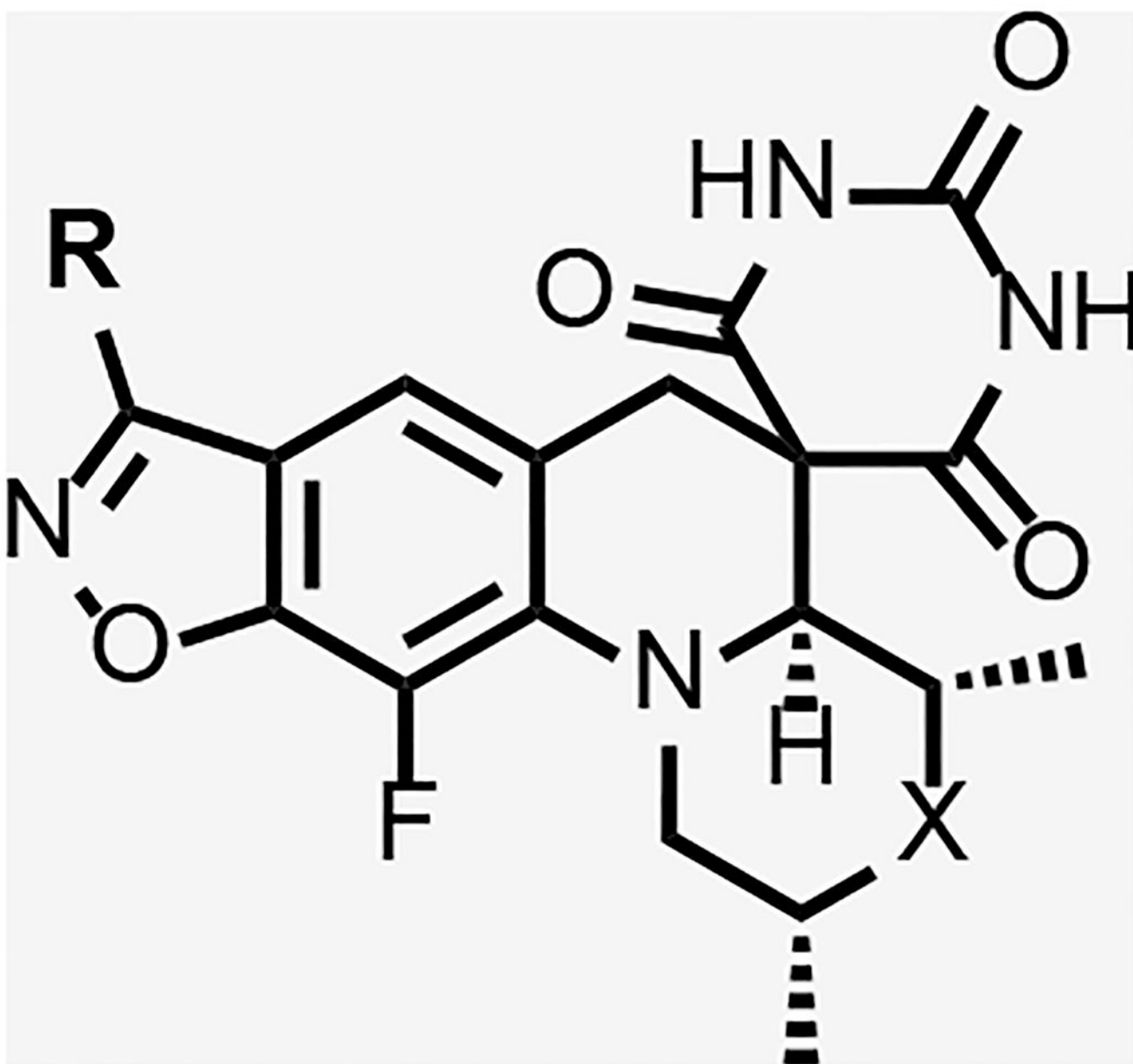
Author Manuscript

Data for SPTs with piperidine and piperazine replacements for morpholine

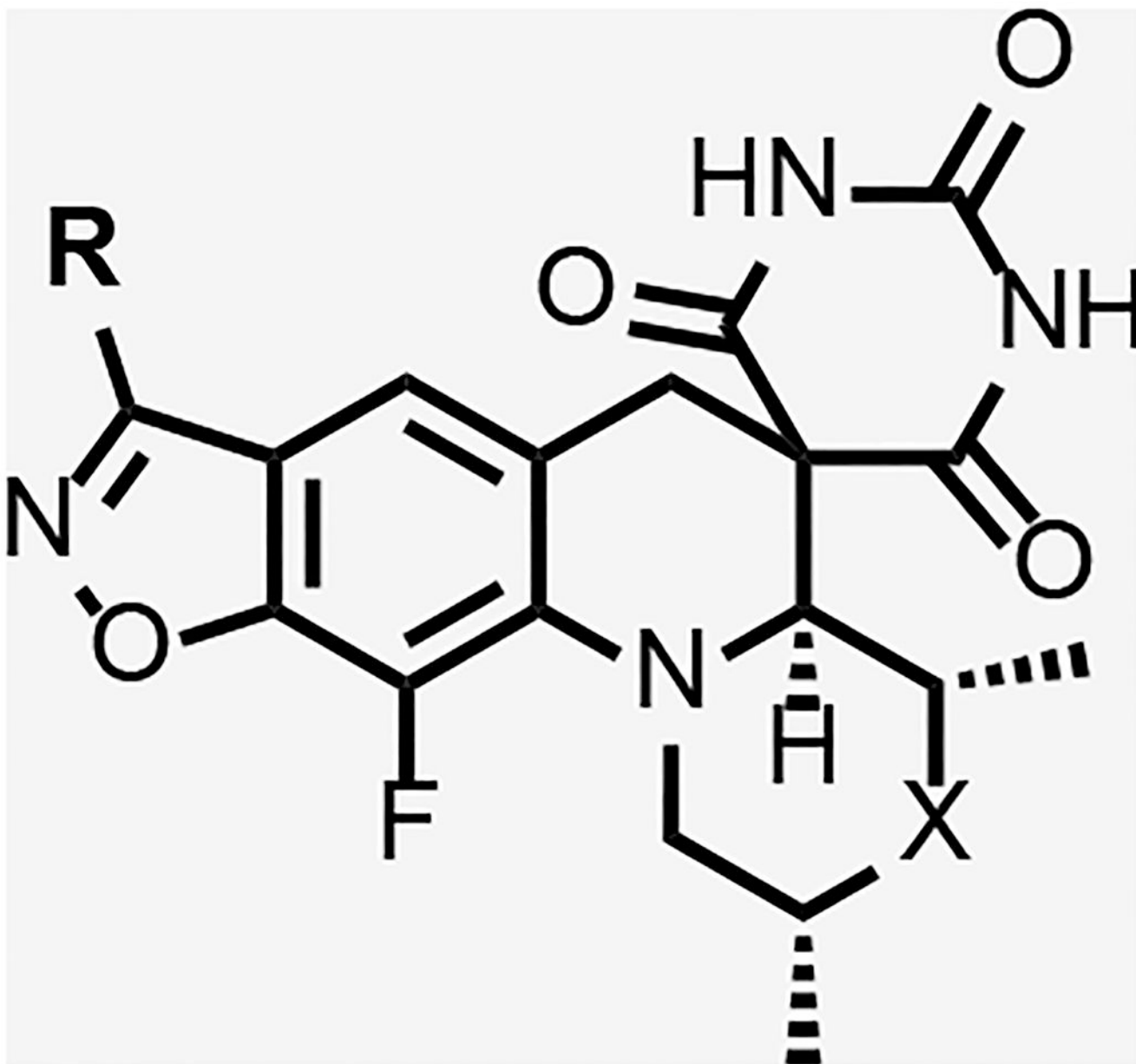


Compound	R	Morpholine Variation	Solubility ( $\mu\text{M}$ )	logD	<i>Mtb</i> gyrase IC <sub>50</sub> ( $\mu\text{M}$ )	<i>Sau</i> gyrase IC <sub>50</sub> ( $\mu\text{M}$ )	<i>Mtb</i> <sup>a</sup> MIC ( $\mu\text{M}$ )	<i>Sau</i> <sup>b</sup> MIC ( $\mu\text{M}$ )	<i>E. coli</i> <sup>c</sup> MIC ( $\mu\text{M}$ )	HepG2 IC <sub>50</sub> ( $\mu\text{M}$ )
34			50	0.30	-	-	>125	63	31	>50

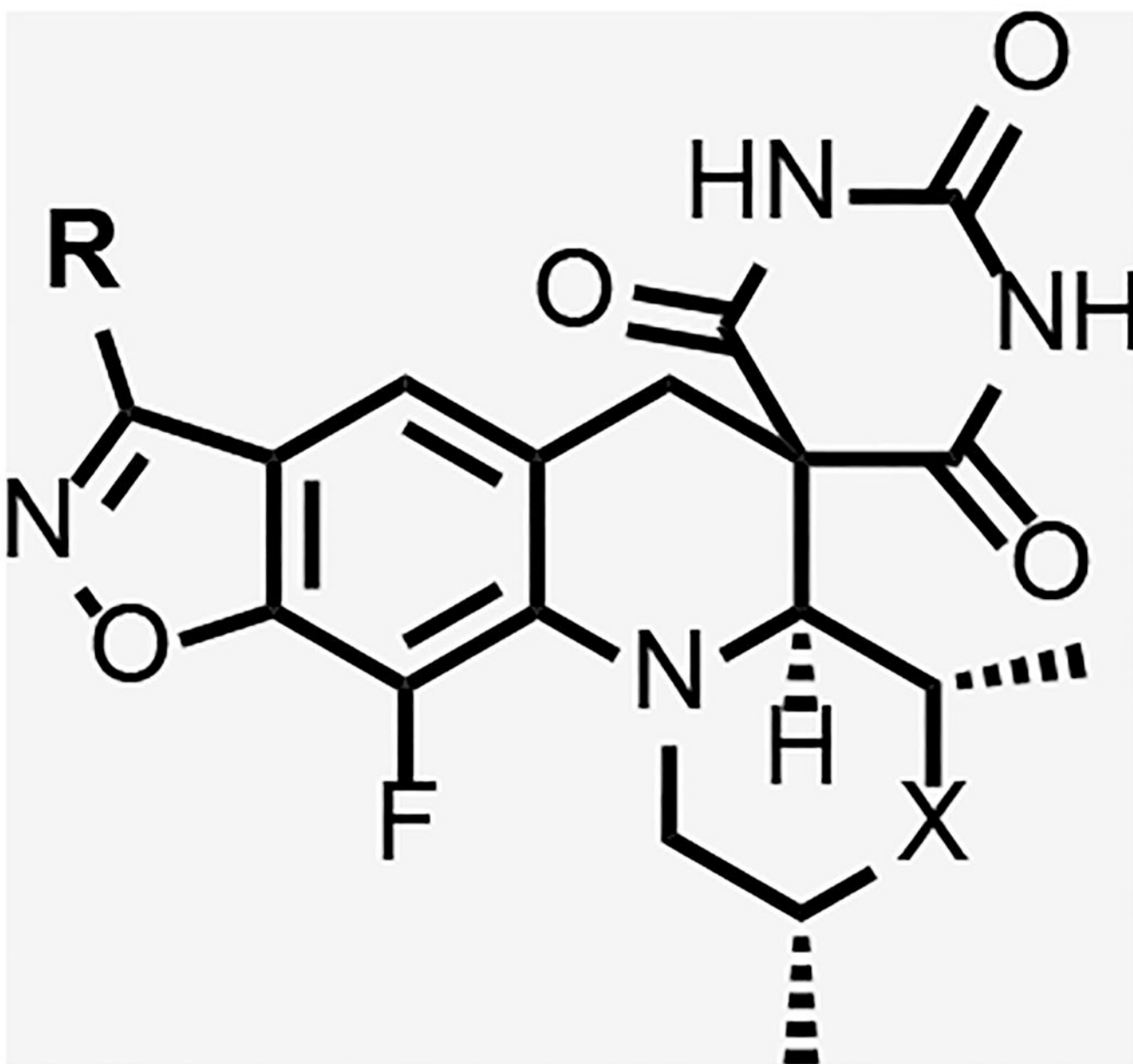
*J Med Chem.* Author manuscript; available in PMC 2022 June 26.



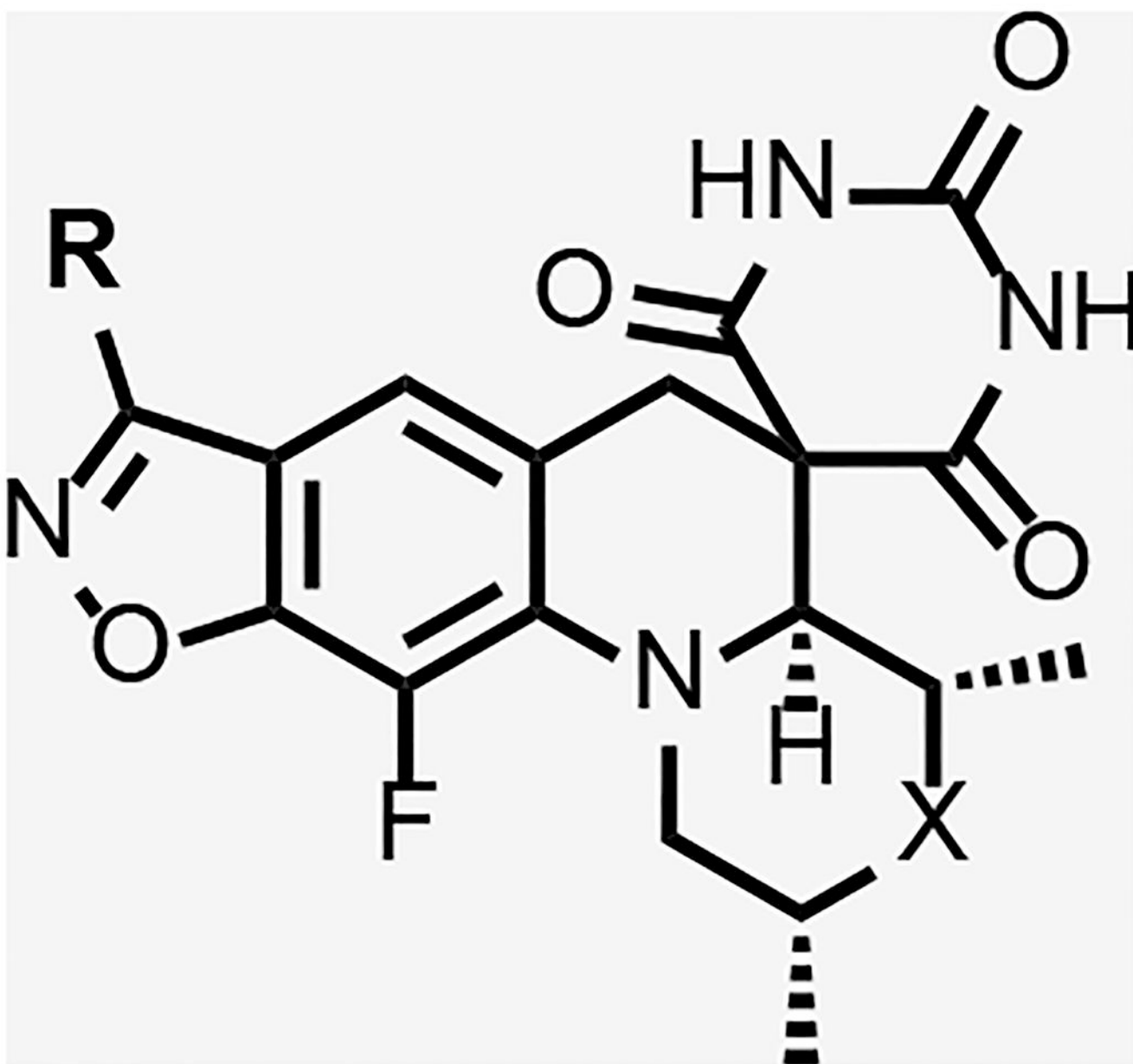
Compound	R	Morpholine Variation	Solubility ( $\mu\text{M}$ )	logD	<i>Mtb</i> gyrase IC <sub>50</sub> ( $\mu\text{M}$ )	<i>Sau</i> gyrase IC <sub>50</sub> ( $\mu\text{M}$ )	<i>Mtb</i> <sup>a</sup> MIC ( $\mu\text{M}$ )	<i>Sau</i> <sup>b</sup> MIC ( $\mu\text{M}$ )	<i>E. coli</i> <sup>c</sup> MIC ( $\mu\text{M}$ )	HepG2 IC <sub>50</sub> ( $\mu\text{M}$ )
35			>200	0.58	207	-	>125	>125	>125	-



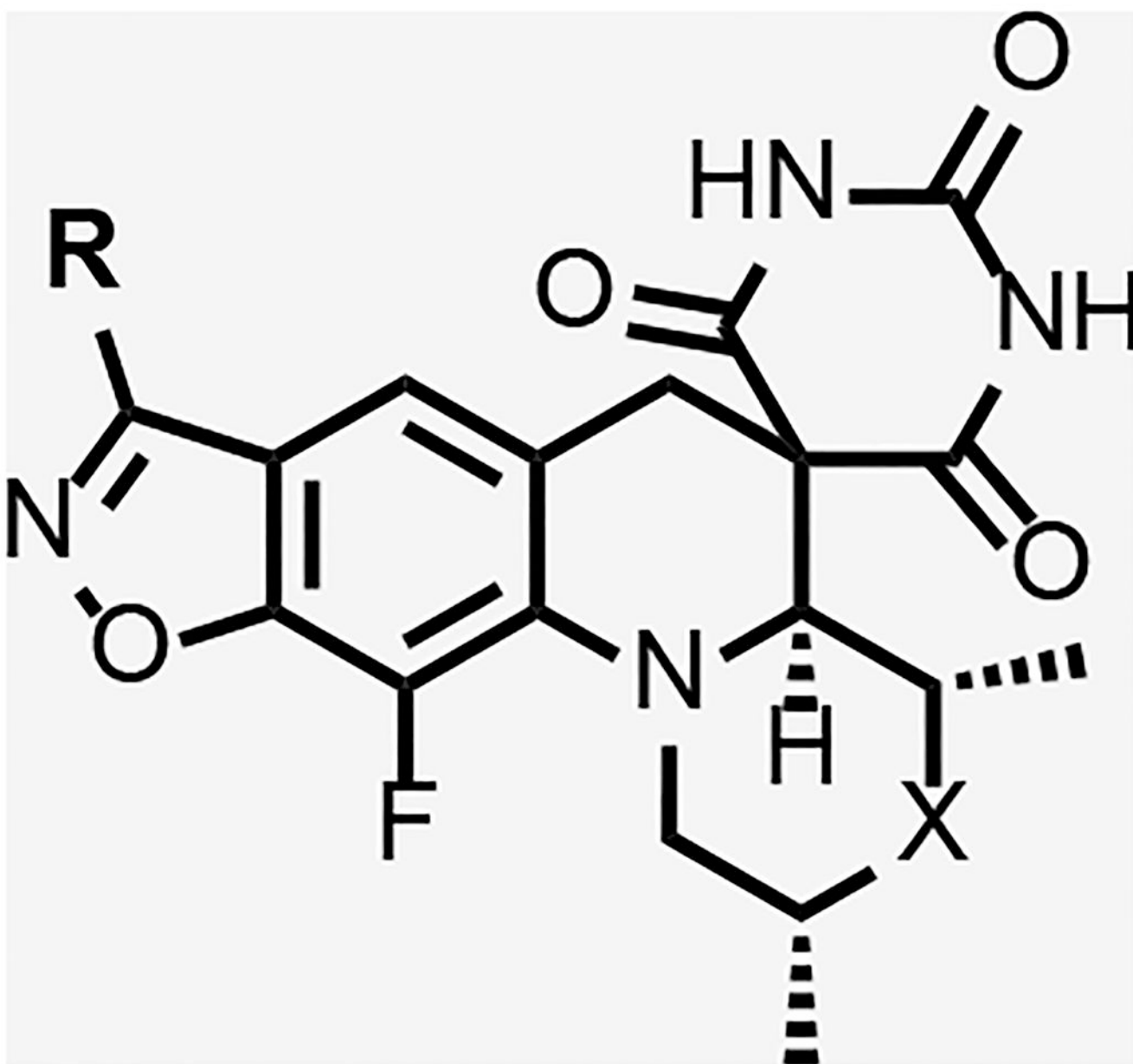
Compound	R	Morpholine Variation	Solubility ( $\mu\text{M}$ )	logD	<i>Mtb</i> gyrase IC <sub>50</sub> ( $\mu\text{M}$ )	<i>Sau</i> gyrase IC <sub>50</sub> ( $\mu\text{M}$ )	<i>Mtb</i> <sup>a</sup> MIC ( $\mu\text{M}$ )	<i>Sau</i> <sup>b</sup> MIC ( $\mu\text{M}$ )	<i>E. coli</i> <sup>c</sup> MIC ( $\mu\text{M}$ )	HepG2 IC <sub>50</sub> ( $\mu\text{M}$ )
36			>200	1.4	>1000	-	>125	>125	>125	>300



Compound	R	Morpholine Variation	Solubility ( $\mu\text{M}$ )	logD	<i>Mtb</i> gyrase IC <sub>50</sub> ( $\mu\text{M}$ )	<i>Sau</i> gyrase IC <sub>50</sub> ( $\mu\text{M}$ )	<i>Mtb</i> <sup>a</sup> MIC ( $\mu\text{M}$ )	<i>Sau</i> <sup>b</sup> MIC ( $\mu\text{M}$ )	<i>E. coli</i> <sup>c</sup> MIC ( $\mu\text{M}$ )	HepG2 IC <sub>50</sub> ( $\mu\text{M}$ )
37			95	-	-	-	>125	>125	>125	>50



Compound	R	Morpholine Variation	Solubility ( $\mu\text{M}$ )	logD	<i>Mtb</i> gyrase IC <sub>50</sub> ( $\mu\text{M}$ )	<i>Sau</i> gyrase IC <sub>50</sub> ( $\mu\text{M}$ )	<i>Mtb</i> <sup>a</sup> MIC ( $\mu\text{M}$ )	<i>Sau</i> <sup>b</sup> MIC ( $\mu\text{M}$ )	<i>E. coli</i> <sup>c</sup> MIC ( $\mu\text{M}$ )	HepG2 IC <sub>50</sub> ( $\mu\text{M}$ )
38			<5	1.8	-	-	3.9	1.0	3.9	>50

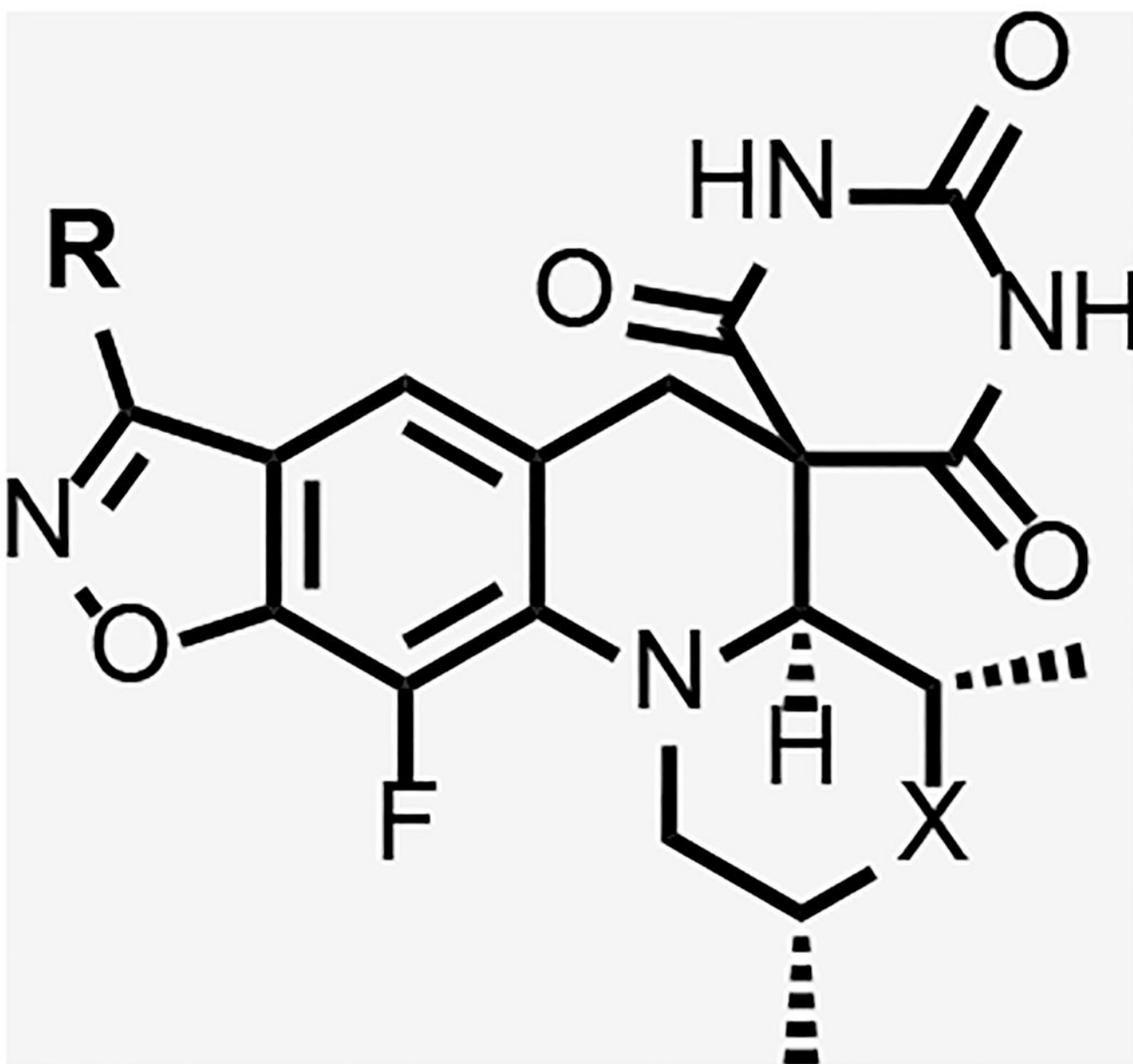


Compound	R	Morpholine Variation	Solubility ( $\mu\text{M}$ )	logD	<i>Mtb</i> gyrase IC <sub>50</sub> ( $\mu\text{M}$ )	<i>Sau</i> gyrase IC <sub>50</sub> ( $\mu\text{M}$ )	<i>Mtb</i> <sup>a</sup> MIC ( $\mu\text{M}$ )	<i>Sau</i> <sup>b</sup> MIC ( $\mu\text{M}$ )	<i>E. coli</i> <sup>c</sup> MIC ( $\mu\text{M}$ )	HepG2 IC <sub>50</sub> ( $\mu\text{M}$ )
39			50	1.7	-	-	0.98	16	63	>300

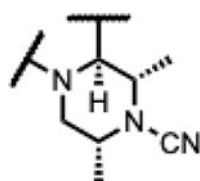
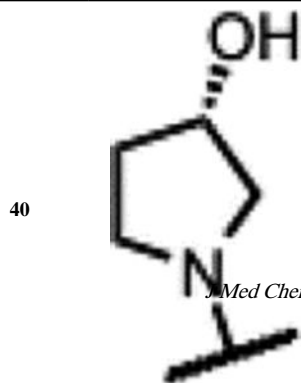
Author Manuscript

Author Manuscript

Author Manuscript



Compound	R	Morpholine Variation	Solubility ( $\mu\text{M}$ )	logD	<i>Mtb</i> gyrase IC <sub>50</sub> ( $\mu\text{M}$ )	<i>Sau</i> gyrase IC <sub>50</sub> ( $\mu\text{M}$ )	<i>Mtb</i> <sup>a</sup> MIC ( $\mu\text{M}$ )	<i>Sau</i> <sup>b</sup> MIC ( $\mu\text{M}$ )	<i>E. coli</i> <sup>c</sup> MIC ( $\mu\text{M}$ )	HepG2 IC <sub>50</sub> ( $\mu\text{M}$ )
----------	---	----------------------	------------------------------	------	--	--	---	---	---	--

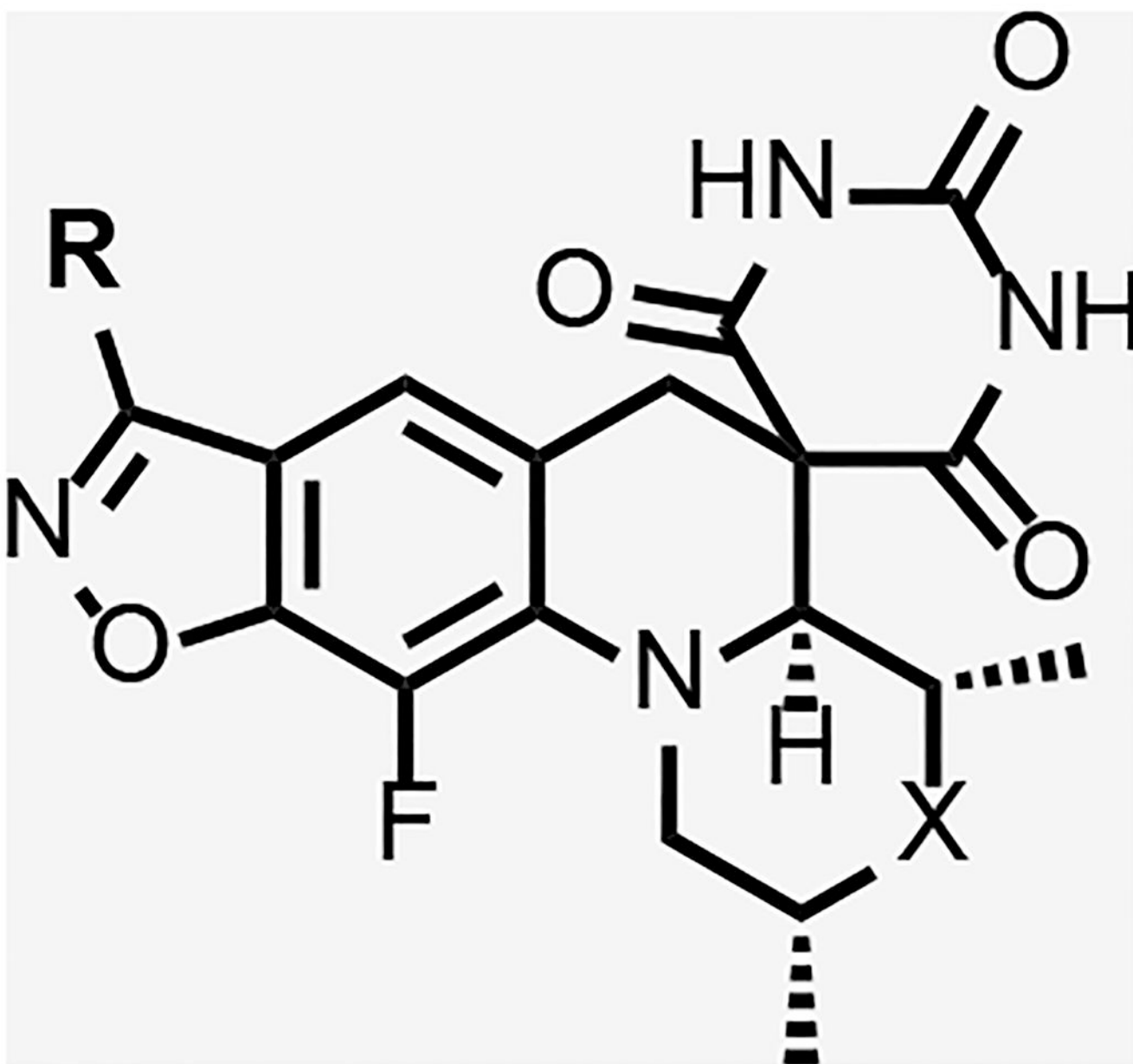


155      1.3      19      3.1      7.8      >125      >125      >50

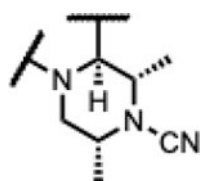
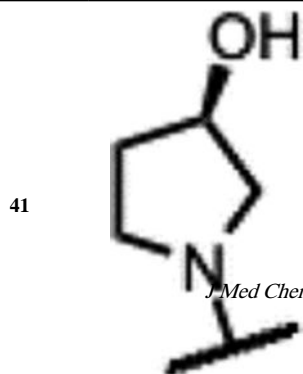
*J. Med. Chem.* Author manuscript; available in PMC 2022 June 26.

Author Manuscript





Compound	R	Morpholine Variation	Solubility ( $\mu\text{M}$ )	logD	<i>Mtb</i> gyrase IC <sub>50</sub> ( $\mu\text{M}$ )	<i>Sau</i> gyrase IC <sub>50</sub> ( $\mu\text{M}$ )	<i>Mtb</i> <sup>a</sup> MIC ( $\mu\text{M}$ )	<i>Sau</i> <sup>b</sup> MIC ( $\mu\text{M}$ )	<i>E. coli</i> <sup>c</sup> MIC ( $\mu\text{M}$ )	HepG2 IC <sub>50</sub> ( $\mu\text{M}$ )
----------	---	----------------------	------------------------------	------	--	--	---	---	---	--



145

1.2

-

-

7.8

&gt;125

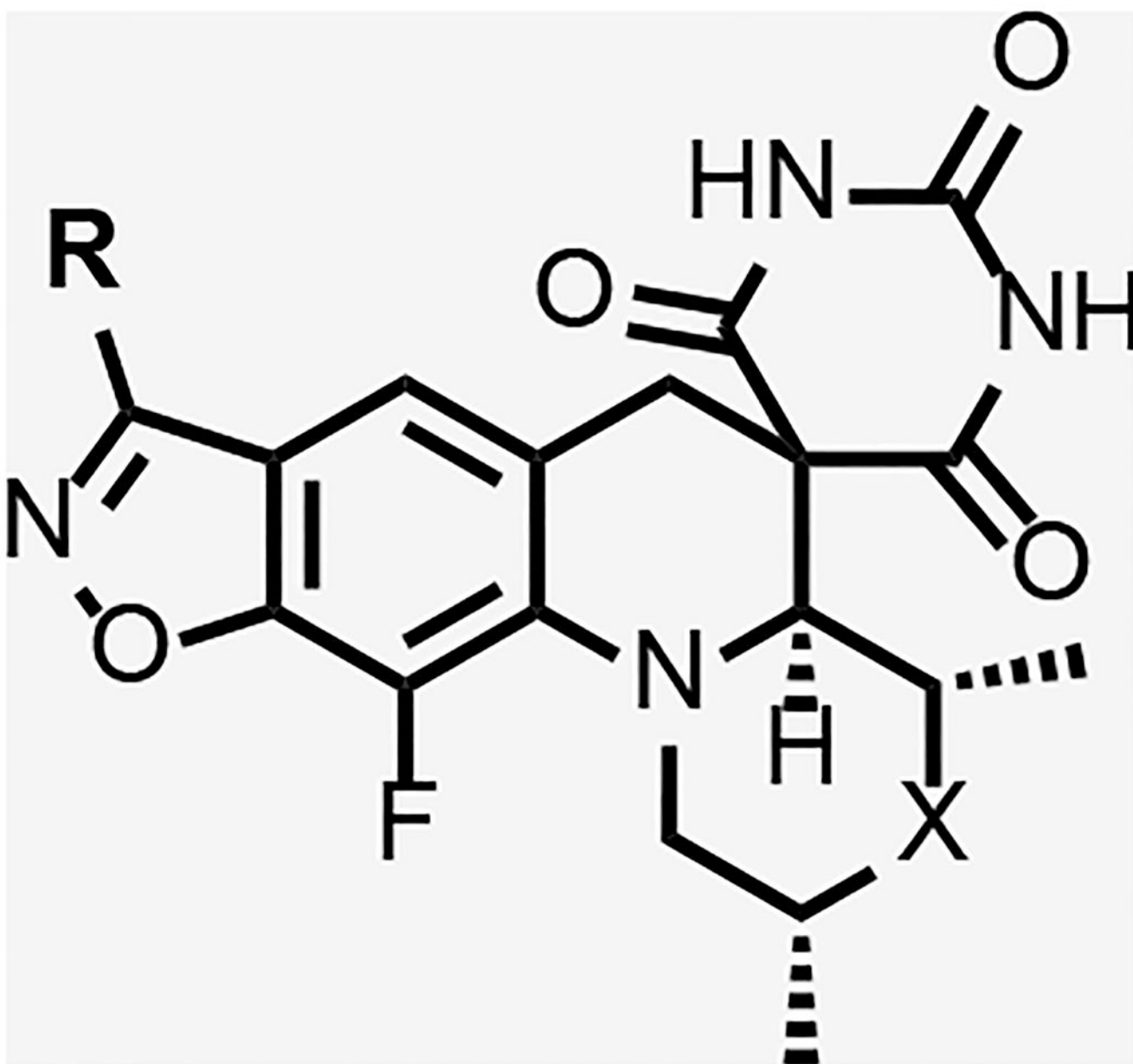
&gt;125

&gt;50

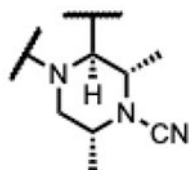
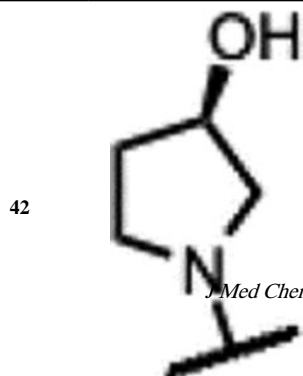
Author Manuscript

Author Manuscript

Author Manuscript



Compound	R	Morpholine Variation	Solubility ( $\mu\text{M}$ )	logD	<i>Mtb</i> gyrase IC <sub>50</sub> ( $\mu\text{M}$ )	<i>Sau</i> gyrase IC <sub>50</sub> ( $\mu\text{M}$ )	<i>Mtb</i> <sup>a</sup> MIC ( $\mu\text{M}$ )	<i>Sau</i> <sup>b</sup> MIC ( $\mu\text{M}$ )	<i>E. coli</i> <sup>c</sup> MIC ( $\mu\text{M}$ )	HepG2 IC <sub>50</sub> ( $\mu\text{M}$ )
----------	---	----------------------	------------------------------	------	--	--	---	---	---	--



130 1.3 2.6 - 0.49 >125 >125 >300

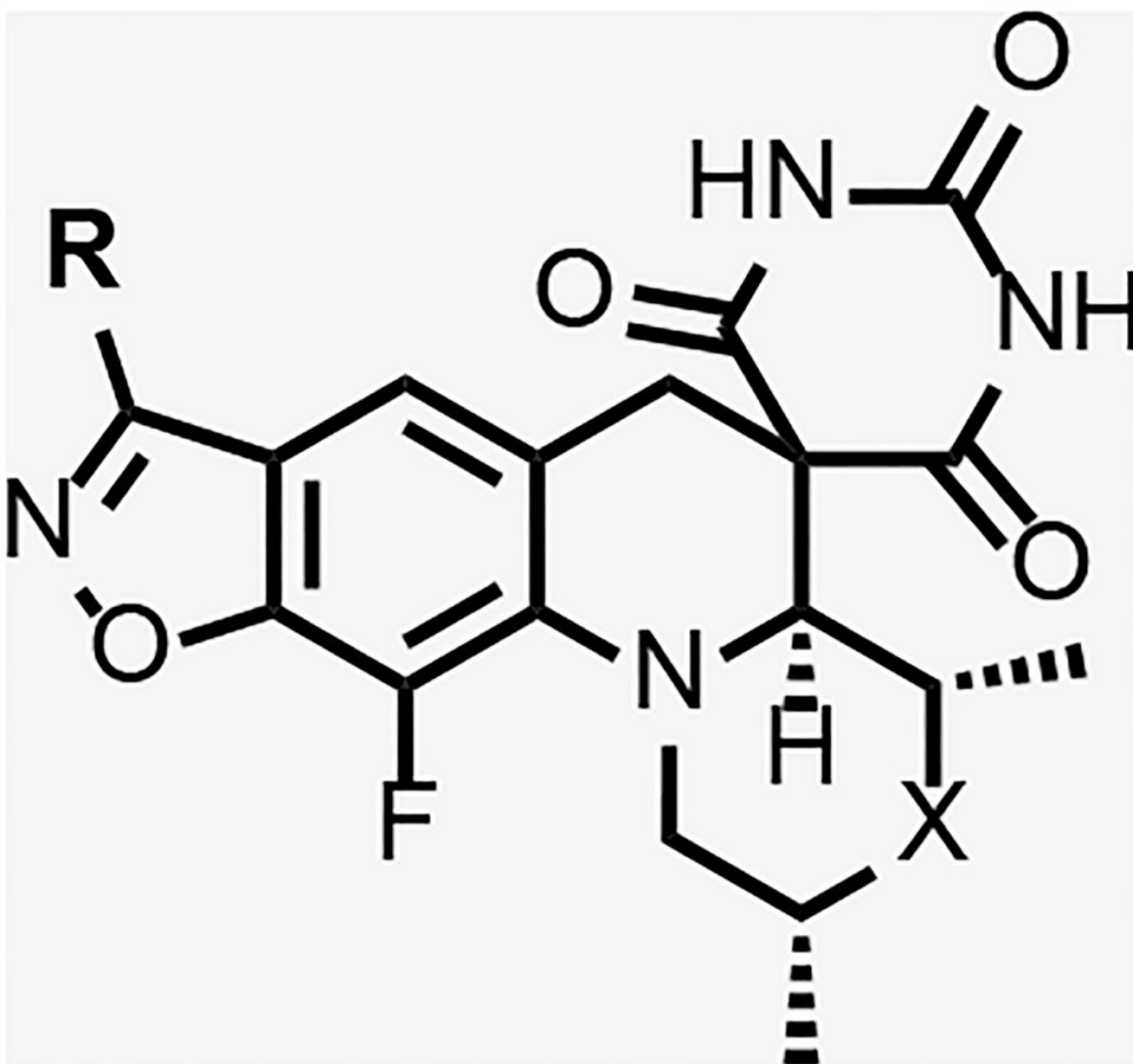
*J Med Chem.* Author manuscript; available in PMC 2022 June 26.

Author Manuscript

Author Manuscript

Author Manuscript

Author Manuscript

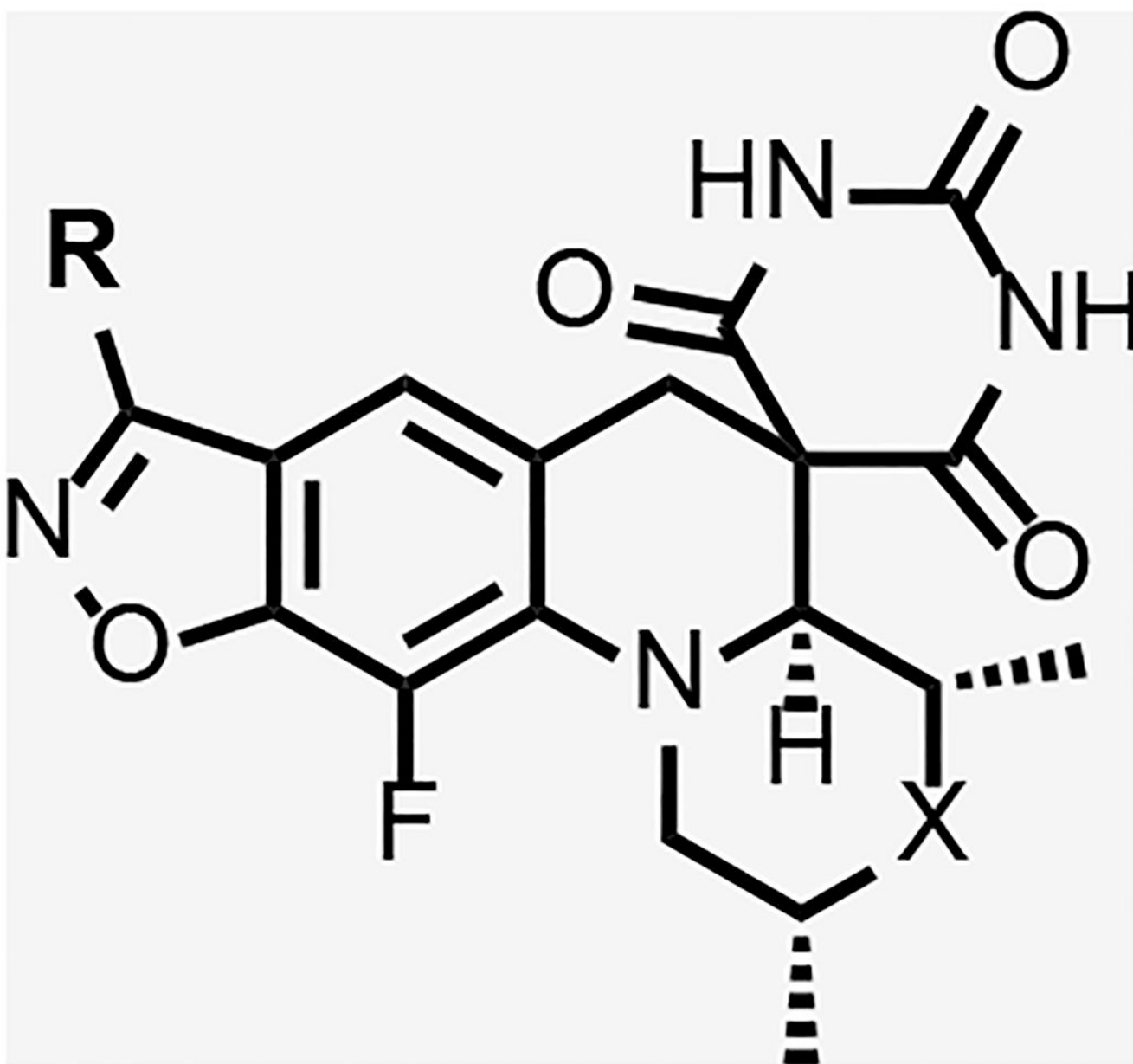


Compound	R	Morpholine Variation	Solubility ( $\mu\text{M}$ )	logD	<i>Mtb</i> gyrase IC <sub>50</sub> ( $\mu\text{M}$ )	<i>Sau</i> gyrase IC <sub>50</sub> ( $\mu\text{M}$ )	<i>Mtb</i> <sup>a</sup> MIC ( $\mu\text{M}$ )	<i>Sau</i> <sup>b</sup> MIC ( $\mu\text{M}$ )	<i>E. coli</i> <sup>c</sup> MIC ( $\mu\text{M}$ )	HepG2 IC <sub>50</sub> ( $\mu\text{M}$ )
----------	---	----------------------	------------------------------	------	--	--	---	---	---	--

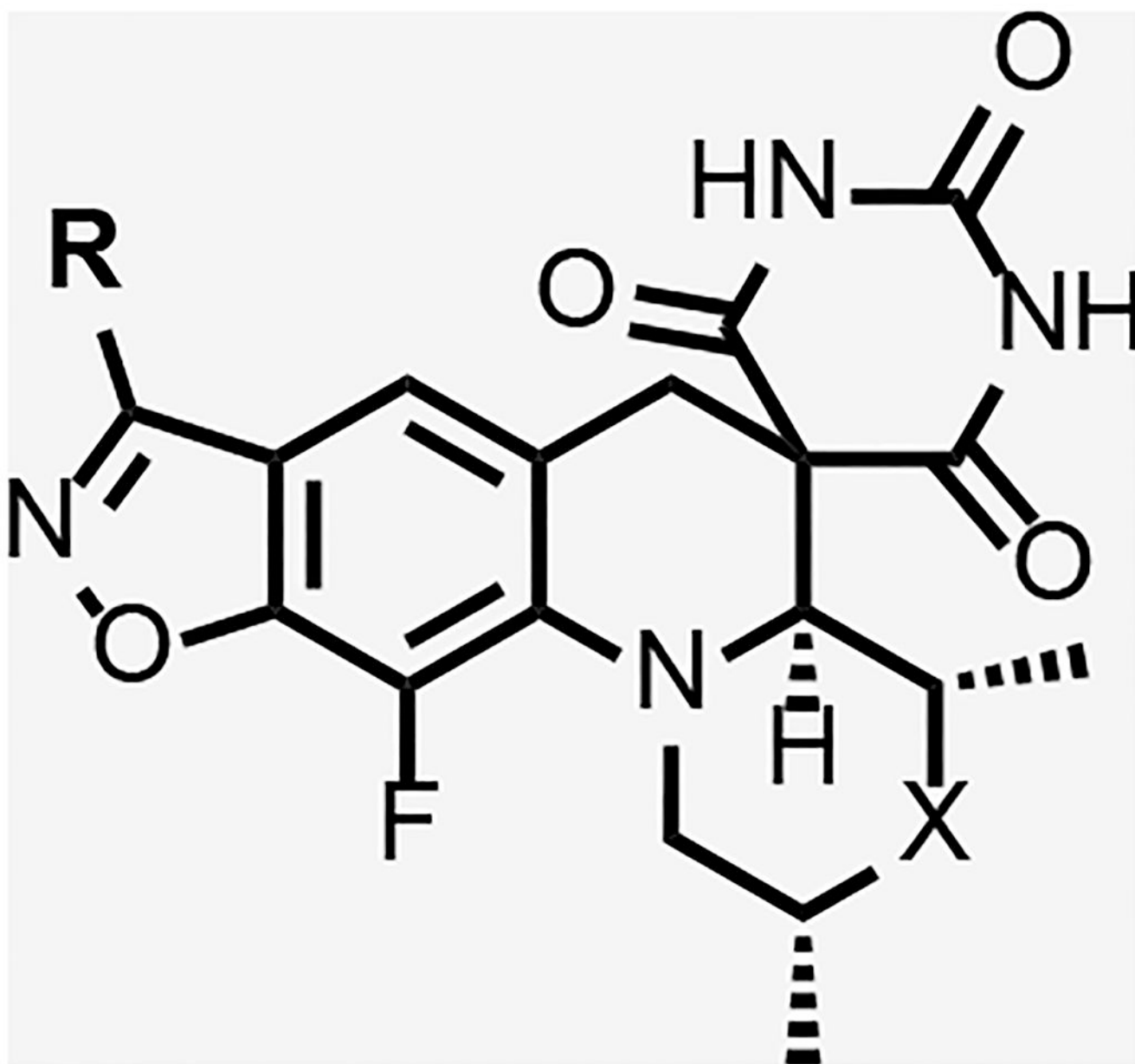
43			40	3.9	-	-	16	7.8	63	>300
----	--	--	----	-----	---	---	----	-----	----	------

*J Med Chem.* Author manuscript; available in PMC 2022 June 26.

Author Manuscript



Compound	R	Morpholine Variation	Solubility ( $\mu\text{M}$ )	logD	<i>Mtb</i> gyrase IC <sub>50</sub> ( $\mu\text{M}$ )	<i>Sau</i> gyrase IC <sub>50</sub> ( $\mu\text{M}$ )	<i>Mtb</i> <sup>a</sup> MIC ( $\mu\text{M}$ )	<i>Sau</i> <sup>b</sup> MIC ( $\mu\text{M}$ )	<i>E. coli</i> <sup>c</sup> MIC ( $\mu\text{M}$ )	HepG2 IC <sub>50</sub> ( $\mu\text{M}$ )
44			45	1.9	-	-	1.5	>125	>125	>300



Compound	R	Morpholine Variation	Solubility ( $\mu\text{M}$ )	logD	<i>Mtb</i> gyrase IC <sub>50</sub> ( $\mu\text{M}$ )	<i>Sau</i> gyrase IC <sub>50</sub> ( $\mu\text{M}$ )	<i>Mtb</i> <sup>a</sup> MIC ( $\mu\text{M}$ )	<i>Sau</i> <sup>b</sup> MIC ( $\mu\text{M}$ )	<i>E. coli</i> <sup>c</sup> MIC ( $\mu\text{M}$ )	HepG2 IC <sub>50</sub> ( $\mu\text{M}$ )
45			15	3.2	-	-	16	>250	>250	>50

<sup>a</sup> *M. tuberculosis* H37Rv;

<sup>b</sup> *S. aureus* ATTC 25923

<sup>c</sup> *E. coli* ATTC 25922

Author Manuscript

Author Manuscript

Author Manuscript

Author Manuscript

**Table 5.**Modulation of MICs against *gyrA* hypomorph

Compound	WT H37Rv		<i>gyrA</i> hypomorph		Ratio (WT/hypomorph)	
	MIC <sub>50</sub> ( $\mu$ M)	MIC ( $\mu$ M)	MIC <sub>50</sub> ( $\mu$ M)	MIC ( $\mu$ M)	MIC <sub>50</sub>	MIC
<b>Rifampicin</b>	0.24	0.041	0.021	0.037	1.3	1.1
<b>Moxifloxacin</b>	0.12	0.19	0.041	0.07	2.9	2.5
<b>Zoliflodacin</b>	20	44	4.6	12	4.3	3.6
<b>7</b>	1.8	3.8	0.26	0.65	7.1	5.8
<b>8</b>	3.3	5.9	0.92	2.4	3.6	2.5
<b>10</b>	3.65	6.75	1.24	3.2	2.9	2.1
<b>40</b>	5.35	10.3	1.75	5.05	3.1	2.0

WT: wild-type; *gyrA* mutant: *gyrA*-FDAS-TetON-1; MIC<sub>50</sub>: The concentration of compound that inhibits bacterial growth to 50% of maximal (DMSO control) growth; MIC: the lowest concentration of the given compound that completely inhibits bacterial growth.